

POLITECNICO DI MILANO

Scuola di Ingegneria Industriale
Corso di Laurea Specialistica in Ingegneria Meccanica
Dipartimento di Energia



**OPTIMIZATION OF A LOW N_q NUMBER PUMP BASED ON
EXPERIMENTATION AND NUMERICAL SIMULATION**

Relatore:

prof. ing. Dossena Vincenzo

Tesi di Laurea Magistrale di:

Claudio LAZARI

Matr. 783312

Anno Accademico 2012/2013

Index:

Introduction	7
Abstract	8
1) The context and the optimization problem	
1.1) Radial pumps: the machine and the system	9
1.1.1) Industrial relevance of the pumps	
1.1.2) Working point	
1.1.3) Specific speed and efficiency	
1.1.4) Range of applications of radial pumps	
1.1.5) Terminology	
1.2) The optimization of a pump	17
1.2.1) Object of the work	
1.2.2) Description of the pump	
1.3) The optimization of the pump: procedure	22
2) Experimental part	
2.1) Introduction	23
2.2) The test rig	24
2.3) Measuring devices	27
2.4) Results and considerations	32
2.4.1) Bearing friction measure	
2.4.2) Behavior of the plastic impellers	
2.4.3) Behavior of the cast iron impellers	
2.4.4) Impellers with reduced diameters	
2.5) Measurement errors.....	46
3) Theoretical loss analysis	
3.1) Introduction.....	49
3.2) Efficiency and loss calculation.....	50
3.3) Mechanical losses: disk friction	52
3.4) Leakage losses measurement	54
3.5) Hydraulic loss outside the pump	57
3.6) Hydraulic loss inside the pump.....	59
3.6.1) Impeller losses	
3.6.2) Volute losses	
3.7) Considerations.....	63

4) Simplified impeller design	
4.1) Introduction	65
4.2) Initial design process	66
4.2.1) Definition of the main dimensions	
4.2.2) Definition of the impeller	75
4.3) Application of the procedure to the original impeller.....	75
4.4) Conclusions	76
5) CFD model	
5.1) Introduction.....	77
5.2) CFD theory.....	78
5.2.1) Balance equations	
5.2.2) Reynolds average and “closure” of the problem	
5.2.3) Boundary layer: the y^+ parameter	
5.2.4) The finite volumes method	
5.2.5) Domain, grid and boundary conditions	
5.3) CFD modeling	83
5.4) Different CFD versions.....	87
5.5) Analysis of the flow in the CFD model	92
5.5.1) Flow at best efficiency point	
5.5.2) Part-load operation flow	
5.6) Conclusions	100
6) Crossing of the results	
6.1) Introduction	101
6.2) Comparison between the real characteristic curves and the ones provided by the company.....	102
6.3) Comparison between CFD and semi-empirical loss analysis.....	105
6.4) Conclusions	108
(consistent view of the pump behavior; hints for the following optimization process)	
7) Optimization of the impeller with CFD iterative process	
7.1) Introduction (modus operandi)	109
7.2) Numerical optimization of a two dimensional geometry.....	110
7.2.1) Intermediate versions	
7.2.2) Final version compared with the original model	
7.3) Numerical optimization of a three dimensional geometry.....	120
7.3.1) Intermediate versions	
7.3.2) Final version compared with the original model	
7.4) Conclusions	126

8) Final considerations	
8.1) Overview on procedure and results.....	129
8.2) Considerations.....	130
8.3) Possible future improvements.....	130
Appendix1.....	131
Appendix2.....	133
Appendix3.....	134
Appendix4.....	135
List of symbols.....	137
List of figures	139
Thanks	142
Bibliography.....	143

Introduction

“Learning is experience, everything else is just information.”

Albert Einstein

The aim of this work is to analyze the functioning of an industrial centrifugal pump and try to improve its efficiency according to the specific working conditions.

Different methods will be used to look at the problem from different perspectives: experimental tests are done to have certain data, the use of semi-empirical formulas furnish an approximate view on the losses, a numerical calculation allows more precise considerations on the flows inside the machine, a one dimensional project is the base for the next step of optimization that is based on the use of the numerical model.

The project started on behalf of a German company that produces and sells the current series of pumps in a number of several thousand pieces per year and had the idea of improving the old design to enhance the performances. To do this, they have turned to the Department of Hydraulic fluid machinery of the University of Graz, an institute active all over the world but especially in the German speaking part; such is its prestige that every year it organizes a big conference on the theme of pumps and their applications.

The theme of the increase of efficiency of machines is particularly relevant today, not only for an obvious economic reason but also for the growing attention to environmental problems: the “end-use of electricity efficiency” is considered by the International Panel for Climate Change as one of the wedges to our disposal to contain the impact of human activities on our planet [5].

Abstract

The aim of this work is to analyze the functioning of an industrial centrifugal pump and try to improve its efficiency according to the specific working conditions.

The machine is produced by a German company that sells it in a number of several thousand pieces per year and this, despite the small dimension of the pump, makes appealing the possibility of enhancing the efficiency characteristic.

To decide on which parameters to act and how to influence the fluid dynamic behavior, it is important to completely understand the functioning of the machine; this will be done by conducting an analysis from four different prospective to get a unified prospective on the problem:

- The experimental analysis produces accurate characteristics curves that are required to validate the numerical model other than to be compared with the commercial data sheet.
- The use of semi-empirical models known in literature makes possible to calculate the amount of losses caused by each component of the pump and most important of all, the relative ratio that occurs among them.
- The simple calculation of the velocity triangles along with the use of some empirical relations is used to provide a good first try in the optimization process. Moreover the distance, for certain geometric dimensions, between the suggested value and the real one could imply the presence of some problems.
- The numerical analysis is done by means of a Computational Fluid Dynamic method and allows taking a look into the flow inside the pump.

The CFD program, which is validated through the confrontation with experimental results, represents the main tool used for the iterative optimization process.

The outputs of the whole procedure are two new impeller versions: Model 8 presents a rise of efficiency of almost 4,5% on all the useful range and has a two dimensional geometry of the blades that is easy and cheap to manufacture. Model 10 attains an efficiency increase of around 7% in the same range but the blades are three dimensional and more expensive to produce.

The relevance of the results, for the company purposes, is proven by their decision of proceeding with the experimental test of the new model; this will be the last step before the commercialization of the product.

Key words: Pump; optimization; efficiency; experimental investigation; CFD; literature models.

Chapter 1: The context and the optimization problem

1.1 Radial pumps: the machine and the system

Radial pumps are dynamic machines in which work is exchanged between an external source of energy (i.e. engine) and the liquid that flows inside the fixed and mobile channels of the machine. Being dynamic, the energy that the liquid acquires is proportional to the square of the speed of rotation. The flow acquires energy in the form of pressure, position and kinetic energy.

Pumps are hydraulic machines that operate with a fluid that can, with good approximation, be considered incompressible, meaning that its specific speed does not change with pressure. The aim of a pump is to transfer energy to the liquid that is inside a system composed by the connection pipes, the tanks and the pump itself [12].

1.1.1 Industrial relevance of pumps

“The rising of water has been one of the man’s earliest need, and indeed, the first call for ingenuity for providing power arose from pumping duties. To this extent it may be suggested that the art of pumping is older than the art of power production.” [1]

Since the beginning of this duty, the evolution of human technique permitted new and better applications, when the stream turbines and electrical engines were finally invented, these opened the possibility of constructing fast spinning centrifugal machines that replaced the older volumetric machines in the middle flow rate applications. These are now the machines of the greater interest.

Radial pumps are one of the most important components in lots of industrial systems; they are generally the most important component whose failure means catastrophic consequences. They also represent an important segment of the market other than an important cause of energy consumption (beware: is not the pump itself that consume the energy but the system does!) whose use must be conscious and aim to minimize unnecessary energy losses.

The fields of applications are almost endless: from the transport of valuable water to the house applications, from the power production plant to the transmission of power, from the transport of solids in the food industry to the civil works of dredging, from the recirculation of flow to the storage of energy. In all of these situations the pump is only part of a more complex system usually characterized by a strong economical relevance.

The quantity of energy transferred by these pumps is often important due to high number of functioning hours or to the big dimensions of the machine. Since a fraction of the energy that is transformed in this component is lost, the total energy losses can sometimes be very relevant and even a small increase in the efficiency can contribute to save valuable energy.

For these reasons, the stress on the efficiency of pumps, along with the reduction of energy required by the system (that is not subject of the present work), has acquired an economical importance as well as environmental.

1.1.2 Working point

From the definition of eulerian work [13], that is proportional to the head produced, we can simplify the formula for the conditions of incompressible liquid and axial incoming flow. The resulting formula is:

$$H = \frac{1}{g} * u_2 * (u_2 - C_{m2} * \cot g \beta_2)$$

The meridian component of the outlet speed is proportional to the flow rate and this means that the value of head can change creating the so called characteristic curve. This is the theoretical curve of head in the ideal absence of losses, when these are considered, the value is reduced. The losses due to the friction and shock are considered to be proportional to the square of the flow rate but the second has a minimum in the design point.

When the real curve is measured, the result shows also the effect of real phenomena such as the recirculation or the flow separation.

Till now the curve that characterizes the behavior of the pump is defined, but also the system has a characteristic resistant curve, this is the energy required to have a certain flow rate inside the pipes of the installation. Of course, when the pump and the system are coupled, the equilibrium point is the one in which the two curves meet each other: there the value of energy necessary is equal to that provided. The curve of the system can be calculated knowing the losses along the pipes, the pressure in the two tanks and their relative geodetic height. A system with high geodetic jump and low hydraulic losses will result in a high and flat curve, while a system with low geodetic jump and high hydraulic losses will have a low but very steep curve. Increasing the losses (by means of a throttling valve) the curve of the system can be made more steep, in this way the working point shifts to lower flow rate giving the possibility of regulation. This is shown in figure 1 where the reduction in flow rate (from Q1 to Q2) is attained or by changing the rotational speed (obtaining H2a with the speed n2) of the machine or by closing the regulation valve (obtaining H2b) and increasing the losses.

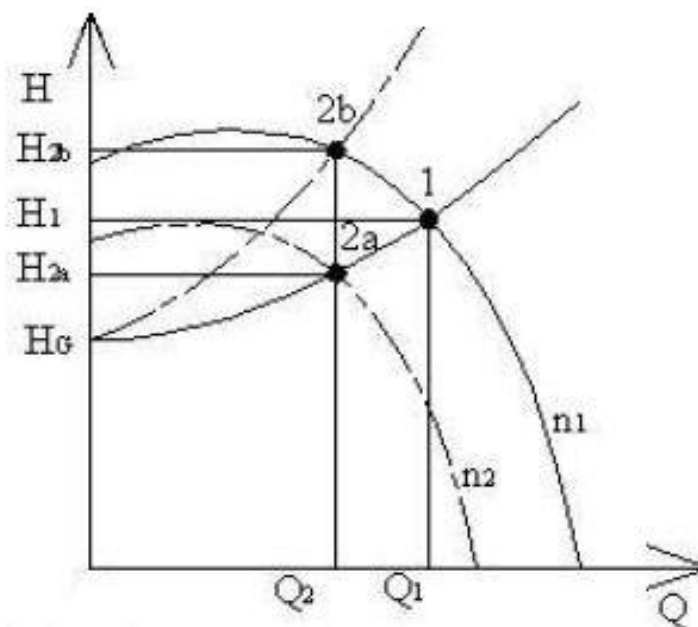


Figure 1: Two possible ways of regulating the flow rate.

1.1.3 Specific speed and efficiency

Not only the characteristic of head changes with the flow rate but also do the power consumption and the efficiency. For the last two terms we will use the following definitions:

$$P_u = g * \rho * H * Q$$

$$\eta = \frac{P_u}{P} = \frac{g * \rho * H * Q}{P}$$

Where “P” can assume different meanings according to which control volume we are considering; the name of the efficiency changes as a consequence.

As a general example, in figure 2 are plotted the characteristics against the flow rate; also the system curve is shown (H_A). At a certain point the efficiency reaches its maximum, that is the best efficiency point (shortened as “BEP”) and is the condition the machine is designed for. That point is characterized by the value of H_{BEP}, P_{BEP}, Q_{BEP}, η_{BEP}.

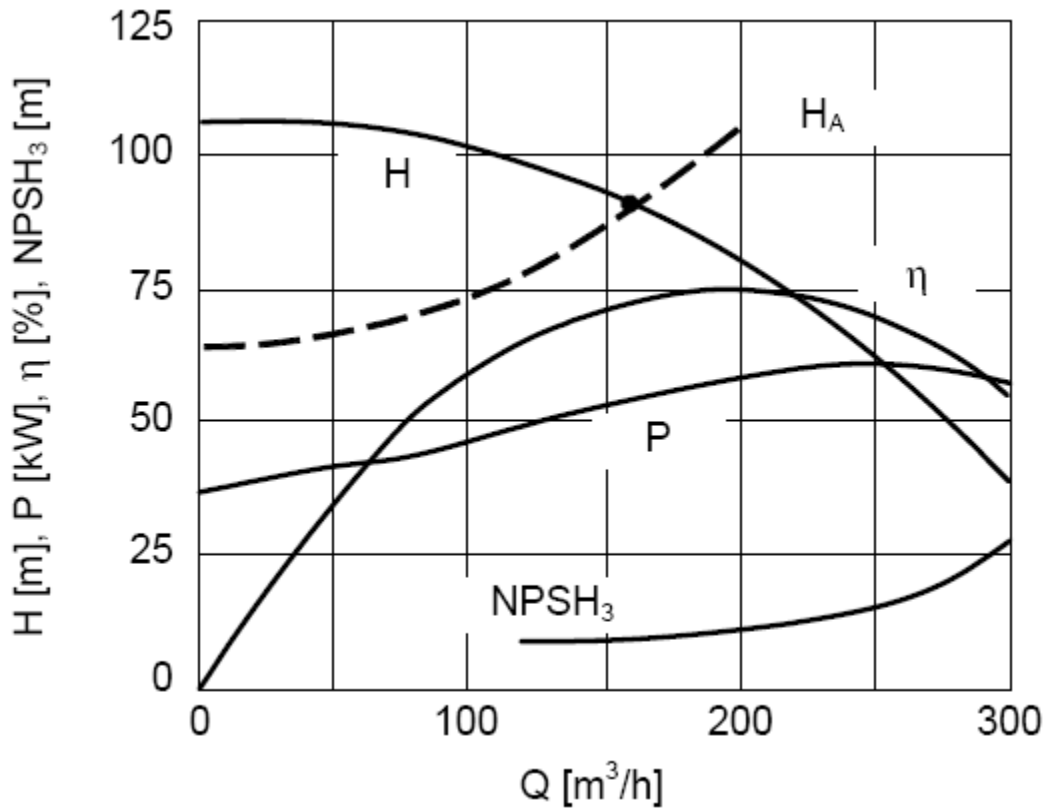


Figure 2: Generic pump characteristics.

The proprieties of different machines can be confronted and generalized by referring them to non-dimensional values: the flow coefficient (φ) and the work coefficient (ψ). They are defined as follows:

$$\varphi = \frac{Q}{\omega * D_2^3}$$

This comes from the consideration that Q [m³/s] is proportional to the cross section times the perpendicular speed, while the section is proportional to a geometrical dimension and the speed is proportional to the tangential speed: $Q \sim A * V \sim D^2 * u \sim D^2 * \omega * D \sim \omega * D^3$.

The work coefficient is, instead, defined basing on the specific work l [J/Kg]:

$$\psi = \frac{l}{\omega^2 * D_2^2}$$

From the definition of eulerian work, applying the previous considerations, we can notice the following proportionality: $l \sim V^2 \sim u^2 \sim D^2 * \omega^2$.

It can be demonstrated that when two machines operate in conditions of similarity, then, when they have the same value of φ and ψ , the hydraulic efficiency is the same [13].

Two machines are in similarity conditions when they have:

- Equal ratio between the main geometrical dimensions (geometrical similarity).
- Equal flow conditions (fluid dynamic similarity).
- Similar velocity triangles in corresponding points of the machine (cinematic similarity).

The consequences of this law are the possibility of defining the performance of a family of turbo-machines by measuring them only on a single component, and the possibility of confronting different families of machines. For the second operation, it is necessary to colligate the previously mentioned coefficients to obtain new parameters: specific speed ω_s and specific diameter D_s .

$$\omega_s = \frac{\varphi^{0,5}}{\psi^{0,75}} = \omega * \frac{Q^{0,5}}{l^{0,75}}$$

$$D_s = \frac{\psi^{0,25}}{\varphi^{0,5}} = D_2 * \frac{l^{0,25}}{Q^{0,5}}$$

These are very useful because they are both only function of D_2 or of ω while being still non dimensional. Considering a single stadium and collecting a big amount of data, Balje developed a diagram where a statistical connection between ω_s , D_s and the maximal efficiency is present. This relation refers only to the best efficiency point of every single machine. The diagram, shown in figure 3, is of a great practical usefulness for the choice of the machine type. To explain this it is better to refer to a simpler version of the same diagram, showing only the relation between the maximum efficiency and the specific speed; see figure 4.

In general we could say that the specific speed permits the confront between impellers with a different shapes but it represents the geometry only in a rough way, the details can actually be different. The meaning of the specific speed can be easily understood considering different impellers with the same design flow rate (and therefore the same inlet geometry), if a lower head has to be obtained, the external diameter must decrease, and this makes the specific speed increase. In figure 5 can be seen the above explained relation between the specific speed and the geometry of the meridian section of the machine: as ω_s rises, the outer diameter is more and more trimmed (increasing number in the figure). In a different way it can be said that higher specific speed impellers permits higher values of flow coefficient with equal work coefficient.

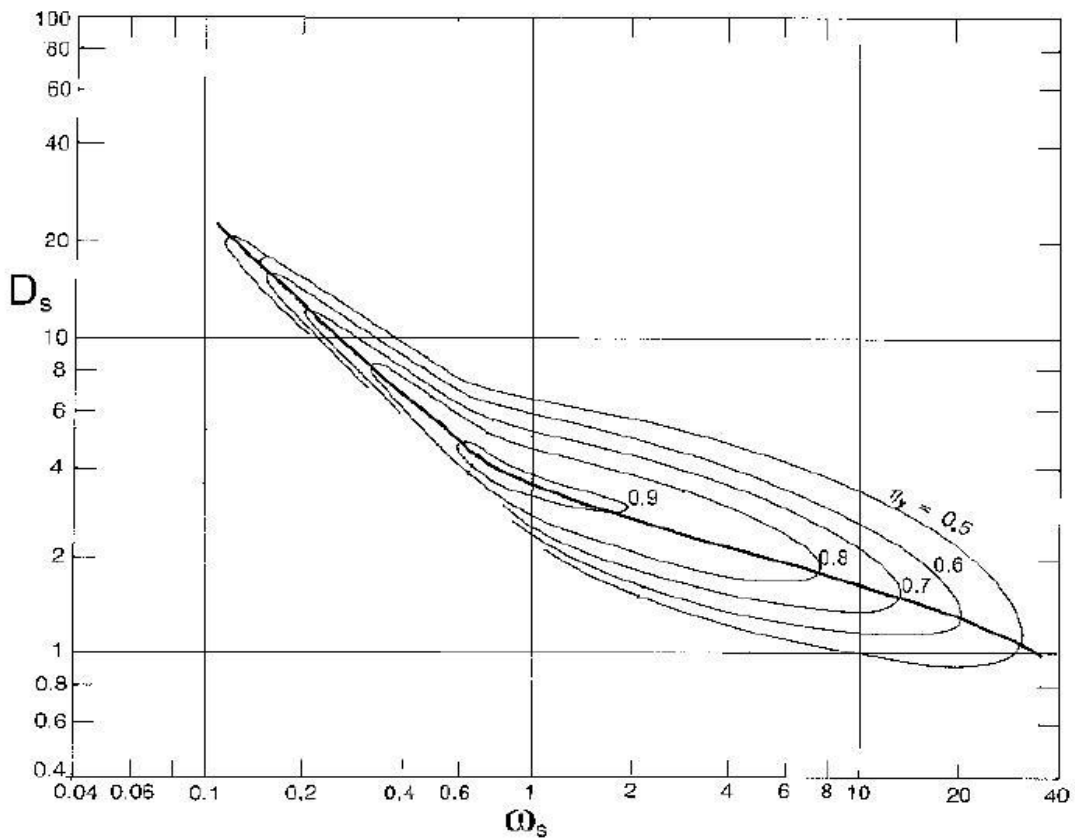


Figure 3: Balje diagram for single stadium of a pump. Elaborated from [13]

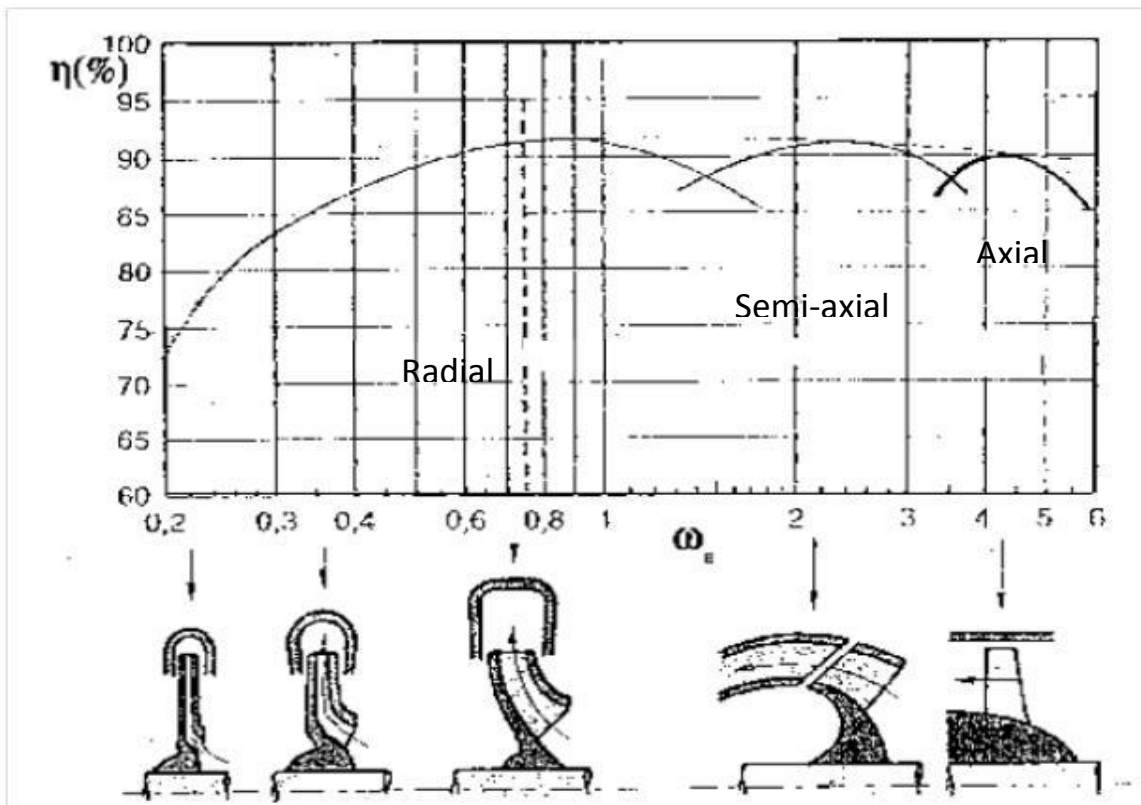


Figure 4: Balje diagram for single stadium. Some typical shapes of impellers are also shown. [12]

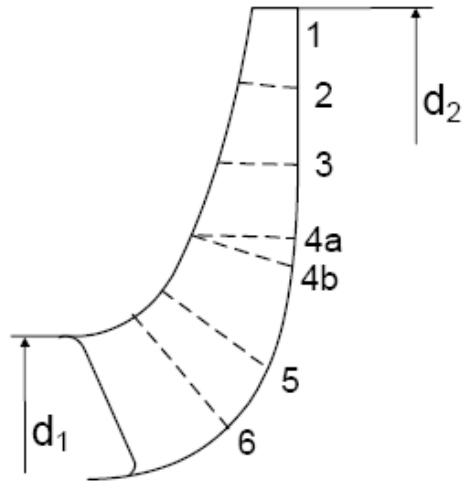


Figure 5: Relation between the impeller shape and the specific speed with constant flow rate.

In figure 4 it is possible to see the difference in the meridian outlook of different specific speed machines. As already explained, the construction of the machine becomes more and more axial when the coefficient ω_s increases. As the type of the machine changes, also do the maximum attainable efficiency because of the difference in the wet surfaces and in the external diameter. In particular, for radial machines, the increase of the diameter means a strong increase of the disk friction losses and a relevant reduction of efficiency (see chapter 3). For this reason, for very low specific speed applications, volumetric machines are preferred.

Instead of the previously mentioned ω_s coefficient, another one is more commonly used in the European industrial world:

$$n_q = n * \frac{Q_{BEP}^{0,5}}{H_{BEP}^{0,75}}$$

This is not a dimensionless parameter but, in practice, it is used in this way without explicitly writing the reference quantities. As it was for the previous expression, also this coefficient must refer to the value of head and flow rate in the best efficiency point.

By means of this coefficient we can introduce a graph (figure 6) that will have further use in this work. It comes from the experience of professor Stoffel of the University of Darmstadt and is a collection of statistical data showing the maximum practically attainable efficiency.

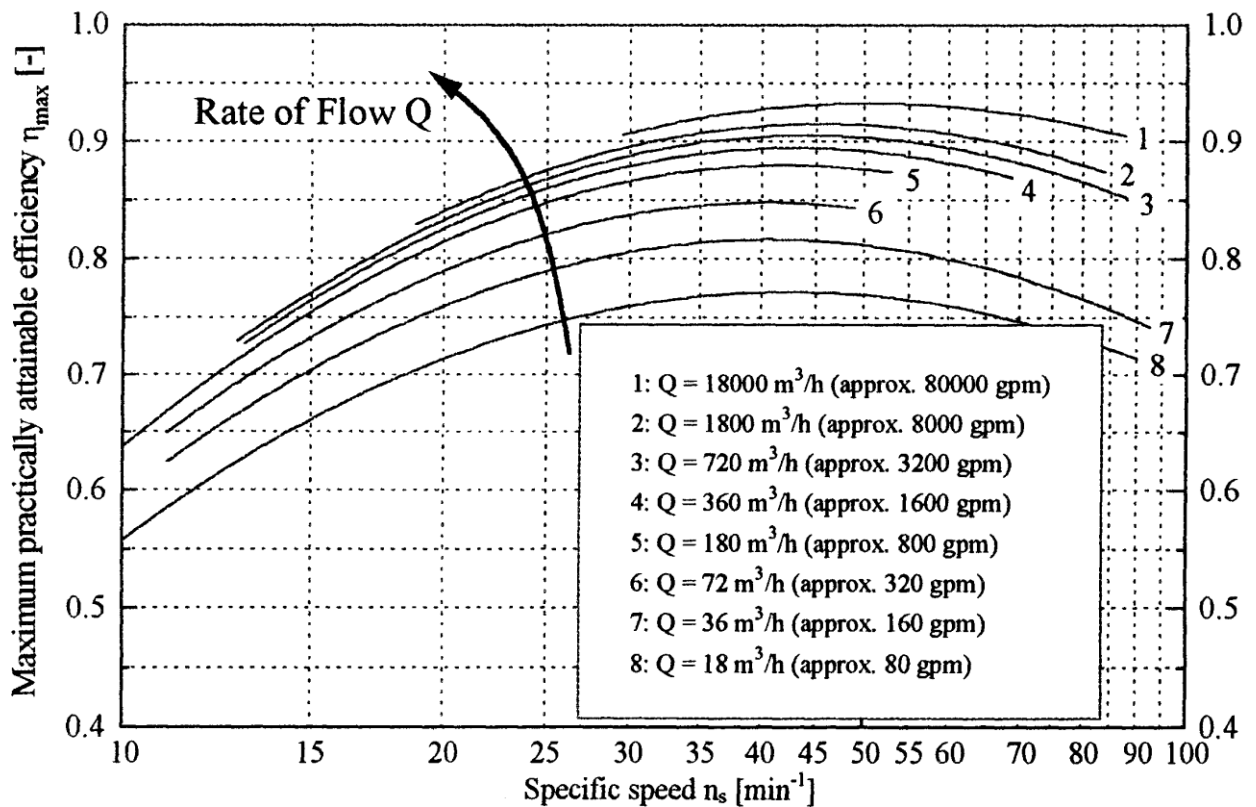


Figure 6: Maximum practically attainable efficiency with respect to specific speed and design flow rate. [14]

1.1.4 Range of applications of radial pumps

Radial machines have a typically wide range of applications: their specific speed can be in a range of n_q number from 7 up to 100. Applications for n_q numbers lower than 10 are reserved to very small impellers where the drop of efficiency is not an issue; this value is also the upper limit for the group of positive displacement pumps that can be applied for $0,5 < n_q < 10$ (see figure 7 for the application field of different type of machines).

The value of efficiency grows from a minimum of 40%, for the smallest machines of very low specific speed, up to a maximum of 92% for around $n_q=50$, after this the efficiency slowly decreases. Typical value of head are from 60 to 1000 [m] but most of the time it is lower than 250 [m]. The work coefficient has a range of $1,2 \div 0,65$ and is in inverse proportion to n_q number. [9]

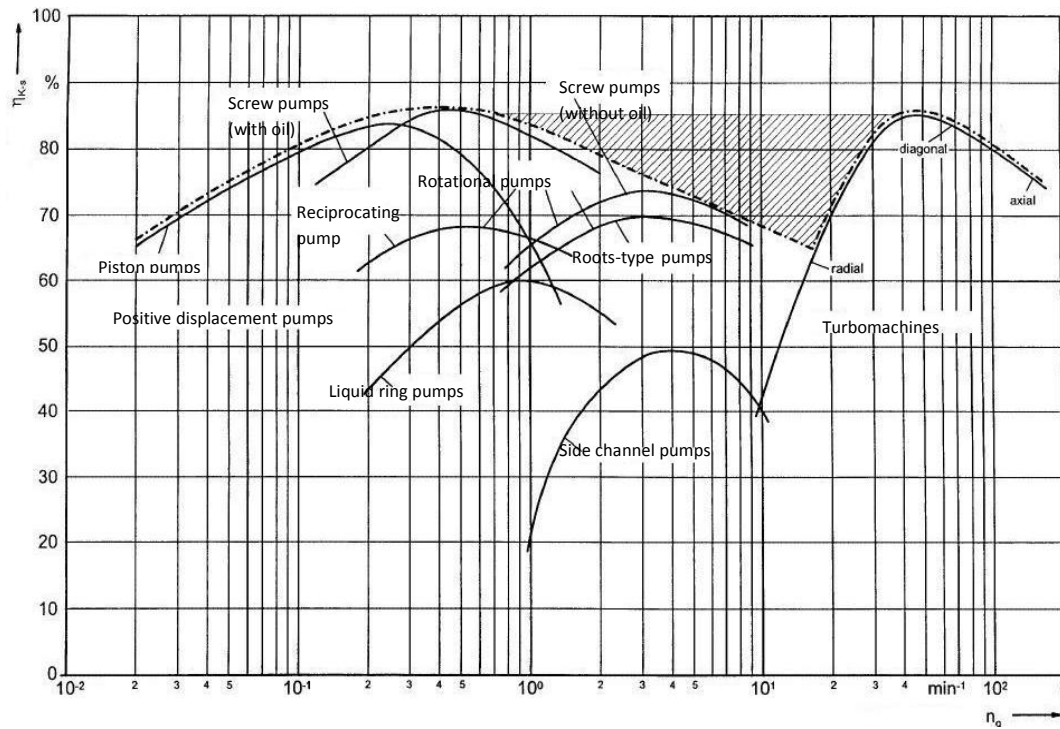


Figure 7: Field of applications for different nq number pumps. [8]

1.1.5 Terminology

A short description of a generic impeller is necessary to define the terminology that will be used in this work.

The fluid, from the admission chamber, enters the impeller and hits the leading edge (LE) of the blade, enters the blade channel where it is constrained by the front and rear (or hub) shrouds and from the suction and pressure sides of two successive blades. After leaving the trailing edge of the blade, the flow leaves the impeller and enters in the diffuser (if there is one) and then in the volute where it is collected and led to the outlet pipe. Not all of the flow that comes out of the impeller is useful: part of it goes into the side cavities that are the vanes between the rotating shrouds and the standing walls of the casing. This flow is under pressure and is pushed out of the small slits between the impeller shrouds and the casing. This kind of volumetric loss is called leakage flow and is sometimes limited through the use of mechanical seals.

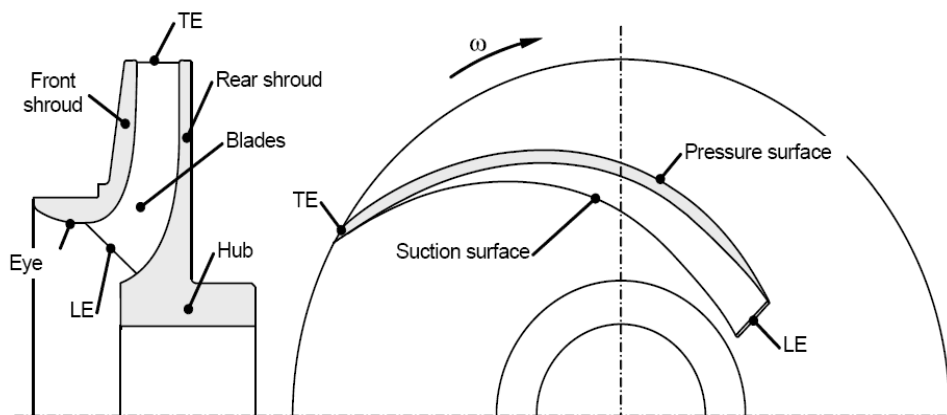


Figure 8: Meridian and planar view of a radial impeller. [9]

1.2 The optimization of a pump

Such is the importance of the pump efficiency that companies that produces or applies one, may eventually decide to switch a currently used model in favor of a better one. For a company that produces and sells a pump series, the optimization of an old model has an economical relevance as well as a marketing one. This operation can be done by an internal research and development division or by a private external studio or university department.

1.2.1 Object of the work

A German company, whose name is preferred not to mention, that produces machinery for industrial machining, produces also the internal components of these machines, one of these is a centrifugal pump. The company produces the complete series of pumps with different dimensions and characteristics, these are applied in various contests as the requirements changes. The design of the machine is pretty old and the company thinks that because of this, there must be room for an improvement of the performances. The use of modern technologies of analysis such as the computational fluid dynamic have been strongly developed in the last years, giving to the designers powerful tools to elaborate even the smaller detail. The idea of the company is that the use of modern techniques could lead to considerable enhance of the performances of their product.

The second motivation that suggested the company to put some effort in the increasing of the pump performances is the number of work-pieces sold: according to what stated by them, several thousand pump of this series are sold every year. The amount of costumers and the dimension of this market stress the importance of an accurate optimization.

A non secondary problem that the company faces is the lack of information regarding the geometry and the real characteristics of the pump. The knowledge of the pump is more or less limited to the geometrical dimensions that are required for the production; also the characteristic curves that the company provides are not totally trustworthy.

The company contacted the Institute for hydraulic fluid machinery asking for a complete investigation of the behavior of the pump, to be done by means of an experimental analysis and a numerical one. The other request is an optimization based on the acquirements of the previous step and on the numerical model that has to be developed.

The aim of the optimization work is to focus on the bigger version of the plastic impeller, the one is then supposed to be cut to create the smaller versions.

1.2.2 Description of the pump

In this paragraph will be explained with more detail the original version of the pump, its behavior, the data provided by the company and the one that we had to measure on our own.

In figure 9 it is shown a picture of the pump. The disposition is supposed to be vertical with the electrical engine on the top and the volute that hosts the impeller under the water level. The fluid enters from below in the suction nozzle and is forced in radial direction by the rotation of the blades inside the closed (shrouded) impeller, after this, it is gathered by the volute and forced into the discharge pipe, a bend changes the direction of the flow and makes it vertical.

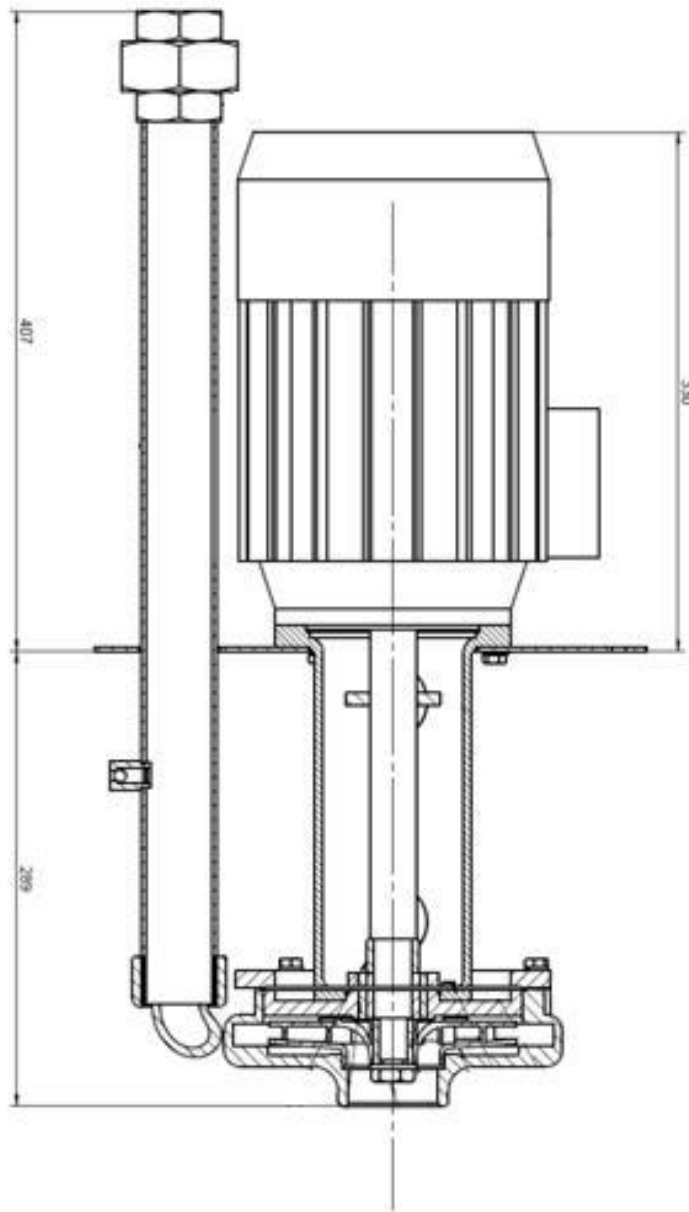


Figure 9: Sketch of the pump.

The series we are referring to, will be from now on called “FP30”. It is composed by 7 plastic (Polyoxymethylene: POM) models having all different diameters: decreasing from 155 [mm] to 110

[mm], all of them obtained from the progressive reduction of the external diameter (operation known as trimming of the impeller); the other geometrical dimensions are clearly unchanged. The same models can also be produced out of cast iron (Grey cast Iron: GG25), therefore the total number of models that compose this series is 12. To simplify the exposition, in table 10, it will be given to each product a name that reminds to the dimension of the external diameter.

Serie	External diameter [mm]	Material	Name
FP30	155	Polyoxymethylene (POM)	Plastic D155
FP30	142	Polyoxymethylene (POM)	Plastic D142
FP30	136	Polyoxymethylene (POM)	Plastic D136
FP30	128	Polyoxymethylene (POM)	Plastic D128
FP30	120	Polyoxymethylene (POM)	Plastic D120
FP30	110	Polyoxymethylene (POM)	Plastic D110
FP30	155	Grey cast Iron (GG25)	Cast iron D155
FP30	142	Grey cast Iron (GG25)	Cast iron D142
FP30	136	Grey cast Iron (GG25)	Cast iron D136
FP30	128	Grey cast Iron (GG25)	Cast iron D128
FP30	120	Grey cast Iron (GG25)	Cast iron D120
FP30	110	Grey cast Iron (GG25)	Cast iron D120

Table 10: Names of the FP30 series components.

These centrifugal pumps, according with the data sheets, are “[..] submersible pumps. They are mounted to non-pressurized containers and immerse into the medium. The flow machines are mainly used on machine tools for conveying coolants. As recirculation pumps, they transport the coolant mixture to filters. The cleaned coolant is then reused in the machines. Thanks to their sturdy and rugged construction, these pumps are extremely durable and have a long service life.” [Data sheet of the pump].

Always according to the information provided by the company, the pre-cleaned coolant mixture is water and the biggest grain size are guaranteed to be always lower than 3 [mm]. Considering this, the company and the department agreed to treat the pump as if it was designed only for water.

The working range of this machine series is up to 7 [l/s] and the head is up to 32 [m]. The range is related to the work that the machine has to do, the presence of a high load of the system, causes the load curve to be very step and the working point to be placed at low flow rate. According to their experience, the most statistically common flow rate is of 4 [l/s]. This value must be kept in mind when it comes to the optimization step.

In figure 11 it is reported the data sheet furnished by the company, it refers both to the plastic and to the cast iron impellers. The trust in this data is limited and, for example, is unlikely that the two versions of the pump have the same characteristics. For this reason one of the tasks is to validate these commercial characteristic curves through the test of more different pumps.

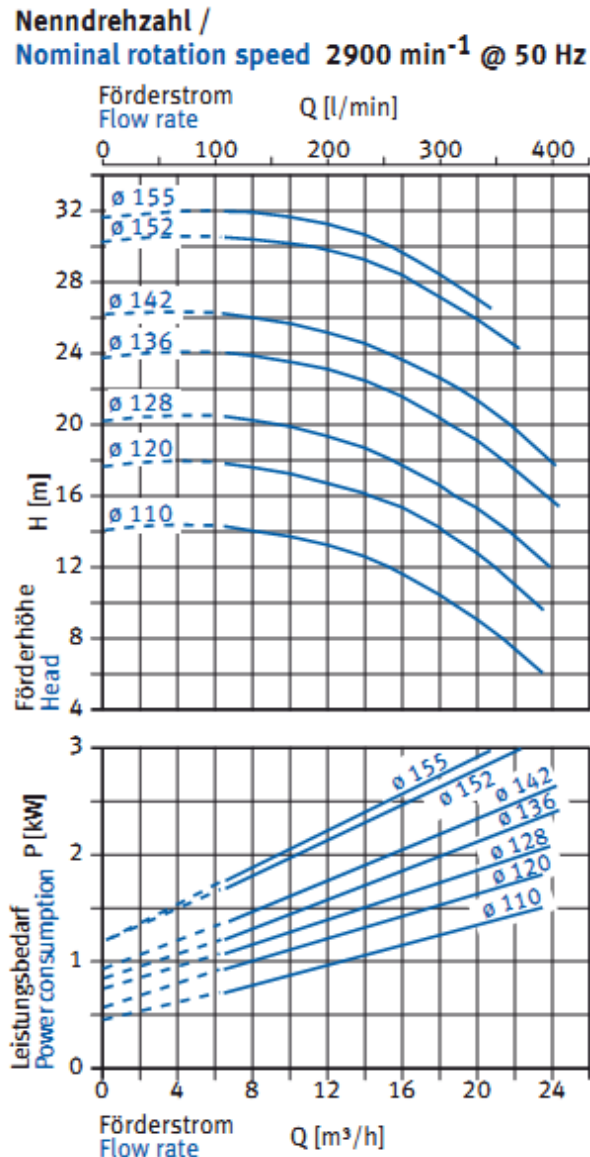


Figure 11: Characteristics curves of head and power consumption furnished by the company.

Other data that are disposed by the company are the drawings of the volute. The drawing of the impeller was, instead, for unknown reasons, not available.

The knowledge that the company has about their product ends here, for the subsequent development of a numerical model, it is necessary to collect other geometrical measure that are jet not available.

The observation of the impeller before the tests permitted the acquisition of additional geometrical measure and some additional considerations.

To a preliminary observation some differences between different material impeller emerge: the roughness inside the channels of the cast iron impeller is definitely higher than in the other situation. Also, and it was a great surprise, the number of blades is different: 5 in the cast iron version and 7 in the plastic one. The detail of the leading edge, visible from the front side through the eye of the impeller, is different in the two versions: in the metallic version the blade stops before entering in the curved region while in the plastic one the leading edge relative to the hub shroud is slightly moved inside the eye. Because of this, in the plastic impeller, the stream lines close to the front shroud will meet the blade

edge only after the curvature is completed; the same is not true for the hub shroud stream lines.

Another difference that can be noticed is again caused by a different production method: the metallic impeller is casted in a single block, while in the plastic one the hub shroud with the blades is casted separately from the front shroud and are then welded together.

The differences between the two models are so big that a relevant distance between the measured characteristic curves is expected from the experimental tests.

In order to study the exact geometry of the plastic impeller, the front shroud was taken away by cutting the weld points exposing in this way the blades. Now it is possible to measure all the geometrical dimensions like the external and internal diameters, the radial position of the leading edges, the angles of the blade and its shape.

1.3 The optimization of a pump: procedure

The objective of the present work is to obtain an improvement in the performances of a pump produced by a German company. The amount of pieces sold per year makes the optimization paramount, while the very old design of the machine suggested to the producer that there would be some room for improvement. Along with this, it is requested, other than necessary for the subsequent steps, to validate the commercial characteristic curves by comparing them with some experimental results. Although the pump we are considering is part of a bigger family of similar machines, the only model that we will try to optimize is the bigger plastic one from which the smaller version come by mean of trimming.

To change some details it is at first important to understand well how the machine works, which are the main causes of losses and whether these can be diminished or not. In other words it is important to completely understand the functioning of the machine to know where to act and which problems to solve. This will be done by conducting an analysis from four different prospective:

- The experimental analysis produces accurate characteristics curves that are required to validate the numerical model other than to be compared with the commercial data sheet. By means of an appropriate test, also the leakage losses will be measured.

- The use of semi-empirical model known in literature will make possible to calculate the amount of losses caused by each component of the pump and most important of all, the relative ratio that occurs among them.

- The simple calculation of the velocity triangles along with the use of some empirical relations (i.e. slip factor and others) is used to provide a good first try in the optimization process. Moreover the distance, for certain geometric dimensions, between the suggested value and the real one could imply the presence of some problems.

- The numerical analysis is done by means of a Computational Fluid Dynamic method and allows taking a look into the flow inside the pump.

All of the considerations summoned from these four different approaches are then confronted to produce a unified view on the physical phenomena that occur inside the impeller. The real optimization will start from these theoretical bases and will exploit the CFD model to start an iterative try and error process.

The expected result of the work is the increase of the efficiency, especially in the working point where it is supposed to operate for most of the time. The big quantity of pieces sold makes even the smallest increase of efficiency welcome for the company, but some kind of considerations about the simplicity of production will have to be done.

To give a first simple idea of the maximum theoretical increase of efficiency that is attainable, we have to anticipate the results of the experimental analysis (Chapter 2): the maximum efficiency is of 58% and it is placed at a flow rate of 5,5 [l/s] where the head has a value of 29 [m], in these conditions the nq number has a value of 17,3. Inserting this coefficient into the graph of figure 6 we get a maximum practically attainable efficiency of 67%. The maximum increase that we may be able to obtain is 9 percentage points.

Chapter 2: Experimental part.

2.1 Introduction

Because of the complex flow phenomena in centrifugal pumps, the design of pump components and their analysis is frequently based on empirical data gained from experimental data. [9].

The experimental investigation has many purposes: it is the fundamental instrument to understand the real behavior of the machine in an operation-like environment, it allows us to determine some kind of losses, it is necessary for the validation of a CFD model.

In this case the main idea was to define the real characteristic curves since they are necessary for successive steps. The company that manufactures the impeller pump, disposes of some curves for obvious marketing reasons but their trust is limited so they asked the Hydraulic fluid machinery department to conduct some experiments before advancing with the optimization of the pump design. Beside this, the use of a non reliable comparison term could lead to a complete wrong evaluation of a further CFD calculation and, as a result, to an incorrect optimization.

Other aims of the investigation are to determine the differences between different work pieces to understand the effects of the production system; moreover, the same model could be produced in a different material (cast iron version) and with a different method, this requires the investigation of differences between the plastic and cast iron versions.

To cap it all, the original model could be cut to reduce the external diameter and to create different variants that have different head characteristics; this variants have to be analyzed as well.

A test rig has been designed to simulate the normal operating conditions and to provide room for the measuring devices. It essentially consists of pipes that conduct the flow from the pump to a regulation valve to the same water tank where the pump is located in. In this way the energy transferred from the pump to the water is then dissipated on the valve.

All the measuring procedure, measuring devices and the test-rig itself must undergo to the rules established by the British Standard guide lines ISO 9906 relative to rotodynamic pumps [6]. This guide lines are not to be considered as an acceptance test code but as a guide for measurements of high accuracy.

2.2 The test rig

The test rig has to meet different requirements: it has to recreate the working condition of the pump, it has to provide the place for the presence of the measurement devices, has to be designed according to the instruction provided by the ISO guide lines for obtaining high measurement accuracy.

The pump operates under the level of non pressurized water (submersible pump) in a depth up to 28 [cm], in accordance to what stated by the company, for reducing the costs and complexity of the plant. For reproducing this working condition, the pump was installed in a way that the whole impeller and the casing are completely covered by at least 10 cm of water. In this way an eventual reduction of the water level (see leakage measure) does not affect the way the pump operates.

According to the ISO standards and in agreement with the company, the fluid used in course of the experiments is water. In the real conditions the pump can operate in different context but always with the requirement of filtered liquid, in this way the maximum size of the particles that can be found must be up to $d=3$ mm.

The tank that holds the water is a cube of around 1,5 m high, width and length. It has two holes on the top, in the first is placed the pump while the second lodges the pipe that comes from the pressure side of the pump. The quantity of water hosted by the tank is big enough to make negligible possible fluctuation of the surface related with losses of fluid, in this way the loss that could causes an alteration of the behavior of the pump is hardly attained.

A basic sketch of the used test-rig is shown with fig.12. The circuit dimensions are related to certain specific goals like the distance between the pump and the outlet of the tube that is of 1 m to put a minimum of distance between the entering streams and the outgoing. In this way the interaction between the two is minimized.

Another distance that is of a high importance is the one between the pump and the flow rate measurement device that is of approximately 80 cm to achieve uniform flow conditions for the measurement.

After the flow rate measurements, the pipe has two bends that lead to the valve and to the tank again; in this part the uniformity of flow does not matter.

The internal diameter of the pipe is of 5 cm and is the same value of the pipe coming out of the pump volute. This dimension affects the kinetic energy of the fluid at the measuring point.

In the figure 12 it is possible to see a sketch of the test rig showing its components:

- 1) Control valve
- 2) Pump
- 3) Speed measuring device
- 4) Torque measuring flange
- 5) Pipe line
- 6) Water tank
- 7) Inductive flow meter
- 8) Pressure transducer
- 9) Electrical engine

the measuring devices will be discussed in the next chapter.

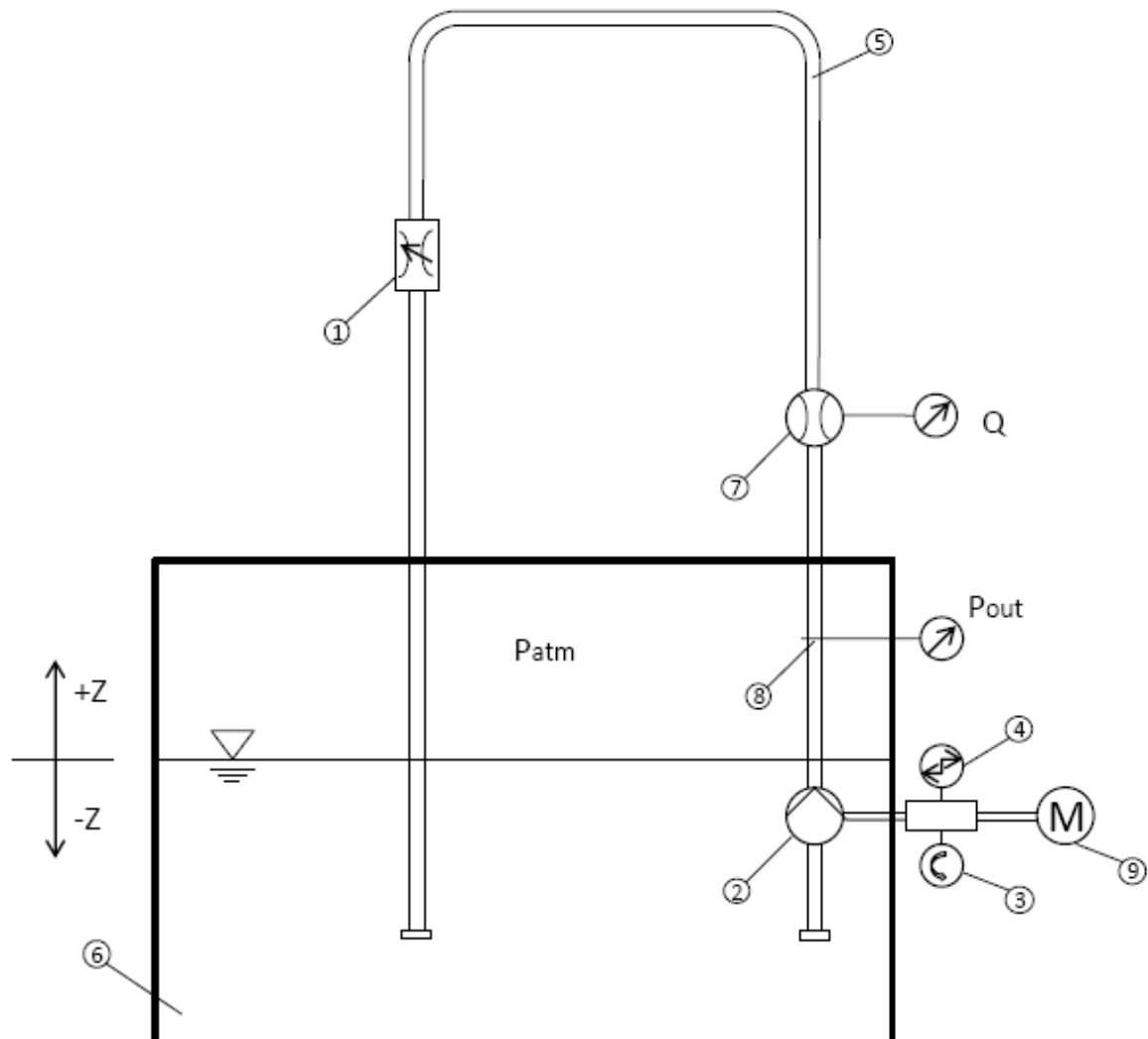


Figure 12: Sketch of the test-rig.

The pump is activated by an electrical engine similar to the one that is actually proposed by the company. The engine has the following characteristics:

Manufacturer = Knoll

Model: D-88348

Serial No.: 909884

Maximum power = 3 KW

Frequency = 50 Hz

Rated efficiency =85%

The power for the engine comes from an electrical inverter that takes the electricity from the grid and allows us to regulate the amount that is transmitted. By this means it is possible to regulate the speed of the motor.

The characteristics of the inverter are:

Maximum power = 5 KW

Speed = 0-4000 Hz

From the charts furnished by the company it is clear that the maximum power required from the pump D55 is higher than 3 KW when the flow rate increases above 20 m³/h. This means that this limit of the engine will prevent the pump from operating in a wider range.

For the purpose of measuring the speed and torque that are transferred by the shaft, it was necessary to split the shaft and interpose a meter. This operation means an extension of the shaft and a loss of stiffness. To overcome this is now necessary to place an additional bearing in front of the impeller. The additional bearing is placed after the torque measuring device and its friction losses are added to the energy consumed by the pump.

These friction losses must be estimated in some way and then subtracted from the measured power. By doing this the calculated efficiency will not be underestimated.

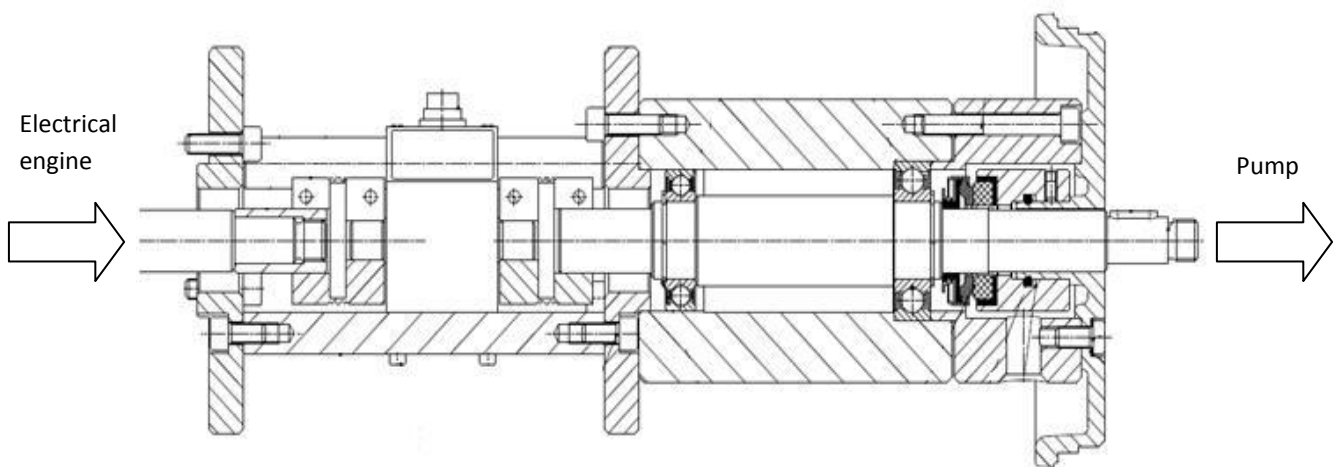


Figure 13: Detail of the shaft split to insert the torque meter.

2.3 Measuring devices

The characteristics of the pump that were investigated are: head, power consumption and efficiency; all measured in different flow rate. The characteristic pump data are defined as follows:

$$P_{mech} = M * \omega = M * 2 * \pi * n$$
$$H = \frac{P_2 - P_1}{g * \rho} + \frac{c_2^2 - c_1^2}{2 * g} + (Z_2 - Z_1)$$
$$\eta = \frac{P_{hydraulic}}{P_{tot}} = \frac{H * g * \rho * Q}{P_{mech} - P_{friction}}$$

Section 1 is the entering section of the pump and section 2 is the outlet one.

Consequently the following measuring categories have to be recorded in course of the measurements:

- Torque and speed of the shaft.
- Difference of static pressure caused by the pump.
- Section area of the pipes to calculate the speed inside it.
- Flow rate.
- Torque and speed required by the bearing alone.

Flow rate

The flow rate is measured by an inductive flow meter that applies a magnetic field to the tube, this results in a potential difference proportional to the flow velocity perpendicular to the magnetic flow lines. The potential difference is then sensed by electrodes.

This non intrusive type of flow meter, with the following characteristic, was integrated in the test-rig:

Manufacturer: BAILEY FISCHER PORTER

Model: DIM

Serial-No.: 9809x1009/A2

Nominal Diameter: ND50

Max. Flow rate: 60 m³/h

Accuracy: ± 0.5% of measured values (relative error expected in the measuring range)

current output: 4-20 mA

According to the ISO guide lines, the distance between the engine and the pump must be of at least five pipe diameters, this is a minimal length of $L = 5 * D = 5 * 0,05 [m] = 0,25 [m]$, more than three times less of the one that was used in the test-rig.

Torque

The torque transferred by the shaft is measured with a torsion dynamometer: the device is connected to the two split half of the shaft by means of two couplings and transfers the information, in an optical way, to the static counterpart. This addition extend the length of the drive train of around 30 [cm] reducing the stiffness and forcing to use an additional bearing. The cage that used to contain the shaft was split as well and was replaced, in the central part, by three columns.

The characteristic data of this device are:

Manufacturer: BHM

Model: T20WN

Serial-No.: 212117806

Nominal (rated) rotational speeds: 10000 rpm

Accuracy: $\pm 0.5\%$ of measured values

Measurement range: 0,1-200 Nm

current output: 8-10 mA



Figure 14: Torque meter.

Power

In order to calculate the efficiency it must be known the exact power transmitted by the engine and the one acquired by the flow. While the latter concerns the pressure and flow rate measure, the former is calculated using the formula:

$$P_{tot} = P_{mech} - P_{friction} = M * 2 * \pi * n - P_{friction}$$

This shows that the torque M , the speed n of the shaft and the losses of the bearing have to be measured.

Another measure concerning the power is the one of the power entering the inverter; this can be used to calculate the efficiency of the electrical engine using the formula:

$$\eta_{engine} = \frac{P_{mech}}{P_{In}}$$

Although this value is not necessary, it can be easily compared with the rated efficiency as to check that there are no big errors in the measured values.

Pressure

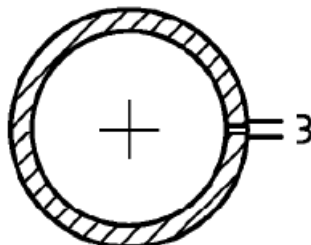


Figure 15: Sketch of a pressure tapping.

According to the ISO guide lines, the head could be calculated using the Bernoulli formula. If we refer to the figure 17, the formula must be adapted:

$$H = \frac{P_{M2'} - P_{M1'}}{g * \rho} + \frac{c_{2'}^2 - c_{1'}^2}{2 * g} + (Z_{2'} - Z_{1'}) + (Z_{M2'} - Z_{M1'}) + H_{j2} + H_{j1}$$

In our situation there are no losses H_{j1} since the pump is submerged and the entrance section does not have an upstream pipe. The local losses referred to the incoming fluid are considered part of the pump itself.

The loss H_{j2} , calculated in chapter 3, is inferior to 0,2% of the maximum head and therefore neglected. The pump is overhung and there is no upstream pipe, the area $A1$ is conventionally considered extremely big and the speed of the incoming fluid negligible. [6]

The pressure is measured using a differential pressure transmitter that measures the displacement of a membrane. It has the following characteristics:

Manufacturer: ROSEMOUNT

Model: 2090

Serial-No.: 74578187/1106

Pressure range: -20,7 / +20,7 bar

Accuracy: $\pm 0.5\%$ of measured values

Current output: 4-20 mA

Pressure is calculated across a membrane that connects two tubes filled with water. One tube comes from the section 2 while the other goes into the water, the difference of pressure measured is therefore the one between section 1 and 2. The difference of high between the two measuring points is none and the term $(Z_{2'} - Z_{1'}) + (Z_{M2'} - Z_{M1'})$ is equal to 0.

The head is therefore calculated as:

$$H = \frac{P_{M2'} - P_{M1'}}{g * \rho} + \frac{c_{2'}^2}{2 * g}$$

The connection between the tube and the pipe is made using small tapings in the wall of the pipe as showed in figure 15. Since just one tapping was used, it is not possible to mediate the values along the perimeter of the pipe section; in these conditions we are not aware of possible non uniformities of flow and for this reason the guide line suggest to refer to the lower of the two classes off accuracy: the second one. All the connecting pipes have an internal diameter of 6 [mm] and, as the guide lines proposes, are made of transparent plastic to make it possible to peer through them and check the absence of air bubbles.

Speed

The speed is measured applying some reflective stripes on the back part of the rotor of the electrical engine and an optical meter calculates the number of passages during two seconds. This system has a relative measurement error of $\pm 0,05\%$.

This device is kept under control by comparing its results with a more reliable instrument: the stroboscope.

The stroboscope is a lamp that can produce an intense pulsing light of various frequencies, when the frequency of the light is the same (or multiple) of a rotating mark, it is possible to see it standing because every time (or once every n revolutions) it is in a certain position it is lighted. The stroboscope used has a range of 0÷3000 rpm and an accuracy of $\pm 2,5$ rpm (0,08%).

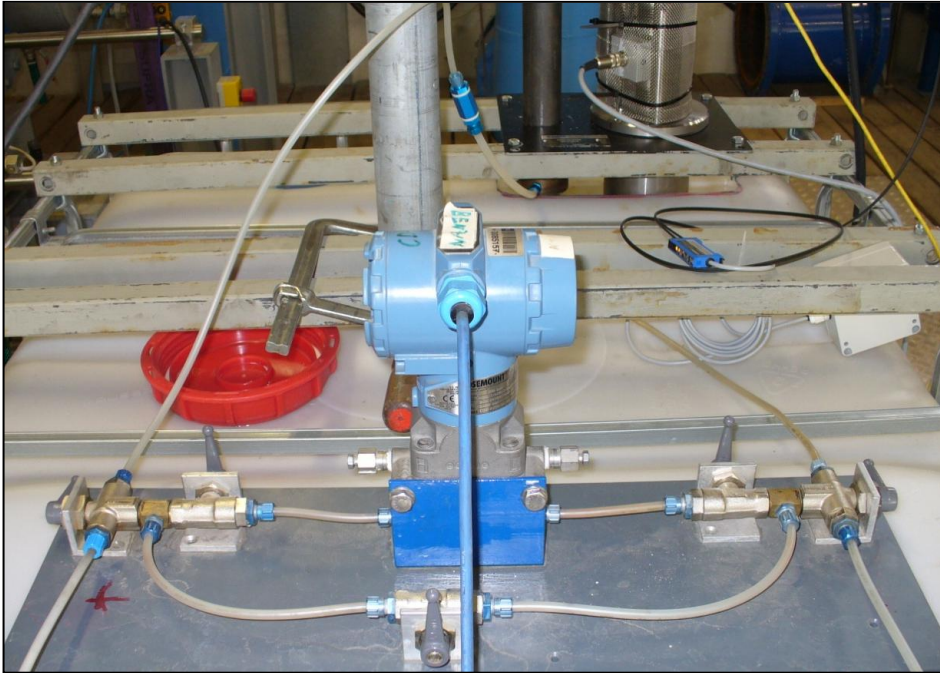


Figure 16: Picture of the pressure measurement device.

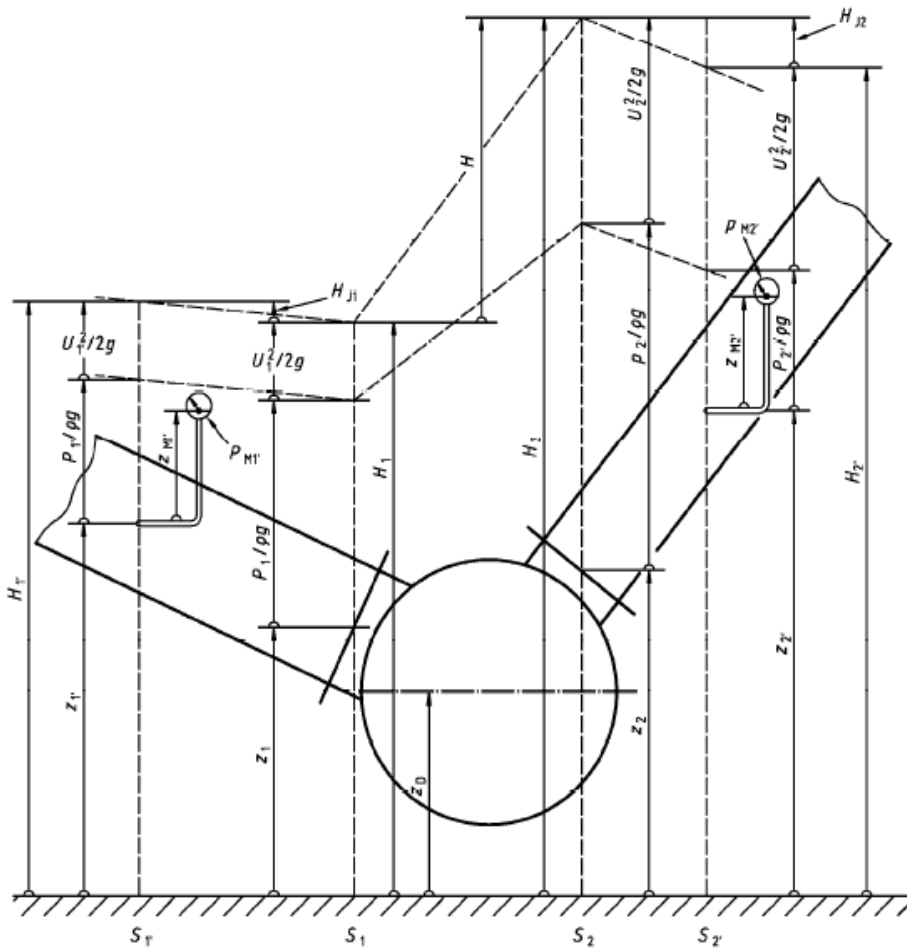


Figure 17: Sketch of the measuring sections. [6].

Acquisition of measurement data

The acquisition of the data is up to a platform called PXI (PCI extensions for Instrumentation) produced by National Instruments®. The model is NI PXI-1042. The main parts are: chassis, system controller and peripheral modulus.

The chassis is the interface between the computer and the measurement devices, the modulus regarding the functioning and the gesture of the peripheral are part of it.

The peripheral modulus is the components necessary for the treatment of the signal such as the voltmeter.

The acquisition of the voltage signals coming from the transducers is up to a voltmeter produced by National Instruments®, the model is the NI PXI-4070.

The second modulus is a multiplexer (model NI PXI-2501) whose purpose is to switch the signals coming from different measuring channels.

The acquisition sheet is the model DAQ-6052E whose role is to transfer the data to the software. The acquisition frequency is of 333 [Ks/s] (kilo samples per second). The maximum number of entrances is 10.

The whole acquisition system is run by software from National Instruments® called "Measurement & Automation".

By means of this program it is possible to control the data acquisition without actually programming a new controller program. This program interfaces with the one used for conducting the tests, that is implemented in Labview®.

2.4 Results and considerations

The test procedure is always the same: the test starts from $Q=0$ [l/s] and different samples are taken at growing values of Q up to 6 [l/s]. The increment of Q wasn't equal in different tests because the regulation valve is triggered by hand limiting the repeatability of the values. The range is limited to 6 [l/s] for two reasons: the range in which the pump will operate is much lower and there is no need of investigate the whole range; the limit on the power of the engine determines a decrease of the speed and if this drops under the 80% of the rated value the flow conditions change too much and the results of the parabolic proportionality are not any more reliable.

The resulting number of measured points is slightly different from one test to one other but is always around 30.

The sampling time accounts for 20 [s] during which 10 total samples are taken and averaged. In the end of the 20 [s] times we have just one mark.

One first tries let us to do some considerations on the fluctuations and variations that affect the measure. Fig.18 shows the first 3 measurements conducted for impeller 1 to demonstrate, as an example, that the error-bars on the head values are inside 0,3%. The same is true for the other parameters of flow rate, speed, power and efficiency. In this way we proved to be inside the ISO permissible variation range.

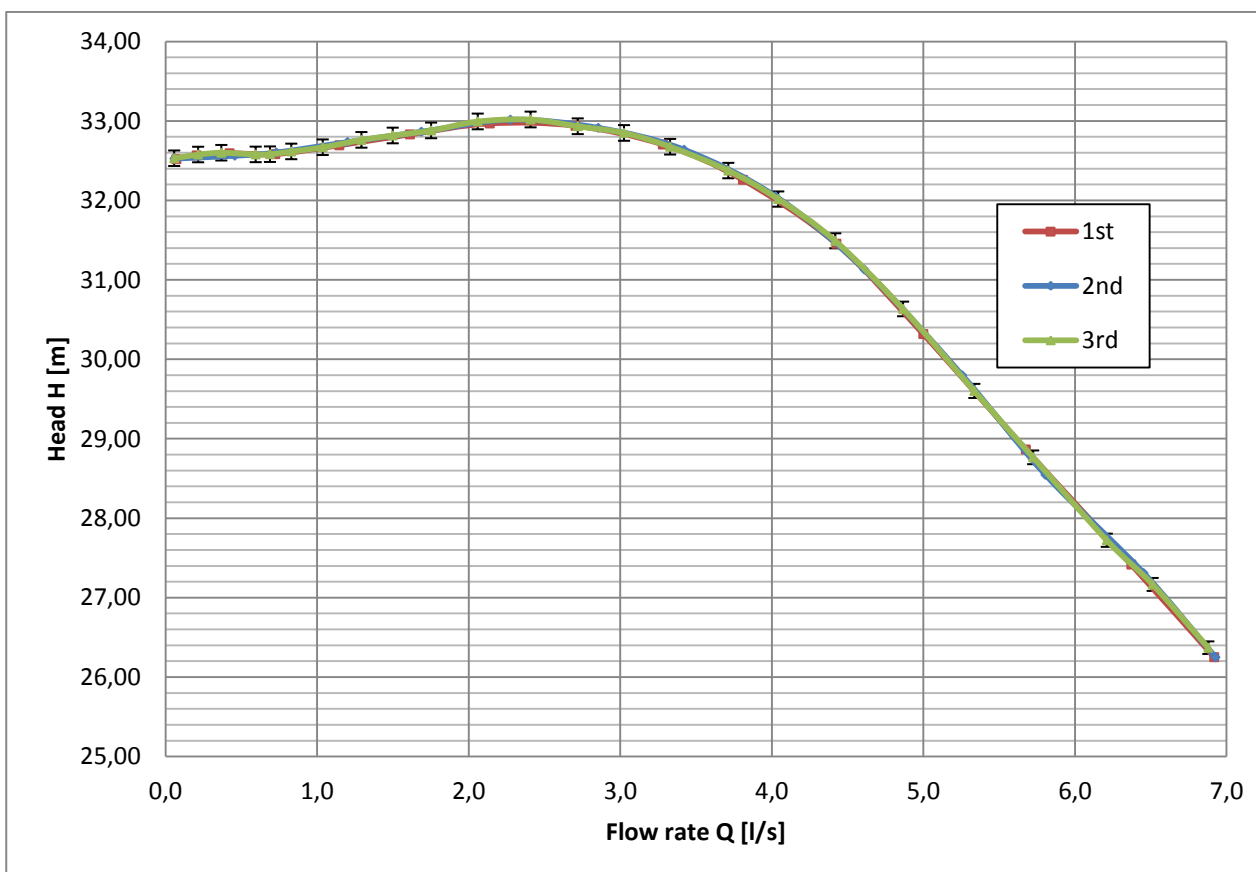


Figure 18: Head characteristics of impellers Plastic D155 number 1.

Using the formulations stated above, it is possible to refer the values H and Q measured at reduced speed to the reference speed of $n=2900$ [rpm] (see similarity parable). Once the data are collected, the values are worked out using the formulas seen in the chapter 2.3:

$$P_{mech} = M * \omega = \frac{M * 2 * \pi * n}{60}$$

$$\eta = \frac{P_{hydraulic}}{P_{tot}} = \frac{H * g * \rho}{P_{mech} - P_{friction}}$$

$$H = \frac{P_{M2'} - P_{M1'}}{g * \rho} + \frac{c_{2'}^2}{2 * g}$$

2.4.1 Bearing friction measurement

As already mentioned, it was necessary to add a bearing to the original construction and the torque measurement is now comprehensive of the friction loss due to the bearing. For calculating the efficiency in the most accurate way is therefore important to subtract the amount of energy lost in friction. This amount is measured by running the shaft without the impeller on its end; the consequence is that the torque meter only sees the bearing friction opposing the rotation. Because of the small surfaces of the shrouds, the relatively low maximum pressure and the pressure compensating back blades, there was no need of simulating the thrust of the functioning impeller.

The data are collected in the very same way as stated for the characteristic curves but with the shaft running at increasing speed from 0 to 2900 [rpm], with 100 or 200 [rpm] of distance between two consecutive measurement points.

The first measurements were done after the measurement of the first impeller, this means towards the beginning of the tests; while the second measurement were taken at the end of all the tests. The effects of the wear can be understood considering this.

Both of the times the tests have been repeated to overcome the problems of the strong variation of the points as well as fluctuation (whose effect is reduced by using a 20 [s] time sampling).

In fig. 19 the friction torque curve of the first measurement is reported. The two curves show a certain difference due to the strong variation of this kind of measurement. The useful value could be considered $M_b=0,26$ [Nm] for $n=2900$ [rpm] and will be used from now when it comes to defining the power lost on the bearing.

The formula used to define the lost power is:

$$P_{mech} = M * \omega$$

$$P_{mech} = \frac{M * 2 * \pi * n}{60}$$

$$P_{mech} = \frac{0,26 * 2 * \pi * 2900}{60} = 75 \text{ W}$$

The use of a different value could be suggested inside a range of $M_b=0,24 \div 0,28$ [Nm] but the use of a different value proved to affect only the third decimal value of efficiency and this is negligible for our purposes.

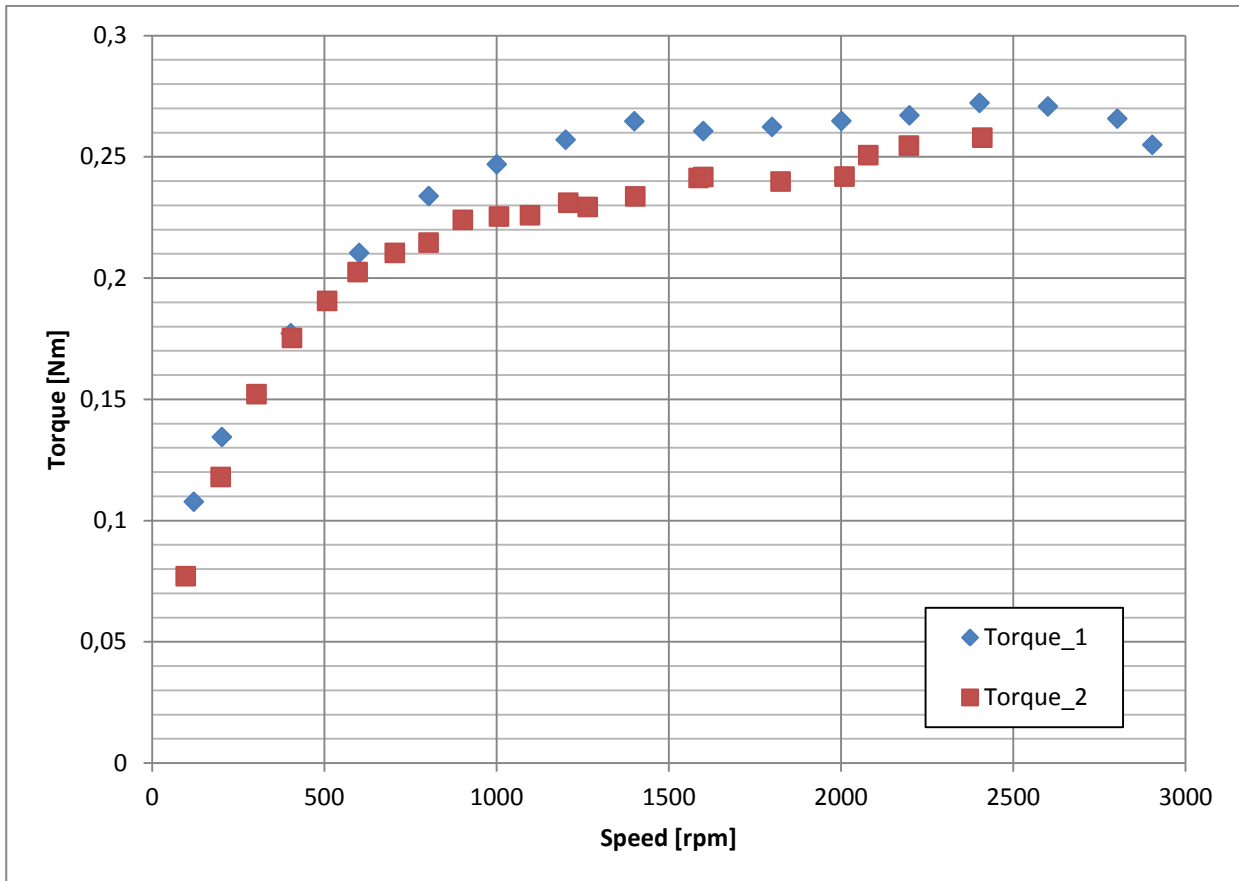


Figure 19: Friction losses on the bearing.

When all the impeller tests were finished, another measurement of the friction losses was carried on to determine possible effects of wear. Fig. 20 shows the results.

As expected, after a period that can be considered a break-in, the friction is reduced. Even if the variations between different measurements are big, it is clear that we had a general reduction of the values. The difference with the previous measure is big and, since it affects the efficiency, it is a good idea to consider this and to use a new value of friction loss of $M_b=0,22$ [Nm] (resulting in a power loss of the last measurements done on the reduced dimension diameters, as we see in the following chapter).

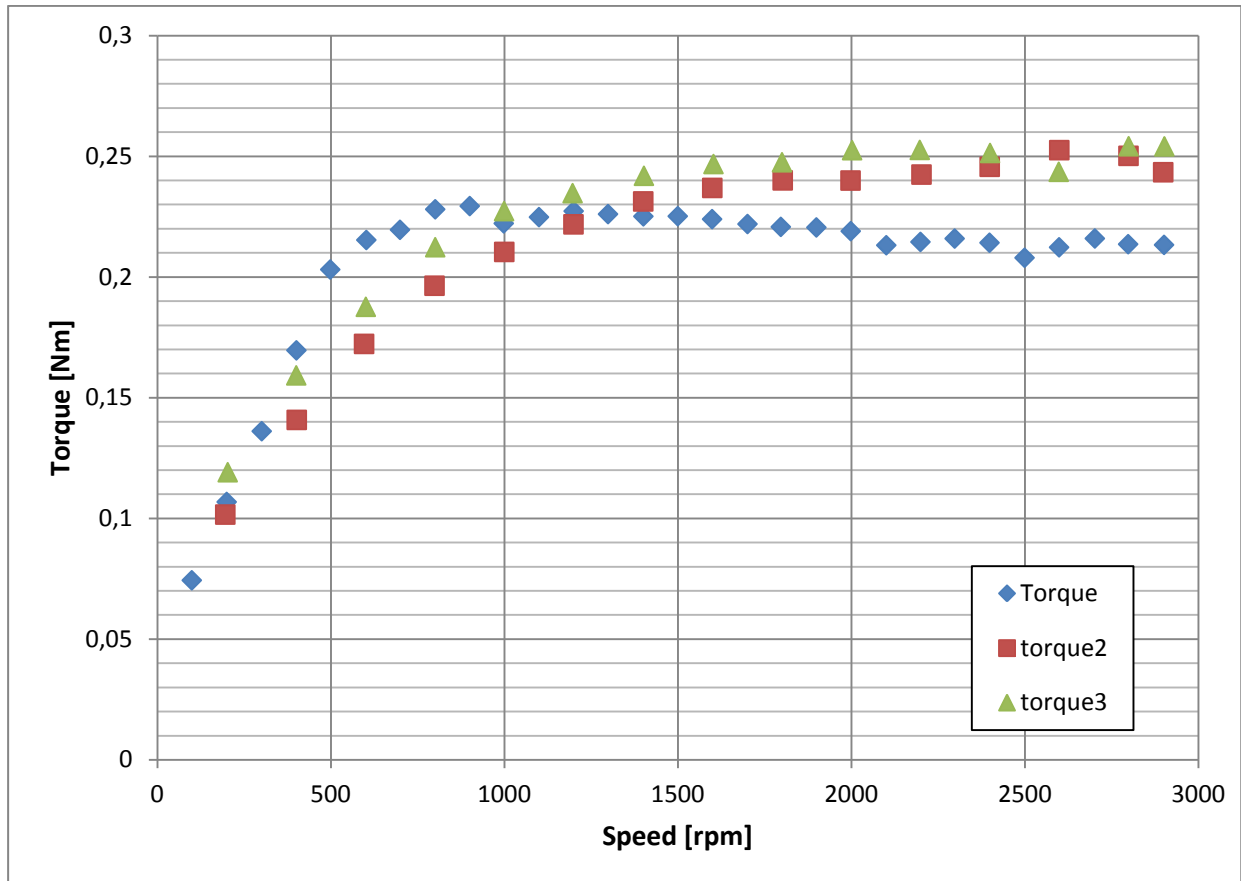


Figure 20: Friction losses on the bearing.

2.4.2 High power operating points

As already mentioned the maximum power that can be released from the electrical engine accounts for 3[KW] while the pump can require even more (when the flow rate goes over the value of around 5 [l/s]). When this happens the inverter has to adapt to meet the limit imposed by the engine, it does this by reducing the speed. If we look at the power that enters in the engine, it is even higher because of the efficiency of this component; this new value is the real limit to the power released. When a change of speed is performed, this also changes the flow condition and, when a stable point is reached, its value of head, efficiency, flow rate and power required are different from the one obtained at rated speed.

To cope with this problem we need a relation between these values and the speed so that we can end up measuring a wrong value and then adjust it for fitting the correct speed. The theory that deals with this problem comes from the use of classical non-dimensional parameters:

Outlet flow coefficient:
$$\varphi_2 = \frac{Q_2}{(\pi * b_2 * d_2 * u_2)}$$

Head coefficient:
$$\psi = \frac{2 * g * H}{u_2^2}$$

Power coefficient:
$$\lambda = \frac{2 * P}{\rho * \pi * b_2 * d_2 * u_2^3}$$

Since we are speaking about the same machine, these values and the diameter are always equal to the same value at a different speed. Therefore the relation between flow rate, head, power and speed is:

$$Q_{2b} = Q_{2a} * \frac{n_b}{n_a}$$

$$H_b = H_a * \left(\frac{n_b}{n_a}\right)^2$$

$$P_b = P_a * \left(\frac{n_b}{n_a}\right)^3$$

Where a and b are two different working conditions characterized by different rotational speed. These relations are actually suggested in the ISO 9906 as an effective mean for bringing the measured values to a reference speed.

In fig.21 we can see the effects of the measured characteristic head of one plastic impeller at various speeds and then brought to the rated value of 2900 [rpm].

The former curve is clearly steeper because the speed decreases along with the head combining the two effects in the drop of the curve. The two curves start to be different after 4 [l/s], approximately when the power required from the grid gets over the limit of 3 [KW].

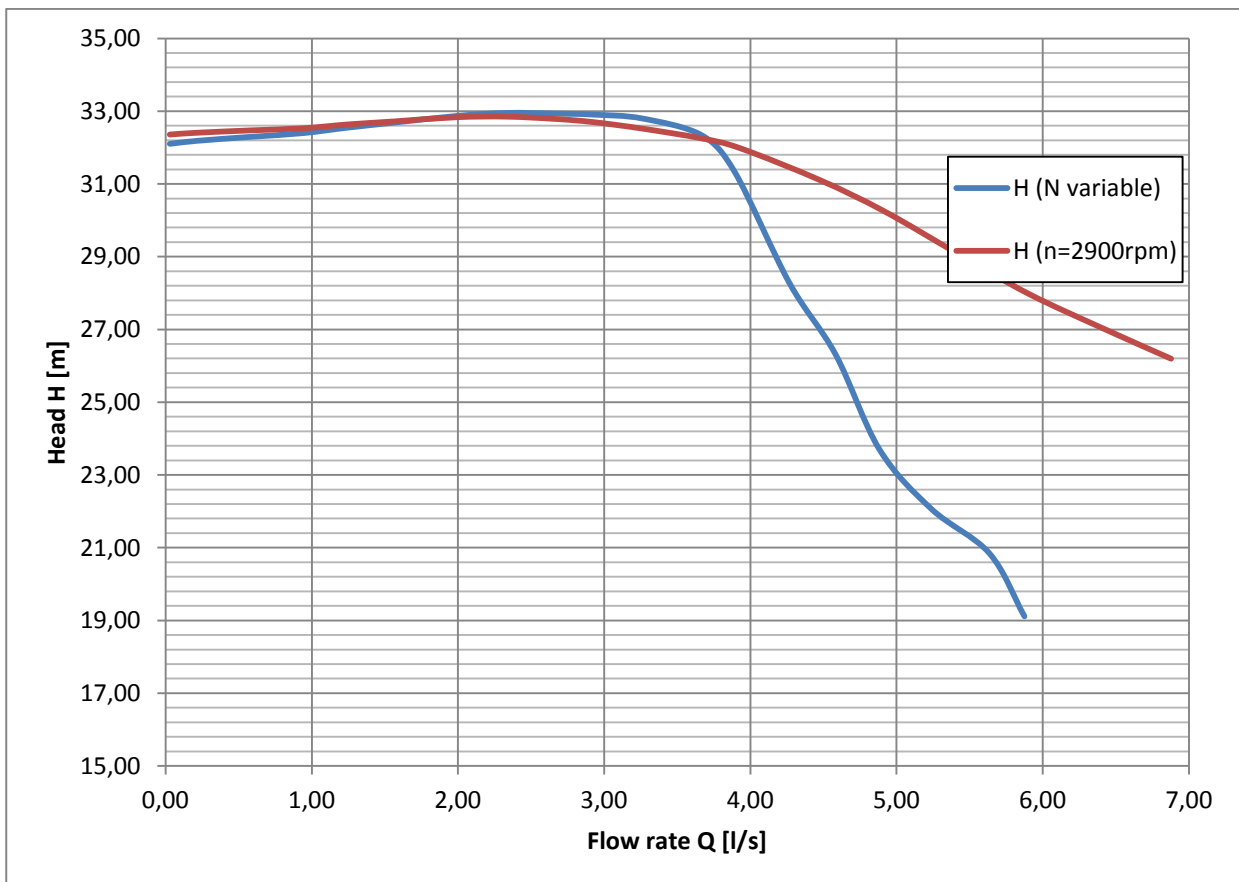


Figure 21: Effects of the rotational speed on head.

2.4.3 Behavior of the plastic impellers

The first group of measurements was conducted on three plastic impellers to determine the characteristic curves and to compare the three of them among each others to highlight the potential influence of manufacturing inaccuracies.

The impellers tested were all models Plastic D155 and were called 1, 2, and 3. The data of pressure difference, speed, torque, flow rate and friction loss are analyzed as explained in chapter 2.4 to obtain the value of head, power consumption and efficiency. Moreover the values have been reported to the rated speed of 2900 [rpm] using the similarity law.

The final result is reported in fig. 22 and 23 for what concerns the characteristic of head and efficiency.

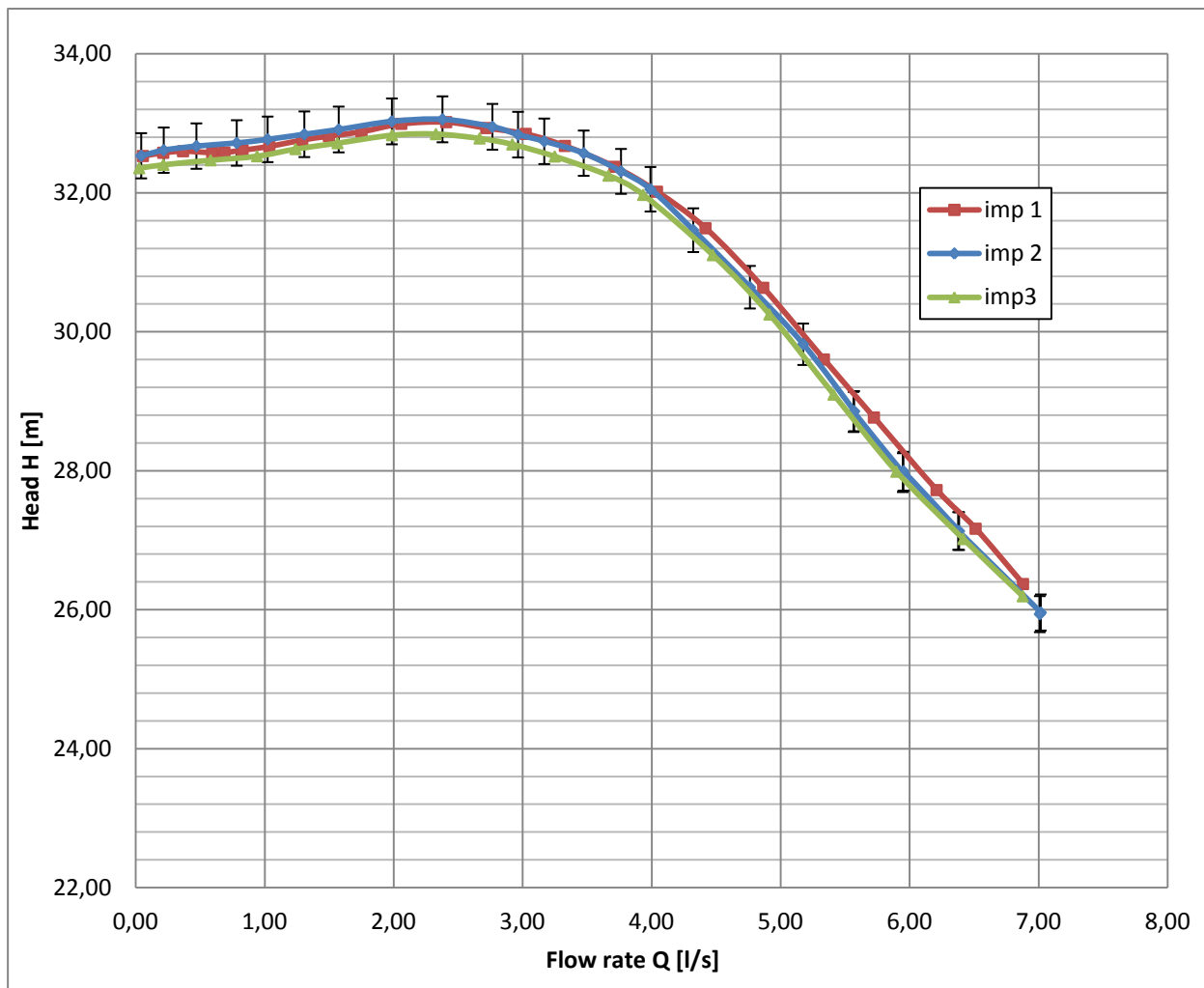


Figure 22: Head characteristic of the plastic impellers

The head behavior is quite typical for this kind of small nq-number pumps and presents the beginning of an instability phenomenon below a value of around 2 [l/s]. Anyway this does not cause problems in the operation of the pump.

The maximum value of head accounts for 33 [m] and is always over the threshold of 32 [m] till a flow rate of 4 [l/s] is reached, after that limit the head drops quite fast.

The presence of the error bars shows that the difference between one curve and the other is always inside a limit of 1,0%, or, from a different prospective, in each point the three curves are within a range of 0,4 [m].

The difference between the three curves means that the production process is affected by geometrical tolerances and tolerances of production that makes the perfect reproduction of the work-piece impossible.

The efficiency of the three impellers is shown in fig.23. From a value of zero (corresponding to $Q=0$ [l/s]) until a value of around 5 [l/s] is reached, then the curve stays more or less flat. If analyzed more closely, the value of the efficiency curves are always slightly lower at $Q=6$ [l/s] than at $Q=5,5$ [l/s]. As a consequence we consider the best efficiency point (BEP) at a value of $Q=5,5$ [l/s]. In that point the head is around 30 [m] for all the impellers and the efficiency accounts for 57%.

Error bars are present in the graph to prove that the efficiency characteristic curves are always inside a range of 2% that means $\pm 0,006$ [-]; this tolerance affects the third decimal number and is to be considered acceptable. In the present situation all the characteristic data, both for efficiency and head, can be found inside a range that is equal to the measurement uncertainty (see paragraph 2,5). This means that the differences between the curves have to be considered in relation to the measurement error rather than to production non-uniformity.

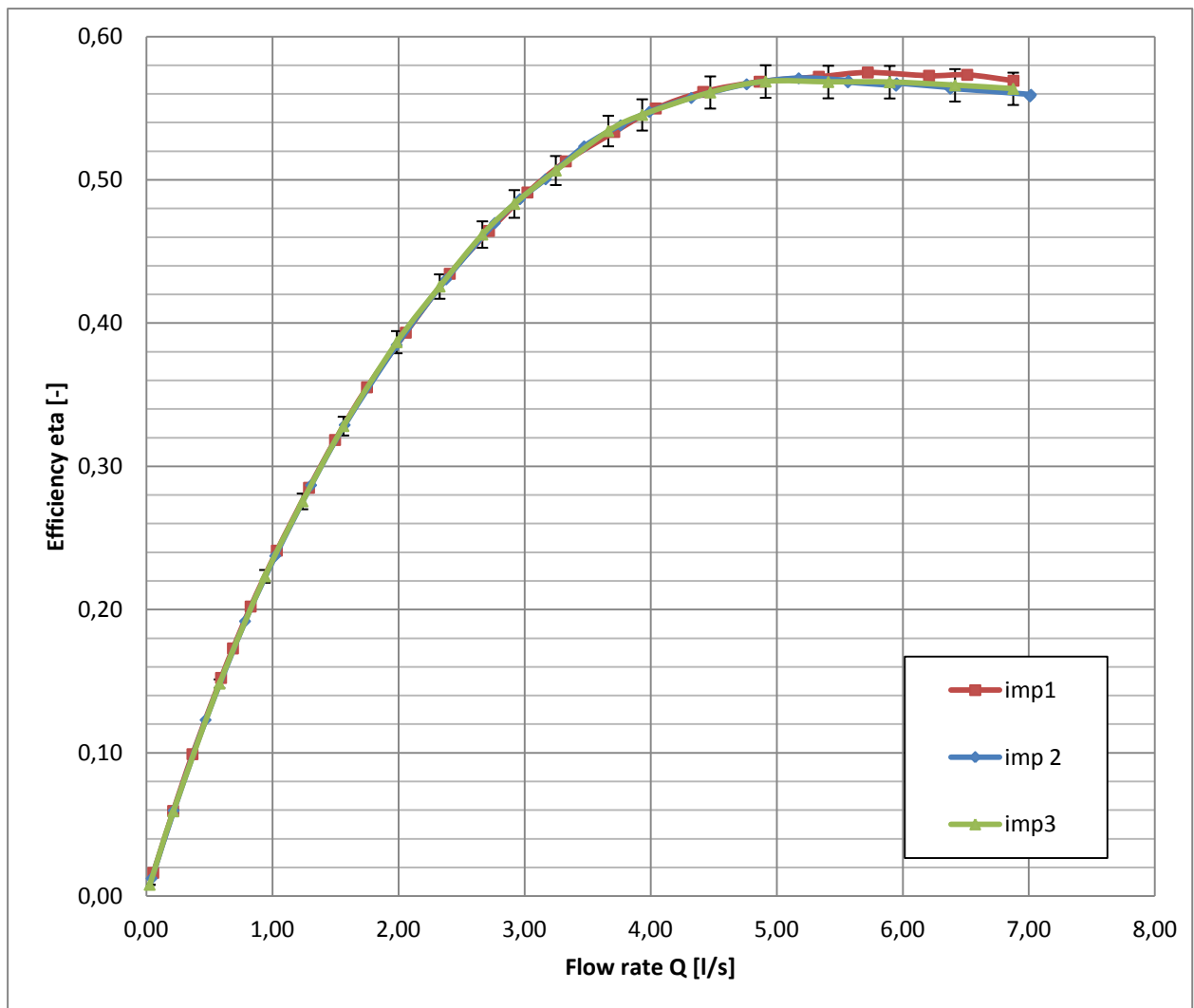


Figure 23: Efficiency characteristic of the plastic impellers.

The power consumption is presented in the picture 24 and it is compared with the (higher) value of power entering the inverter. This value was read on the display of the inverter and, due to the strong fluctuation, the measurement could be considered to have an accuracy of $\pm 0,005$ [KW]. Only the curves referred to the impeller 1 are presented to make it easier to compare them.

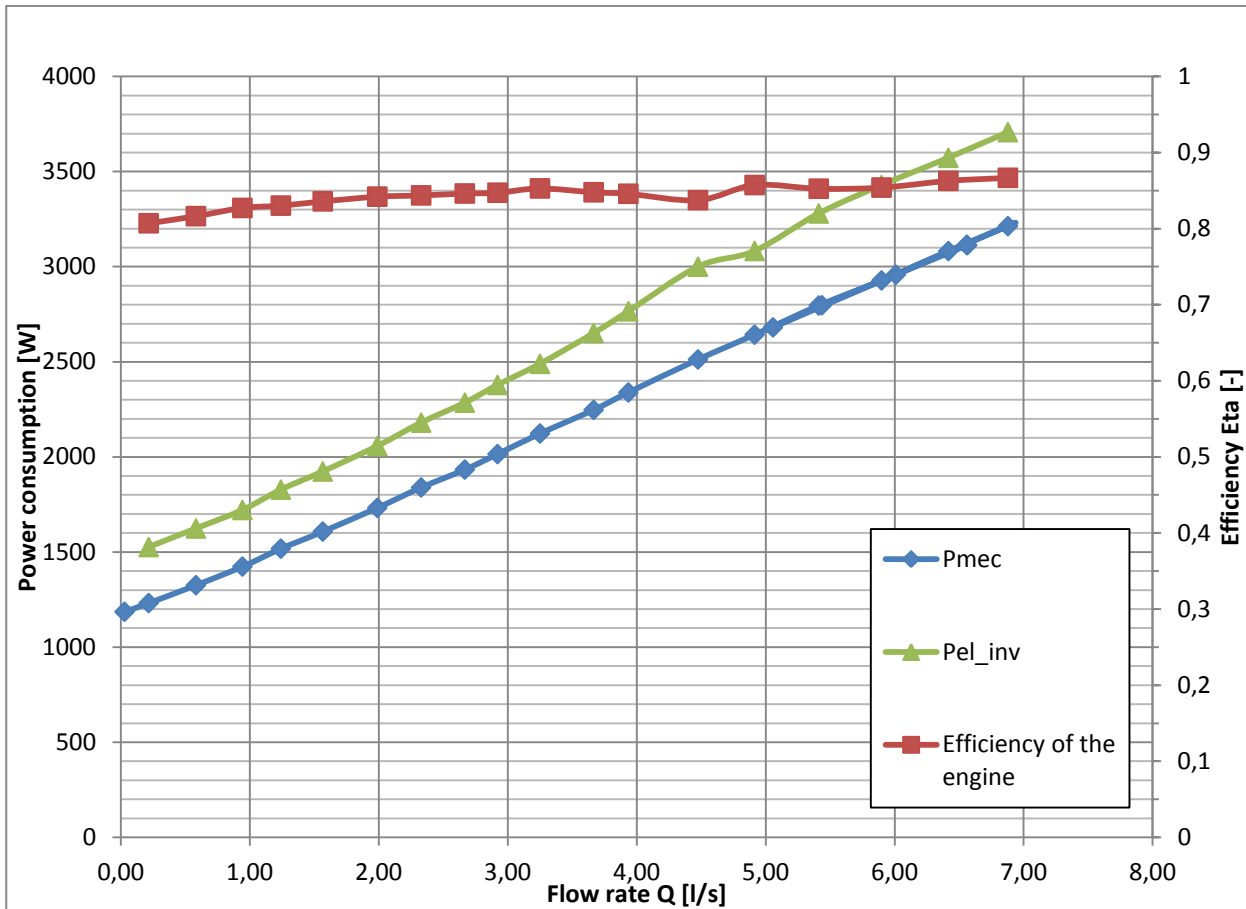


Figure 24: Power consumption of impeller 1.

The difference between the two curves is related to the efficiency of the electrical engine that converts the electricity into mechanical power. This calculated electrical efficiency is in the range of 84 ± 3 [KW], close enough to the declared value (see paragraph 2.2); this was considered a prove that the equipment was working properly. The efficiency of the electrical engine grows from 0,8 to 0,85 when the power consumption becomes close to the rated power of the engine.

2.4.4 Behavior of the cast iron impellers

The three cast iron impellers have been tested in the same way as the plastic ones. In fig.25 the characteristic curves of the impellers models Plastic D155, number 4, 5, 6 are presented compared with the number 1,2,3 (plastic) to show the differences between the two groups. The main idea is to compare two different production systems but this is made difficult by the other geometrical differences between the models: the number of blades is 5 for the cast iron versions and 7 for the plastic ones; also the detail of the leading edge is different in the two versions.

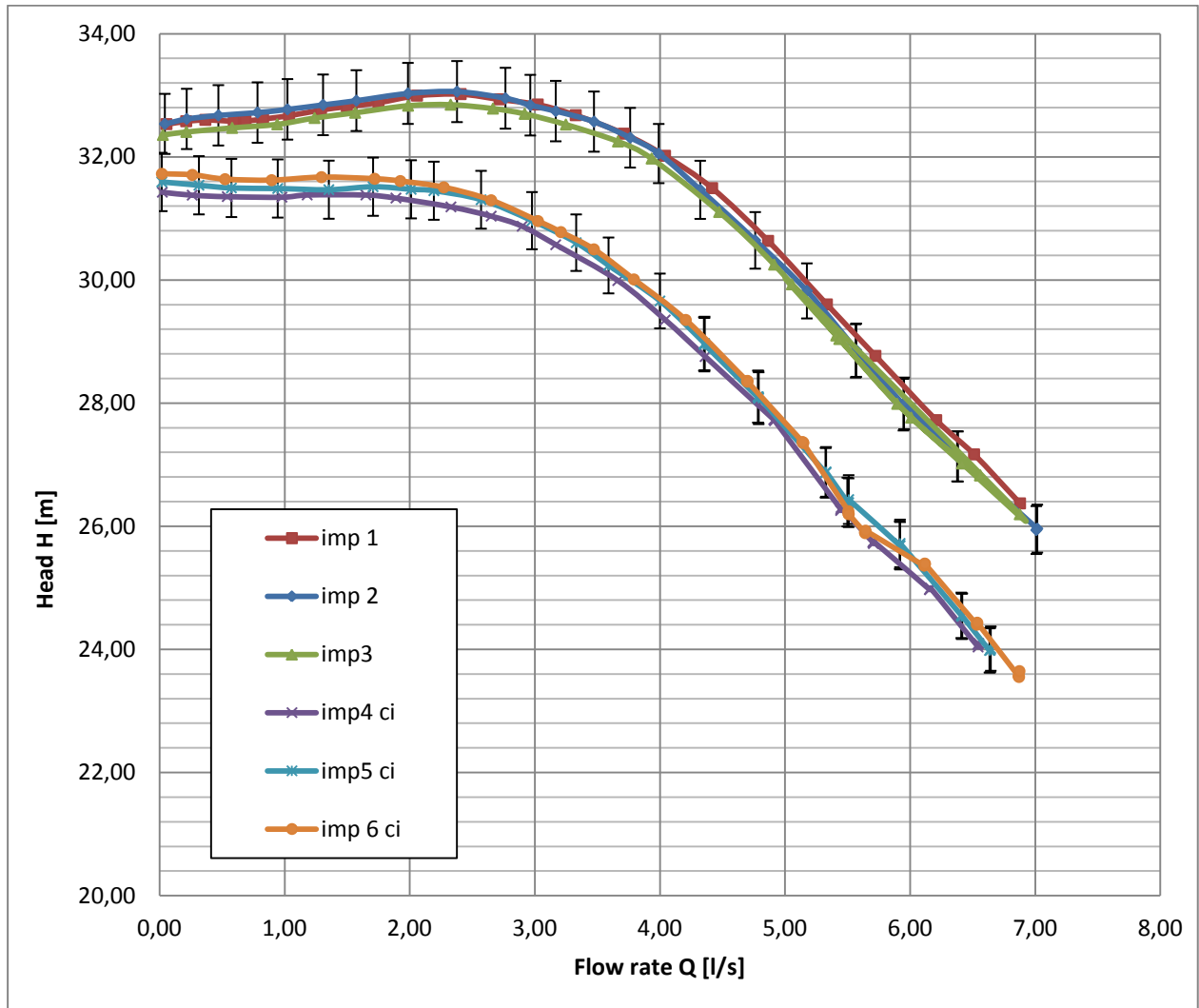


Figure 25: Head characteristic of the plastic and cast iron impellers.

As for the plastic versions, the head curves are all close together within a range of $\pm 0,2$ [m], that means a span of 1,5 %: even the process of iron casting allows a degree of repeatability that can be compared with the manufacturing of the plastic, as far as it concerns the tolerances.

The head has a maximum around the value of 31,5 [m] that means a loss of approximately 1,5 [m] with respect to the plastic impeller series. This reduction is attributed to three factors: an improved slip factor due to the use of 5 blades instead of 7, bigger hydraulic losses due to the more rough iron walls (that was not measured) and perhaps to a slightly different geometry of the blades. The shape of the curve is all in all the same as the one seen in the chapter 2.4.2.

The efficiency curves are all inside a range of 1,5% that, as for the other versions, means $\pm 0,006$ [-]. The curves are superposed to the previous ones until a flow rate of 2,5 [l/s] is reached, then they start to be lower. The maximum value is 0,55 [-]; 0,02 points lower if compared with the plastic versions. This distance is caused by three main factors: a higher surface roughness due to the different production method; the fact that the blades, unlike in the plastic project, don't enter in the eye of the impeller (not even for a small part) but remain entirely in the blade channel and, most important of all, a higher load of the blades that increases the separation. This feature of the leading edge makes the incoming stream to meet the leading edge only after the curvature where the flow is faster and less uniform.

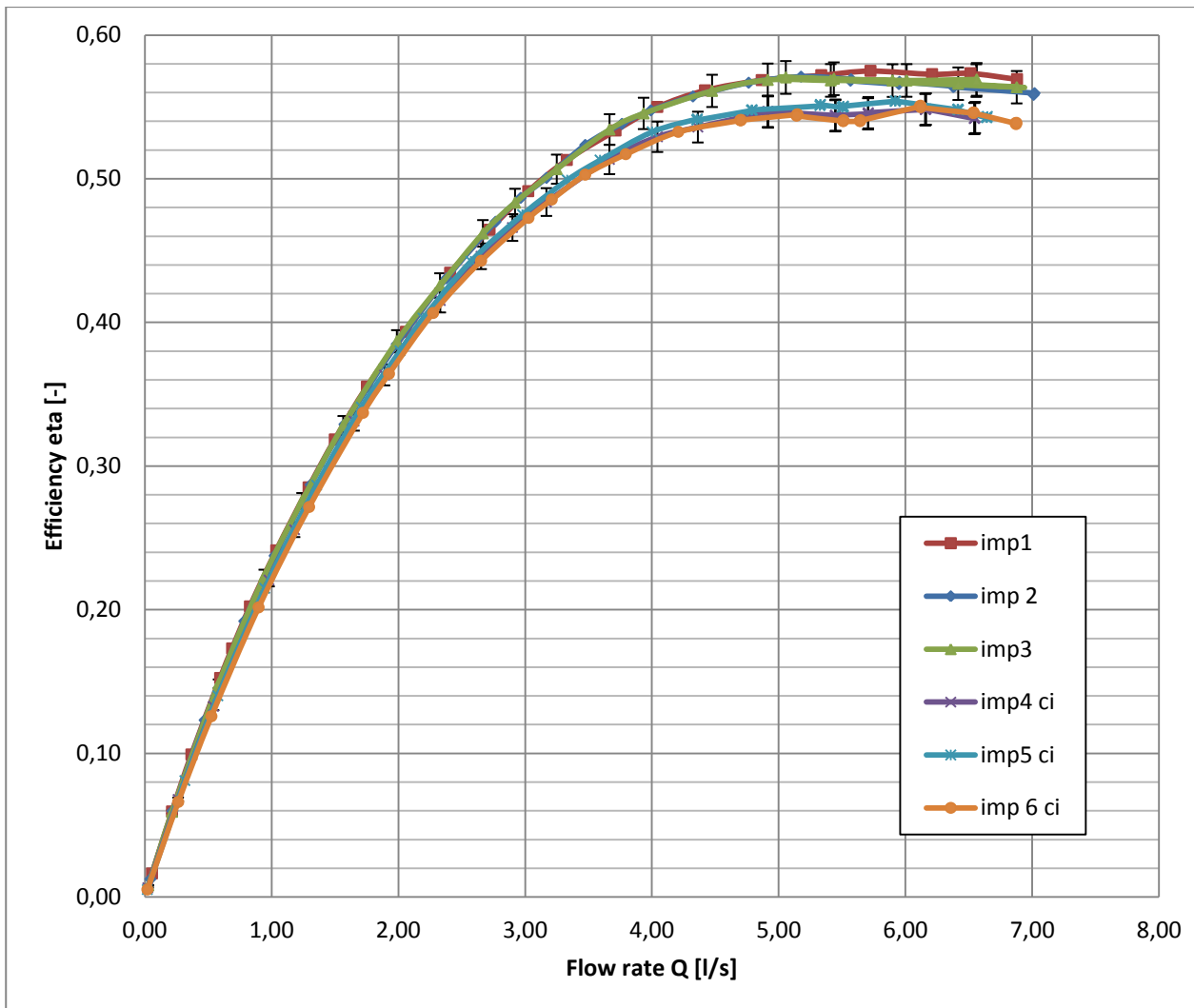


Figure 26: Efficiency characteristic of the plastic and cast iron impellers.

2.4.5 Impellers with reduced diameter

The last group of measurements is made on the impellers with reduced diameter. The original model could be trimmed to reduce the diameter and obtain reduced head characteristics. These smaller models are used on the same plant without changing anything of it, not even the volute is different. It was important to compare the data of these models with the one furnished by the company to understand whether they are valid or not.

The data are collected and analyzed in the very same way as for the previous experiments. The analyzed impellers have the following diameters: 142, 128, 110 [mm]. They are obtained from the impeller 2 by trimming its edges in a vertical plane.

In fig. 27 and fig. 28 the characteristics of head and efficiency are reported compared with the original diameter $d=155$ [mm].

As expected the head characteristics drop as the external diameter is reduced. Even the efficiency shows a reduction because of the bigger distance between the blades and the volute that increases the mixing loss due to the bigger space that the flow has to interact with the slower water that surrounds it. This reduction could be estimated with an empirical formula from [9]:

$$\Delta\eta = \varepsilon * \left(1 - \frac{D_2'}{D_2}\right)$$

Where ε should be set $0,15 \div 0,25$. The results are shown in the tab. 29 where, to attain a good compatibility, a value of $\varepsilon = 0,01$ has been chosen. The impeller 2, D142 shows a slightly increased efficiency that was not predicted. This is due to the fact that the disk friction losses decrease with the 5th power of the diameter while the head is proportional to the 2nd power.

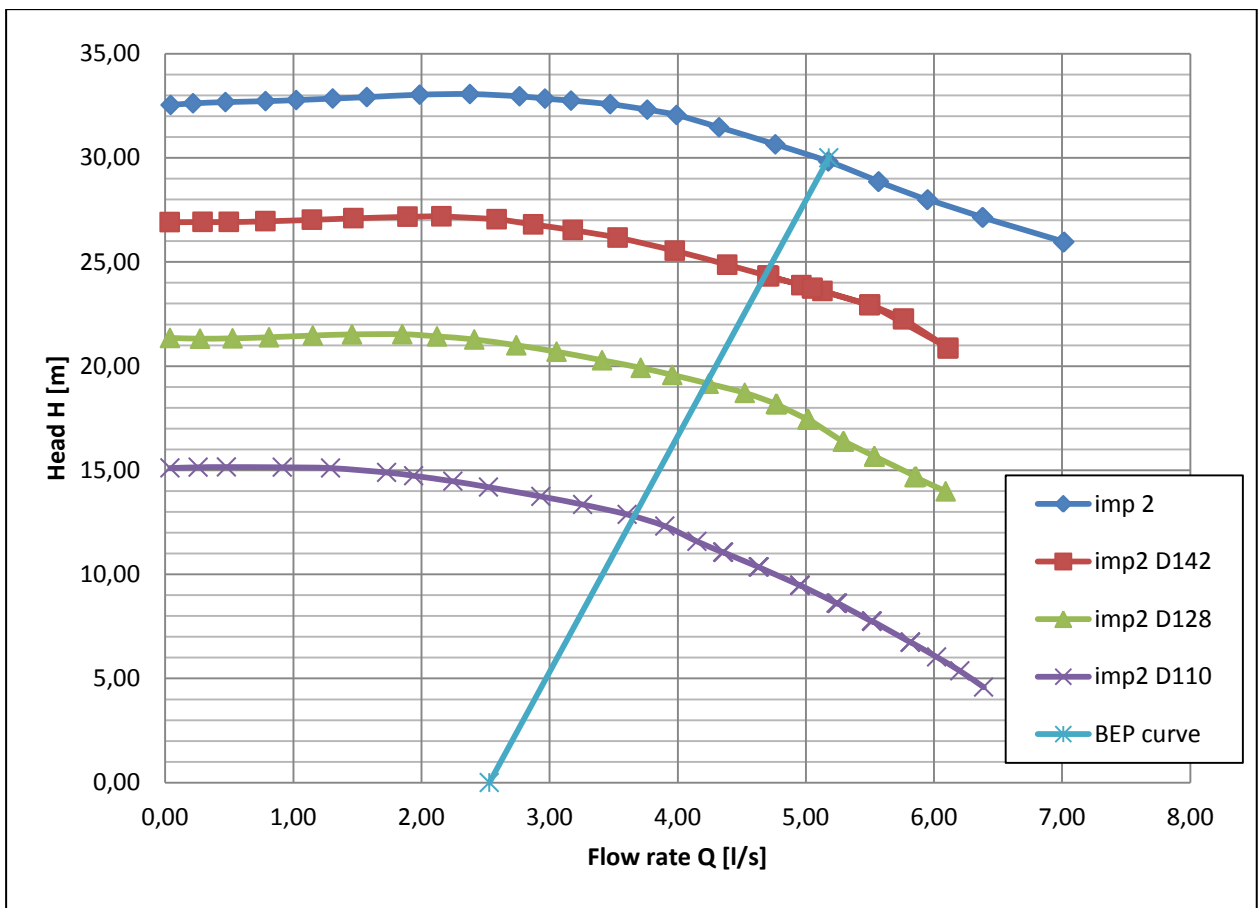


Figure 27: Head characteristic of the plastic impellers with reduced diameter.

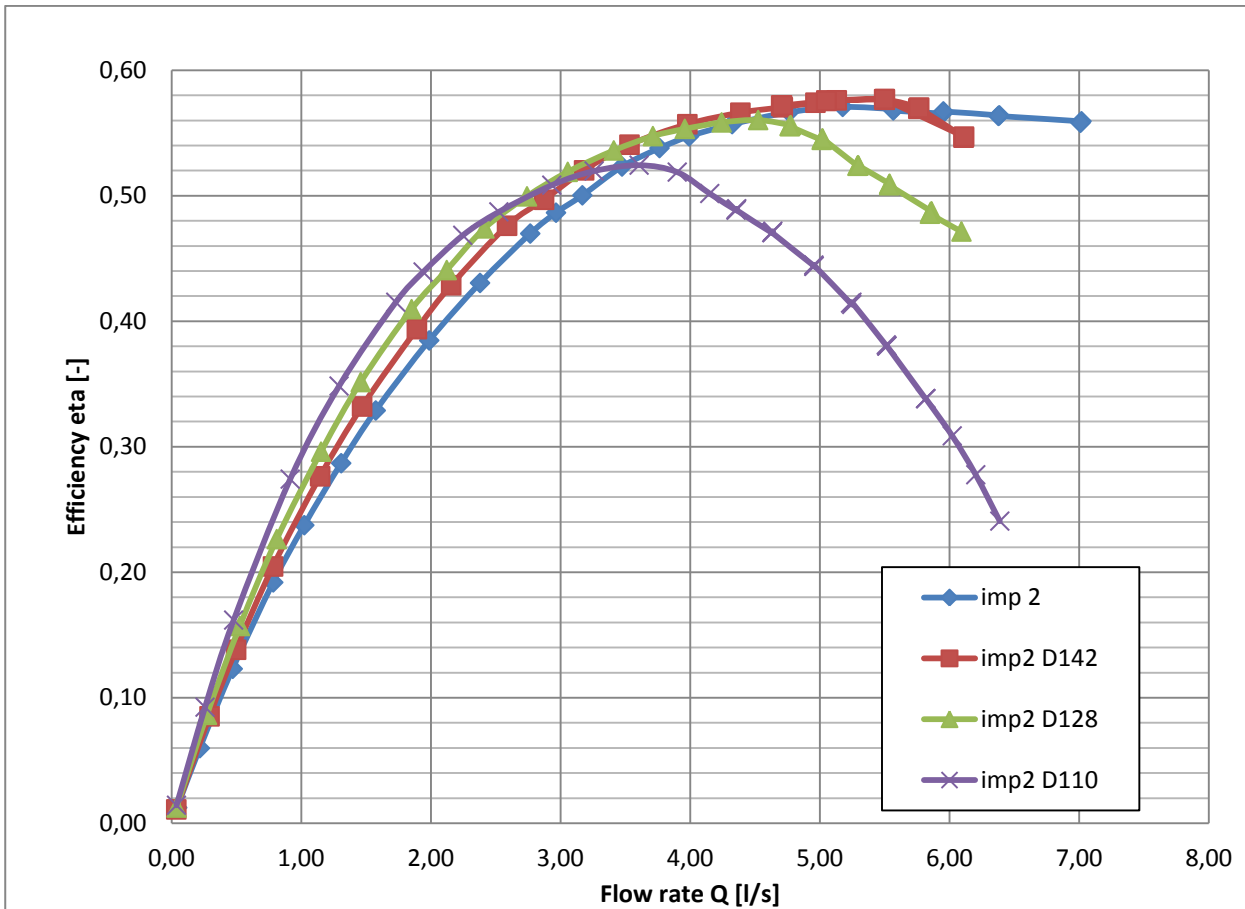


Figure 28: Efficiency characteristic of the plastic impellers with reduced diameter.

D2 [mm]	η max. [-]	$\Delta \eta$ [-]	$\eta_{\text{calculated}}$ [-]
155	0,571	0,0000	0,571
142	0,576	0,0017	0,574
128	0,560	0,0035	0,557
110	0,524	0,0058	0,518

Table 29: Reduction of efficiency in plastic impellers with reduced diameter.

Another, more complex behavior can be observed: the best efficiency point shifts towards lower flow rates.

This can be explained considering that, while the impeller changes, the volute remain the same; the best efficiency point is the result of the combined operation characteristics of the volute and of the impeller.

From the definition of eulerian work we can express the tangential component of the speed outside of the impeller:

$$C_{2t} = \frac{g * H}{\eta} * \frac{1}{u_2} + \frac{u_{1m} * C_{1t}}{u_2}$$

A simple hydraulic calculation of the collector can express the relation between the flow rate and the volute sections:

$$Q = \int C_{2t} * \frac{r_2}{r} * b * dr = C_{2t} * r_2 * J_{sp}$$

Where

$$J_{sp} = \int_{r_4}^{r_a} \frac{b}{r} * dr$$

If we insert the C_{2t} expression in the Q expression we obtain:

$$Q = \left(\frac{g * H}{\eta} * \frac{1}{u_2} + \frac{u_{1m} * C_{1t}}{u_2} \right) * r_2 * J_{sp}$$

This equation can be modified to express Q as a linear function of H:

$$H = \frac{\eta}{g} * u_2 * \left(\frac{Q}{u_2 * J_{sp}} - \frac{u_{1m} * C_{1t}}{u_2} \right)$$

This linear relation between H and Q represents the hydraulic behavior of the volute. The best efficiency point will be determined by the intersection of the characteristic curve of the pump and the characteristic curve of the volute because that is the point in which the operation is optimal, both for the impeller and the volute. When a smaller impeller is used, its characteristic curve is lower while the volute curve is unchanged. The new intersection between the two curves is shifted to lower values of Q determining a shift of the BEP to a lower flow rate [9].

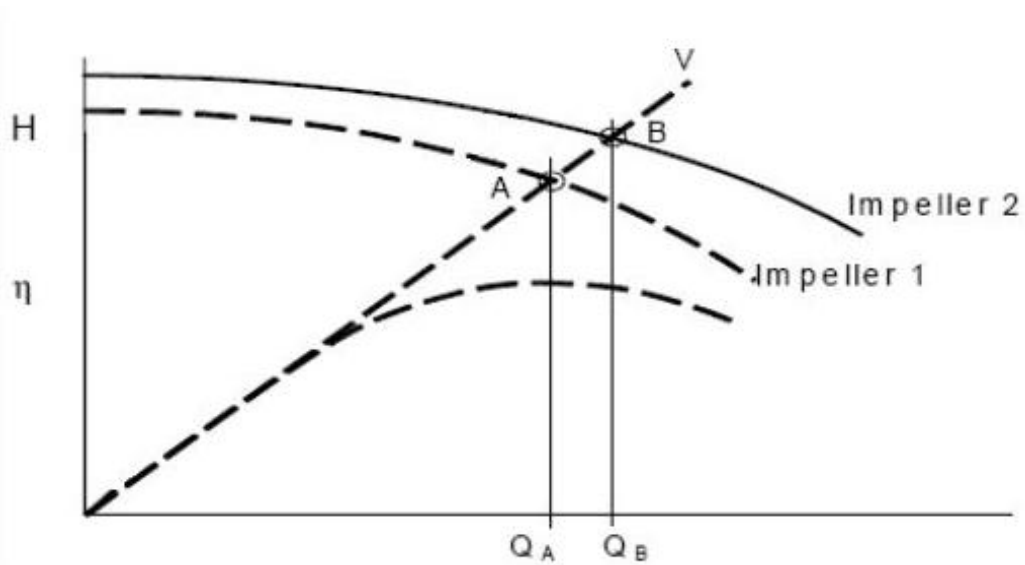


Figure 30: Head curves of two different impellers and volute.

In fig.30 is possible to see the graphical representation of this idea: the curve (V) is not changed but the head curve decreases and their meeting point is shifted from B to A.

Some empirical formulas are also used to estimate the position of the new BEP:

According [9], all the BEPs of the trimmed pumps, are situated on a line that connects the BEP obtained with the maximum diameter to the point on the abscissa $Q' = \phi * n_q * Q_{BEP(Dmax)}$ where $\phi=0,01\div0,05$. This line can be seen in the figure 27 and 28 and the intersection point with every characteristic curve roughly determines the new BEP. For drawing the line an $\phi=0,03$ was used.

2. 5 Measurement errors.

Even if the measuring procedure and the measurements instruments used follow the rules suggested by some international standards, a measurement uncertainty will be anyway affect the collected data. When the instruments are well calibrated and properly installed, an error will be always present and cannot be reduced no matter how many times the measure is repeated. This error is called “systematic uncertainty”[6]. The instruments used were calibrated in previous experiences of the Hydraulic fluid machinery laboratory and showed an error lower or equal to the one reported for each instrument. All the measurement devices have a value of uncertainty that is below the maximum permissible value stated in the ISO guide lines (see Appendix 1). The normative suggests that the systematic uncertainties have to be within this limit. The degree of accuracy to which we refer is the number 2. This is one of the two possible levels of accuracy and is the one that is supposed to be used when nothing else is specified in the agreement with the company.

In table 31 all the uncertainties concerning both the instruments and the calculated values are reported. Some values are not directly measured but calculated, in this situation the uncertainty is to be calculated as the square root of the sum of the squares of the systematic and random uncertainties:

$$e_{tot} = \sqrt{\sum e_{S i}^2 + \sum e_{R i}^2}$$

In this way the systematic uncertainties for the measurements of head, pump power input and efficiency were calculated according to [6]:

$$e_{S \text{ power input}} = \sqrt{e_t^2 + e_n^2}$$

$$e_{S \text{ Head}} = \sqrt{e_Q^2 + e_p^2 + e_s^2}$$

$$e_{S \eta} = \sqrt{e_Q^2 + e_H^2 + e_t^2 + e_n^2}$$

Device	Uncertainty symbol	Uncertainty: ± %
Flow rate	eQ	0,5
Pressure	eP	0,5
Section	eA	0,1
Head_calculated	eH	0,71
Head_normative	eH	1,5
Speed	eS	0,05
Torque	eT	0,5
Pump power input	eS power input	0,50
efficiency	eS η	1,66

Table 31: Uncertainties.

The random uncertainty acquired during the measurement on the same impeller showed a random uncertainty of $\pm 0,15\%$ for the head and $\pm 0,15\%$ for the efficiency. Using the values of random and systematic uncertainty, we can calculate the total uncertainty of the measured head and efficiency:

$$e_{TOT\eta} = \sqrt{e_{S\eta}^2 + e_{R\eta}^2} = 1,66\%$$

The uncertainty that affects the head and efficiency curves is well inside the accuracy range permissible value stated in ISO 9906 (see Appendix 1): 6,1%.

Chapter 3: Theoretical loss analysis

3.1 Introduction

The goal of this chapter is to inspect the experimentally investigated pump from a theoretical point of view. The aim is to better understand the distribution of the losses and their relative importance. This was accomplished by applying some loss models that can be found in literature. The main source of information is [9] since it contains a specific chapter dedicated to this purpose, referred to outstanding researchers and to a great number of experimental tests.

The approach used is mainly semi empirical, this means that the formulas have a simple theoretical base (such as the proportionality to certain physical dimensions) but are then completed exploiting some experimental coefficients. In this way the physical meaning is preserved and the model makes sense of a massive number of measurement data.

Although the great amount of data that are summoned to produce this models, the tolerance on the result is often very big and it is not uncommon for it to reach the 25%; this is certainly a non negligible quantity when the overall expected efficiency is lower than 70% as it is the case we are facing. The reason for this big uncertainty is a great complexity of the hydraulic phenomena that are not only difficult to study but also different in different situations. Small features can strongly influence the evolution of phenomena. Formulas that refer to just a few main parameters could not be enough to ensure good results.

The lack of accuracy of the method is not a problem because the aim of this chapter is to have an idea of which are the weak points of the pump and to try to recognize a general trend rather than to calculate the efficiency in the most accurate way possible.

The normative ISO 9906 [6] suggests simple formulas for calculating certain kind of losses such as the loss that occur in the flow from the pump to the measurement devices. Even here, the approach is always semi empirical.

In order to improve the quality of the overall calculation, when it was possible, some losses should be measured instead of calculated. In this way their value is much more trusted and there is one factor of uncertainty less in the final result.

3.2 Efficiency and loss calculation

Every time a fluid is in contact with a surface in relative movement, some losses arise and the power lost from friction is dissipated into heat. This happens both if a fluid flows into a tube or if a component of a machine moves inside the fluid. In a machine there are a lot of different source of losses that can be observed. Some end up heating the flow and are called “internal” and some other don’t and are called “external”.

The presence of losses means that the energy applied to the shaft to run the pump is higher than the resulting mechanical energy transferred to the fluid.

The sources of loss can be divided into three big categories:

-Mechanical losses.

They contain both internal losses as disk friction on the frontal and back shroud and external losses as bearing and seals friction losses. The last two don’t generally produce a heating of the fluid and their name comes from this. In this pump there are no bearings between the engine and the impeller and there are no seals between the chasing and the impeller, therefore the only mechanical losses are the ones given by the friction of the water between impeller and the chasing (called Pd in figure 32).

-Leakage losses.

Part of the fluid that enters the impeller goes then in the lateral vanes and a fraction of this leaves trough the gaps between impeller and chasing. This exiting fluid has already acquired energy by passing the impeller and therefore its energy is lost (the relative power loss is now Pl). The leakage flow was measured and there is no need to calculate it since the real value is known.

-Hydraulic losses.

Hydraulic losses are all internal losses related to the fluid being in contact with moving or standing parts of the machine. For this analysis the path of the flow is divided into different sections: the impeller, the diffuser, the volute, the losses in the pipes between the impeller and the measuring points. The hydraulic power lost on the pump parts is called PHin while the power lost outside the volute and the impeller is called PHout. All these sections of the machine can be analyzed using simple semi empirical models. The complexity of the geometry and of the phenomena involved is an obstacle to the accuracy of this method. The real flow distribution and its effects on the efficiency can only be evaluated by means of experimental tests and/or CFD calculations.

As a general rule, these losses are the main source of efficiency reduction in a pump and even a rough evaluation of them could help understanding the behavior of the pump and suggest what to improve.

Fig.32 shows a graphic interpretation of the power balance of a pump: the power that enters the shaft is partly lost in form of different losses.

The value of efficiency is defined as the ratio between the energetic benefits and the effort made:

$$\eta_{tot} = \frac{P_u}{P_{in}} = \frac{g * \rho * H * Q}{\frac{(g * \rho * H * Q)}{\eta_{vol} * \eta_{Hin} * \eta_{Hout}} + P_d} = \frac{g * \rho * H * Q}{M_{in} * \omega}$$

It can be re written as:

$$\eta_{tot} = \frac{\eta_{vol} * \eta_{Hin} * \eta_{Hout}}{1 + \eta_{vol} * \eta_{Hin} * \eta_{Hout} * \left(\frac{Pd}{g * \rho * H * Q} \right)}$$

In this definition, instead of the absolute values of power losses, the partial efficiency values are used, defined in the following way:

$$\eta_{vol} = \frac{Q}{Q + Q_{leakage}}$$

$$\eta_{Hin} = \frac{H}{H + \Delta H_{impeller} + \Delta H_{volute} + \Delta H_{diffuser}}$$

$$\eta_{Hout} = \frac{H}{H + \Delta H_{enter} + \Delta H_{bending} + \Delta H_{tube}}$$

All the values we refer to are related to the best efficiency point that has the following conditions:

$Q=Q_{bep}= 0,0055$ [m³/h]

$H=H_{bep}=30$ [m]

$n=2900$ [rpm]

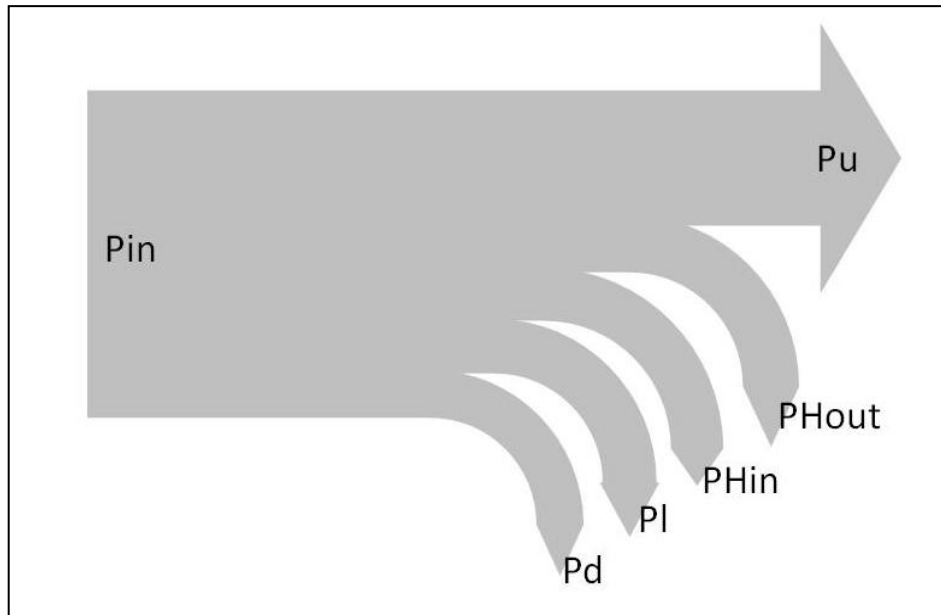


Figure 32: Power balance.

3.3 Mechanical losses: disk friction

When a disk rotates in a fluid, shear stresses develop on the surfaces. A theoretical explanation of this can be the following:

we calculate the shear stress as:

$$\tau = \frac{1}{2} * \rho * c_f * u^2$$

With $u_2 = R * \omega$. The force generated on an infinitesimal surface $dA = 2 * \pi * r * dr$ is:

$$dF = \tau * dA = 2 * \pi * \tau * r * dr$$

And the torque generated is:

$$dM = r * dF = \pi * \rho * c_f * \omega^2 * r^4 * dr$$

The power lost on each side of the disk is therefore:

$$P_M = \omega * dM = \left(\frac{\pi}{5}\right) * \rho * c_f * \omega^3 * r_2^5 * \left(1 - \frac{r_1^5}{r_2^5}\right)$$

The friction coefficient for turbulent flow could be calculated from the formula[9]:

$$C_f = \frac{0,136}{\left(-\log\left(0,2 * \frac{\varepsilon}{r_2} + \frac{12,5}{Re}\right)\right)^{1,15}}$$

And the Reynolds number could be calculated in this way [9]:

$$Re = \frac{u * r_2}{\nu} = \frac{\omega * r_2^2}{\nu}$$

In the end the power lost due to shear stresses on a disk is proportional to the fifth power of the diameter of the machine, to the third power of the speed, to the Reynolds number and relative roughness.

This model does not take into account the conditions of the flow into the narrow gap between the shroud and the chasing wall. In particular the dimension of the gap has an influence because if it is too large the boundary layer can grow too much but if it is too small the velocity gradients are too big and the friction rises.

In order to consider this and to better match the model with the experimental evidences, a semi empirical method is suggested by Gülich:

$$P_M = \frac{K_R}{\cos\delta} * \rho * \omega^3 * r_2^5 * \left(1 - \frac{r_n^5}{r_2^5}\right)$$

Where:

$$K_R = \frac{\pi * r_2}{2 * Re * S_{ax}} + \frac{0,2}{Re^{0,2}} * \frac{1 + \frac{S_{ax}}{r_2}}{1 + 2 * \frac{S_{ax}}{r_2}} * f_L * f_R$$

Where f_R takes into account of the influence of the roughness:

$$f_R = \left(\frac{\log\left(\frac{12,5}{Re}\right)}{\log\left(0,2 * \frac{\varepsilon}{r_2} + \frac{12,5}{Re}\right)} \right)^{2,15}$$

And f_L considers the effects of leakage:

$$f_L = \exp\left(-350 * \varphi_{sp} * \left(\left(\frac{r_2}{r_{sp}}\right)^a - 1\right)\right)$$

$$\varphi_{sp} = \frac{Q_{Leakage}}{\pi * r_2^2 * u_2}$$

If φ_{sp} is >0 then it must be $a=1$, otherwise $a=0,75$.

The variables considered can be seen in the figure 33.

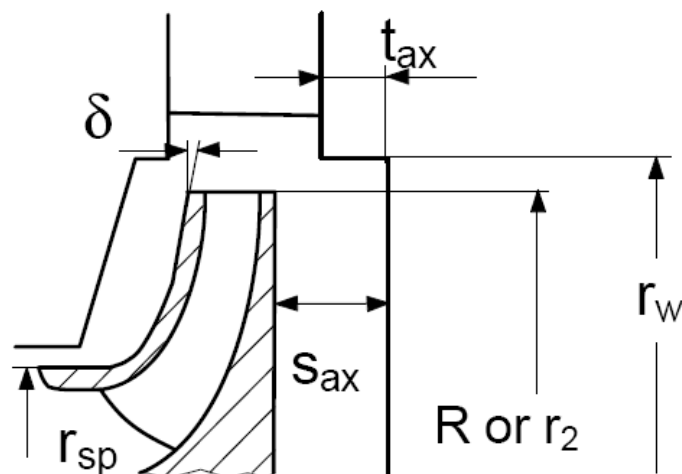


Figure 33: Sketch of the meridian section.

The frontal shroud presents some bumps due to the productive procedure in which the blades are welded to the shroud through some point, the sign of this operation remains and therefore the surface is not flat and the roughness cannot be considered the same as in the blade channels. A Value of roughness of 0,01 [mm] has been chosen. The distance between disk and the chasing wall is $S_{ax}=5$ [mm] but is a mean value because wall and impeller have a relative angle between each other.

In this conditions the power lost by friction on the front shroud is $P_m = 104,7$ [W].

The rear shroud presents some back blades to create a pressure gradient that helps to balance the forces generated on the front shroud. At the same time the pressure gradients opposes the leakage losses forcing it to a higher radius. The behavior of the flow forced by the back blades was not considered because of the lack of a simple modeling. To have a rough evaluation of the friction losses even on the back side of the impeller, the same model used for the front shroud was applied. The value of roughness used is 0,01 [mm] and this gives good results (as we will see from the CFD analysis). The distance between disk and the chasing wall is $S_{ax}=3$ [mm].

In this conditions the power lost by friction on the rear shroud is $P_m = 101$ [W]. Despite the bigger surface wet by the water, the value is lower than the one lost on the front shroud because the smaller gap reduces the development of the boundary layer, while the additional surface is in a low radius region and causes little additional losses.

The partial efficiency reduction caused by the disk friction can be calculated as:

$$\eta_{\text{disk}} = \frac{P_u}{P_u + P_m} = \frac{g * \rho * H * Q}{g * \rho * H * Q + P_{m \text{ front}} + P_{m \text{ back}}} = 0,89$$

The value of Q_{leakage} used for the calculation comes from the experimental tests explained in the following sub-chapter.

3.4 Leakage losses

After the flow comes out of the impeller, a part of it goes in the lateral vanes instead of going into the volute (or after having been in it). In the lateral vane the movement of the flow is subjected to different forces like the friction of the walls, the initial momentum and the difference of pressure across the clearance between impeller and chasing. The last component causes an outgoing flow called leakage flow that is a lost since it has already been energized by passing into the impeller mobile vanes.

Lots of factors influence the amount of leakage flow and the following are of a particular importance:

- dimension of the clearance: height and length
- roughness of the clearance walls
- difference of pressure
- flow distribution inside the lateral vanes
- production tolerances are an issue because of the small dimensions of the geometry

It is clear that the interaction between the leakage flow and the disk friction is not easy to understand and to describe with simple models. To overcome this problem, and since the experimental analysis was possible, we refer to the measured values.

The expected result is calculated using an empiric formula suggested by [9]:

$$Q_{\text{leakage}} = Q * a * n_q^{-m}$$

If n_q is lower than 27 the value of “a” is 4,1 and “m” is 1,6. If n_q is greater or equal to 27, the value of “a” is 0,15 and “m” is 0,6. The negative exponential law reflects the fact that leakage losses reduces when the n_q number increases. This is due to the fact that a bigger flow rate means a relative reduction in the flow loss: as already discussed, the main flow rate is not a parameter that affects the behavior of the water in the lateral vanes.

In our case the expected leakage loss is 0,000247 [m³/s] resulting in a volumetric efficiency of 0,948 in the best efficiency point.

3.4.1 Experimental setup and results

To measure the leakage flow in the test rig, the following procedure was applied:

The leakage flow that comes out of the back part of the impeller is forced into a tube that permits to collect it into a bucket. The bucket is filled for a time Δt and then weighed. The difference between the total weight and the weight of the empty bucket is the amount of water stored collected in the time Δt :

$$W_{\Delta t} = W_{\text{tot}} - W_{\text{empty}}$$

For the time measurement a stopwatch was used. This instrument has an accuracy of $\pm 0,005$ [s]. For the weight measurement, it was used a balance with the accuracy of $\pm 0,05$ [kg]. To compensate the low accuracy of the balance, it was necessary the use a long measurement time of 200 [s] to increase the amount of water to weighed and to reduce the final relative uncertainty of the measure up to a value of $\pm 0,025$ % that is smaller than the one of the flow meter.

$$Q_{\text{leakage}} = \frac{W_{\Delta t}}{\Delta t} \cdot \frac{\rho}{\rho}$$



Figure 34: Test-rig for the measurement of leakage losses.

Fig.34 shows a detail of the system used to collect the leakage flow. The structure that holds the pump has three holes that allow the lost flow to exit, two of them were closed and the third connected with a tube that leads the flow into the bucket. This construction shouldn't produce a different pressure condition in the out-coming leakage flow. For being sure of this, the characteristics of head, power consumption and efficiency were measured during the test and, as expected, they didn't show any difference from the original behavior.

The measurement was repeated for different flow conditions: one measurement every 0,5 [l/s] from 0,5 [l/s] to 6,0 [l/s].

The test was conducted at the original speed of 2900 [rpm] in order to recreate the operative flow conditions. As already explained, the power limitation coming from the engine forces the speed to drop at high flow rate, making the leakage measurement incorrect in that situation. To find the real value, it was necessary to repeat the leakage measurement at the same flow rate but with reduced speed (to be repeated at least two more times) and then linearly extrapolate the value for 2900 [rpm]. The results are reported in the graph 35 in terms of relative flow: $Q_{R\ leakage} = \frac{Q_{leakage}}{Q}$ and show the reduction of the relative value when the flow rate increases, this behavior fits well with the above explanation.

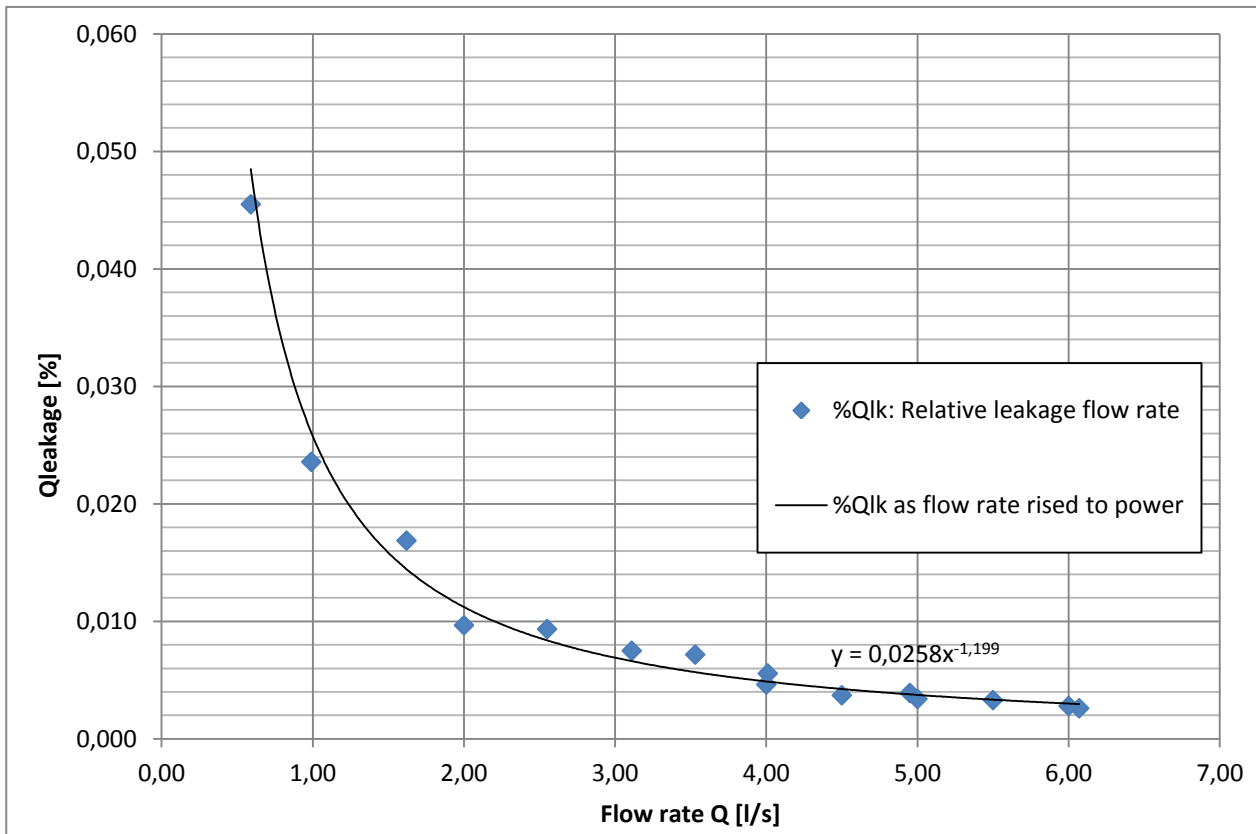


Figure 35: Leakage losses.

In the best efficiency point the relative leakage value is of 0,3% and the absolute value is $Q_{leakage}=0,019$ [l/s]. This means a volumetric efficiency of

$$\eta_{vol} = \frac{Q_{leakage}}{Q + Q_{leakage}} = 0,997$$

This value is very high if compared to the expected value, probably because of the smart construction of the back blades and because of the narrow and long clearance between casing and impeller.

This experiment concerns only the back part of the leakage flow but a similar flow will be present in the frontal part of the machine. This additional source of loss would have been too complicate to be measured.

Even if the geometry is completely different, the order of dimension shouldn't be too different and it could be a good idea to think at the frontal loss as if it was equal to the rear one.

3.5 Hydraulic loss outside the pump

From the point of view of the measurement system, the control volume does not only comprehend the pump itself but even the connections between this and the pressure measurement points. Therefore the losses produced in these regions are regarded as internal to the pump.

The calculation of these losses is very standard and is done following the suggestions of the ISO 9906 guide line [6].

From the pump to the pressure tapping, the stream flows into 20 [cm] of piping and the friction caused by this contact with the wall is called distributed loss and can be calculated in the following way:

$$\Delta H_{j2} = \lambda * \frac{L_2}{D_2} * \frac{V_2^2}{2 * g}$$

Where $L_2=0,2$ [m] , $D_2=0,044$ [m] and $V_2=3,54$ [m/s] is calculated using the obvious ratio between flow rate and cross section, λ comes from the following calculation

$$\frac{1}{\sqrt{\lambda}} = -2 * \log_{10} \left(\frac{2,51}{Re * \sqrt{\lambda}} + \frac{\epsilon}{3,7 * D_2} \right)$$

This has to be solved in an iterative way.

The value of ϵ (absolute roughness) is chosen to be of 0,3 [mm], a common value for new steel pipes. The result of this calculation gives a head loss of $H_{j2} = 0,1$ [m].

Additionally to this loss, it must be considered the concentrated loss corresponding to the entrance of the flow into the channel that eventually leads to the impeller. The classical way to calculate this is by using an experimental coefficient that takes into account the deflection of the stream lines and the losses related to this process. The classical theory for the calculation sees the loss as proportional to the square of the flow velocity:

$$\Delta H_{enter} = f_{in} * \frac{V_1^2}{2 * g}$$

Where $V_1 = 1,9$ [m/s], which comes from the dimension of the intake section whose diameter is of 0,06 [m], f_{in} is the coefficient related with the geometry similar to the one shown in fig.36. The classical value of this coefficient is 0,5 and causes a head loss of $H_{enter} = 0,092$ [m].

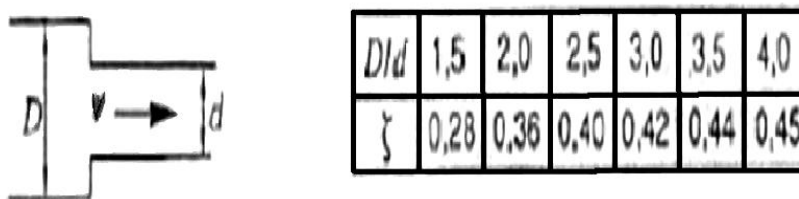


Figure 36: Localized loss coefficients. [4]

As already mentioned in chapter 2, the relative value of head reduction due to this loss is smaller than 0,5% and, according to the ISO guide lines, it can be neglected for the calculation of the head from the pressure measurements.

Another source of loss is the bending of the pipe that leads the flow out of the horizontal volute and into the vertical pipe. Again the concentrate loss could be calculated with the same model but in this case the situation is completely different because the approaching flow is definitely not uniform and there is no experimental coefficient that can represent this situation. Although the model is clearly incorrect, the absolute value of the loss is expected to be very low and a high percentage of uncertainty is admissible.

As a loss-coefficient the value of $f_{bend}=0,25$ was used, representative of a 90° bending with turbulent approaching fluid and a speed of at least 2 [m/s].

This results in a head loss of:

$$\Delta H_{bend} = f_{bend} * \frac{V_2^2}{2 * g} = 0,16 [m]$$

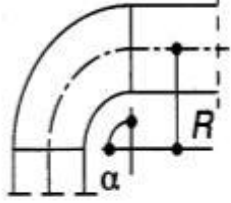
Component	Sketch				K
	α	R = 1·D	R = 1,5·D	R = 2·D	
Bend, Turbulent flow (Minimum speed 2 m/s)		180°	0,28	0,21	0,14
		120°	0,28	0,21	0,14
		90°	0,25	0,19	0,13
		60°	0,16	0,12	0,08
		45°	0,12	0,09	0,06
		30°	0,08	0,06	0,04

Figure 37: Localized loss coefficients. Elaborated from: [4]

The overall loss external to the pump is given by the sum of all the previous values:

$$\Delta H_{tot} = \Delta H_{bend} + \Delta H_{enter} + \Delta H_{j2} = 0,35 [m]$$

The relative efficiency is given by the following definition:

$$\eta_{Hout} = \frac{H}{H + \Delta H_{enter} + \Delta H_{bending} + \Delta H_{tube}} = 0,988$$

3.6 Hydraulic losses inside the pump

The subject of this sub-chapter is the analysis of the losses in the components present between the suction and the discharge nozzle. The two main sources of losses are the friction on the surfaces of the components and the vortex dissipation. In particular the second is more related to separated flows (that can have many causes). Strong flow non-uniformities or high gradients permit the growth of vortices whose energy is then dissipated creating smaller vortices. Contrary to what occurs in the turbulent dissipation, the friction dissipation is the most important in accelerating and attached flows and it is influenced by the wall roughness and Reynolds number.

The complexity of three dimensional flows, the great amount of causes that could produce flow separation and the difficulty in the description of interaction in a separated flow, make it almost impossible to develop a simple model that describes the losses. Thus, this calculation must have a strong empirical character and is mainly based on formulas that can be found in literature and have an experimental origin. An important uncertainty has to be taken into account: 25% of error in the result is not surprising.

The components that should be considered are: impeller, diffuser and volute. In the pump that we consider there is no real diffuser and its analysis will not be done.

All the models used are referred to the best efficiency point and are not meant to describe the behavior when a recirculation is present. Literature reference for them can be found in [9].

3.6.1 Impeller losses

For the calculation of the impeller losses a method based on the separation between the so called chock losses and the friction and mixing losses was used. The chock loss occurs since the flow has to adapt its direction to the one of the blade, it does so losing some energy. The energy lost by the flow is proportional to the difference of velocity of the flow before and after entering the blade channel. The friction loss is based on the calculation of the average relative velocity and on an empirical dissipation coefficient.

The average velocity in the blade channel can be calculated using the following formula:

$$W_{av} = \frac{2 * Q}{N_{blades} * (a_2 * b_2 + a_1 * b_1)}$$

Where the “a” is width of the blade channel and of “b” is the high in the sections 1 (entrance) and 2 (outlet). The dimensions were measured from the physical component and the values are: a1= 15 [mm], a2= 27 [mm], b1=10,0 [mm], b2=8 [mm]. The average speed of the flow is: $W_{av} = 4,45 \left[\frac{m}{s} \right]$.

The friction coefficient was calculated using the same approach seen for the disk friction but using a roughness of $\epsilon=0,002$ [mm] typical for plastic surfaces. The Reynolds number has to be calculated in the following way:

$$Re = \frac{W_{ave} * L_{blade}}{\nu}$$

Where the length of the blade is measured and is equal to 85[mm]. With these values, the friction coefficient is $C_f=0,0055$.

The dissipation coefficient could then be calculated using this empirical formula:

$$C_d = (c_f + 0,0015) * \left(1,1 + 4 * \frac{b_2}{D_2}\right) = 0,0091$$

The hydraulic diameter comes from the formula:

$$D_h = \frac{2 * (a_2 * b_2 + a_1 * b_1)}{a_1 + b_1 + a_2 + b_2} = 0,012 [m]$$

In the end the loss of head has to be calculated with the following method:

$$\Delta H_{friction-imp} = 4 * C_d * \frac{L_{blade}}{D_h} * \frac{W_{ave}^2}{2 * g} = 0,3 [m]$$

To calculate the chock losses we have to estimate the velocity of the flow before and after entering the blade channel. The head loss will be proportional to that value.

The speed in the blade channel could be estimated knowing the dimension of the channels:

$$W_{1q} = \frac{Q}{N_{blades} * a_1 * b_1} = 5,31 \left[\frac{m}{s}\right]$$

The speed of the approaching flow comes from the velocity triangles theory:

$$W_{1m} = \sqrt{C_{1m}^2 + (u_1 - C_{1u})^2} = \left[\frac{m}{s}\right]$$

In the end the loss of head has to be calculated with the following method:

$$\Delta H_{chock-imp} = \frac{0,3}{2 * g} * (W_{1m} - W_{1q})^2 = 0,32 [m]$$

The total hydraulic efficiency of the impeller can be calculated in the following way:

$$\eta_{H imp} = \frac{H}{H + \Delta H_{chock-imp} + \Delta H_{friction-imp}} = 0,97$$

3.6.2 Volute losses

To calculate the hydraulic losses in the volute, the mixing loss of the entering flow is neglected. The cross-section of the volute changes in every angular position and this affects the speed of the flow and therefore the friction. To calculate the friction losses inside the volute, it is necessary to consider different sections each with a different surface, length, mean speed and mean friction coefficient.

Basing on the volute-section sketch provided by the manufacturer of the pump it is possible to identify 9 sections placed at 45° of distance to each other to define 8 segments as it is shown in fig.38.

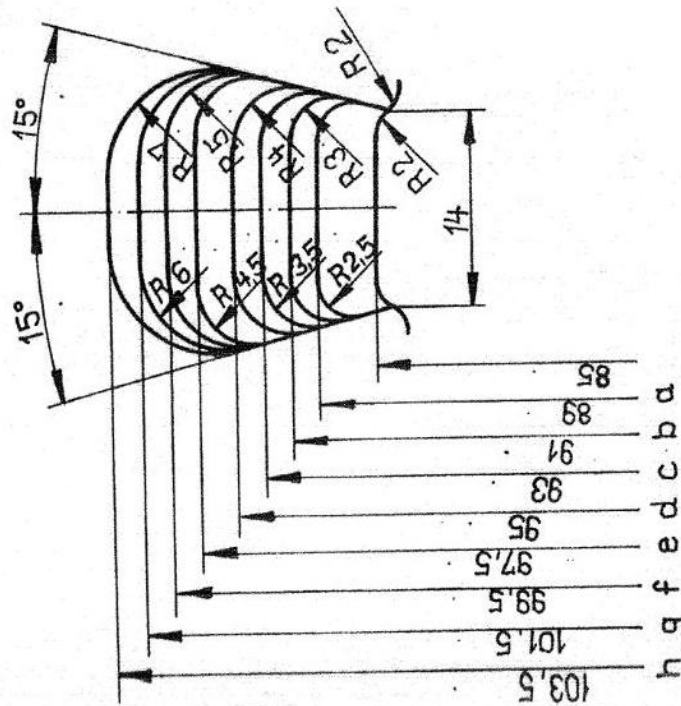


Figure 38: Sections of the volute.

Each segment is associated with an angular angle of 45° and a maximum radius from 82 to 106 [mm]. For each segment is calculated the length:

$$\Delta L_i = \frac{r_i - r_{i-1}}{2} * (\theta_i - \theta_{i-1})$$

The wall area is calculated with the following formula:

$$\Delta A_i = \Delta L_i * \pi * (r_i - r_0)$$

The speed can be calculated from the flow rate in each segment:

$$c_i = \frac{Q_i}{S_i} = \frac{Q_i}{\left(\frac{r_i - r_0}{2}\right)^2 * \pi}$$

Where Q_i is the fraction of flow entering in the "i" section of the volute.

To calculate the friction coefficient we use the classical approach for the turbulent flows:

$$C_{f i} = \frac{0,136}{\left(-\log\left(0,2 * \frac{\varepsilon}{r_i} + \frac{12,5}{Re}\right)\right)^{1,15}}$$

Where the roughness value is $\varepsilon=0,003$ [mm] and the Reynolds number could be calculated in this way:

$$Re_i = \frac{r_i - r_{i-1} * C_i}{\nu}$$

The semi empirical formula that describes the total head loss is:

$$\Delta E_{tot} = \frac{1}{Q * 2 * g} * \sum (C_i^3 * \Delta A_i * (C_f + 0,0015)) = 10,1 \text{ [m]}$$

The total hydraulic efficiency of the volute can be calculated using the definition:

$$\eta_{H imp} = \frac{H}{H + \Delta E_{tot}} = 0,75$$

The pump has a small dimension, a relatively small nq number and a measured efficiency lower than 60%, these considerations let us suppose that the turbulent effects inside the components might have a certain importance and that separation of the flow occurs inside the impeller or in the volute. In this situation the mixing losses could gain importance. The presented loss model for the volute neglects these losses so the real value of volute efficiency should be lower than the calculated one.

3.7 Considerations

It is now possible to collect all the data relative to the losses and to calculate the total effect on the hydraulic efficiency. Using the final formula shown in the chapter 3.1 we obtain a total efficiency of:

$$\eta_{tot} = \frac{\eta_{vol} * \eta_{Hin} * \eta_{Hout}}{1 + \eta_{vol} * \eta_{Hin} * \eta_{Hout} * \left(\frac{Pd}{g * \rho * H * Q} \right)} = 0,65$$

This result is subjected to a big uncertainty due to the compulsory simplification of the model. The way to calculate this uncertainty is suggested together with the model itself:

$$\Delta\eta_{tot} = 0,2 * (1 - \eta_{tot}) = 0,07$$

This means that the measured value ($\eta_{BEP} = 0,59$) is comparable with the calculated efficiency whose range is: $\eta_{tot} = 0,58 \div 0,72$. The use of a simple model that neglects the mixing losses in the volute contributes to place the real value in the lower part of the range.

For each type of loss we can now compare the amount of power lost in the component. The result is presented in the table 39. The calculation refers to the following formula:

$$\Delta P_{lost} = H_{lost} * Q * g * \rho$$

In the case of the volumetric loss:

$$\Delta P_{lost} = H * Q_{lost} * g * \rho$$

Type of loss		P lost [W]	P lost [%]	dη
Leakage losses from the back part:	dPvol	6	0,01	0,002
Leakage losses from the front part:	dPvol	6	0,01	0,002
Mechanical losses:	connection losses: dPH	19	0,02	0,008
	disk friction losses: dP PRR	206	0,25	0,083
Hydraulic losses:	impeller losses: dPh	34	0,04	0,014
	diffuser losses: dPh	0	0,00	0,000
	volute losses: dPh	550	0,67	0,224

Table 39: Table of the calculated losses inside the impeller.

The main source of loss is clearly the one in the volute. These are strongly influenced by the velocity inside the volute that is proportional to the speed outside of the impeller (especially true for a pump that lacks of a proper diffuser). It is clear that the speed inside this component is very high (with a peak of speed higher than 35 [m/s]) and the first idea to improve these conditions is to use a volute with bigger cross sections.

The second cause of loss is the disk friction. This is normal for low nq numbers where the ratio D2 / D1 is high: the head grows with the square of the diameter, the friction grows with the fifth exponent.

The Impeller losses are very small and under the 5%. This result is not plausible and could be caused by the use of too simple models that cannot properly describe the complicate flow conditions: especially separation phenomena that may occur, where actually not taken into account. Despite the big value of uncertainty that the formulas leave, it is clear that the losses inside the impeller are not so important and should not be considered as the main target of the optimization. This is true for the BEP but for lower flow rate values, it could be completely different. This concept has to be stressed because the working point of the pump is placed at part-load, there, these considerations loose of their numerical relevance.

The volumetric losses have been calculated and proved to be very small in comparison with other values. The other losses have a marginal influence and are not interesting as far as it concerns the optimization.

The whole procedure can be summarized as an application of simple semi empirical models that allows us to calculate a rough approximation of the losses inside the pump. Even if the uncertainty is high, and some phenomena are completely neglected, the result can be successfully compared with the measured value.

The most important finding is the evaluation of the relative importance of the different losses: the volute losses proved to be the most important, contributing for 67 % followed by the disk friction losses that have the 25 % of the importance; the impeller is a less important source of losses contributing for less than 5 % of relative losses.

Chapter 4: Simplified impeller design

4.1 Introduction

The goal of this chapter is to provide the theoretical basis for the numerical optimization of the impeller and to furnish a comparison term to evaluate how and where the old geometry must be changed. The numerical optimization should be the last passage that comes after the definition of a valid geometry. From this prospective the CFD based optimization is just something that comes after the definition of a good first-try geometry.

The aim of this chapter is to define an impeller that is close enough to the perfect one. When this model has been defined, it is also possible to apply it to the original project in order to understand the differences from the suggested values, to help understanding the weak point of the original project.

The approach that is used is mainly semi empirical, this means that the formulas have a simple theoretical base (such as the reference to the celerity triangles theory) but are then completed exploiting some experimental coefficients that come from a great number of experimental evidences. The physical meaning is guaranteed by the connection with the theory while the accuracy of the model is improved by the comparison with similar empirical situations.

The process of designing a new impeller could be summarized in the following steps (this is the current industrial approach):

- Calculation of the main dimensions (strong use of empirical correlations)
- Draw of an initial geometrical design
- Use of a 3D design software for a pre-optimization of the geometry
- Optimization through try and error approach (use of Navier Stokes programs)
- Experimental tests for evaluating and perhaps optimizing again the last calculated version

The current chapter is about the first three points of the list. The results of this procedure will be exposed latterly in the 7th chapter where it will be applied every time to a different particular situation.

A simplified approach for the definition of an ideal geometry requires several different inputs such as the flow conditions and the expected head characteristic, both considered in the best efficiency point. Beside this, there are also some other hydraulic specifications that have to be considered during the process. These considerations are mostly general and are related to all the characteristic curve and not only to the BEP point:

- The working conditions along all the characteristic curve should be stable.
- The value of head in with a flow rate equal to 0 [l/s], causes the maximum rise of pressure that could compromise the structural integrity of the pipe system. It must be paid attention to this value.
- There could be some limitations on the development of axial trusts and cyclic pulsations.
- Material and production method may have influence on the hydraulic proprieties.
- Cavitation characteristics must always be compared with the one of the plant in order to work in safe conditions.
- The hydraulic design must undergo to mechanical limitations on axial extension, shaft diameter, production costs, presence of seals.

-As a general rule the head and efficiency must be as higher as possible to reduce fixed and operational costs and to have a smaller machine.

Not all of these considerations have an importance in our particular context. As an example, the NPSH characteristics do not have any importance since the pump is submerged (see appendix 4). Other conditions are determined by the decision of the company that already produces the old model of the pump; this is, for example, the case of the production system.

4.2 Initial design process

In this paragraph will be explained the theoretical base and the semi-empirical approach that is used for the definition of the main dimensions. The main reference for the use of these models is the book published by Gülich [9], here a lot of experimental data form the base for the development of a simple design process that takes into account the main features of the pump. In particular, during the entire paragraph, we will focus only on what concerns centrifugal pumps, avoiding more general formulas that are pointless in this context. The procedure is composed by two successive steps. At first the main dimensions are defined with reference to the expected characteristics and with the hydraulic specifications. The next part is the definition of the impeller geometry: blades and blade channels can be drawn using some software that helps to attain smooth variations of the variables.

4.2.1 Definition of the main dimensions

The process of optimization starts with the definition of the main geometrical dimensions. These values are the bases for the definition of the complete geometry.

The input data that are required in this part are: speed, flow rate in the BEP, head in the BEP, inlet flow conditions and other hydraulic conditions as already mentioned in the introductory chapter. The entering flow is considered to be axial since there is not a distributor component that changes the absolute angle. The distribution of velocity over the approach flow cross section is assumed constant.

The first value that has to be calculated is the **n_q number**. It is important to define the general behavior of the machine and some of its dimensions. It is defined as follows:

$$n_q = n * \frac{\sqrt{Q_{BEP}}}{(H_{BEP})^{\frac{3}{4}}}$$

The definition of a certain optimal flow rate can affect the value of n_q number and, through it, other part of the optimization process. With reference to the measured impeller, the flow rate at which the maximum efficiency is obtained, is around 5,5 [l/s] and the relative head has a value of 29 [m]; considering that the rotational speed is of 2900 [rpm], the n_q number of the original project has a value of 17,3.

The n_q number allows us to enter the 40th diagram and to estimate the efficiency. This will be useful for the determination of the head.

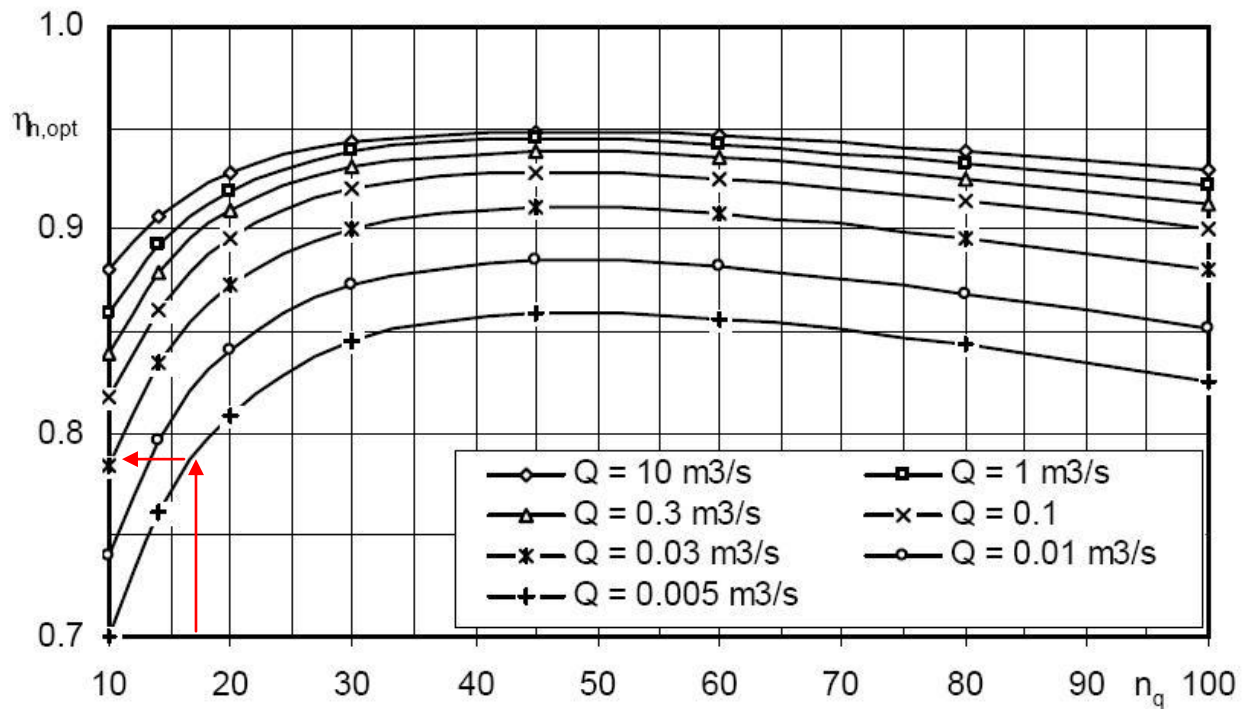


Figure 40: Hydraulic efficiencies of single-stage single-entry radial pumps. [9]

The volumetric losses can be estimated using the following empiric formula:

$$Q_{leakage} = 4,1 * Q * n_q^{-1,6}$$

The volumetric efficiency is then calculated as:

$$\eta_{vol} = \frac{Q}{Q + Q_{leakage}}$$

The internal diameter of the impeller is limited by the presence of the shaft that transmits the torque coming from the electrical engine. The decision is to maintain the shaft unchanged to avoid a complete re-design of the whole machine and of the electrical engine.

The head coefficient is connected with the load of the blades and it must be selected within a range of value that is defined in fig.41 as function of n_q . The range has an upper limit because a high load causes bad part-load flow conditions and reduction of efficiency. The minimum value is related with the need of containing the dimensions and costs of the machine. When the coefficient is chosen, the external diameter is calculated as:

$$D_2 = \frac{84,6}{n} * \sqrt{\frac{H_{opt}}{\Psi_{opt}}}$$

It is to be noticed that with small n_q numbers is a good idea to keep the head coefficient high to decrease the diameter of the machine and the disk friction losses that are supposed to be high.

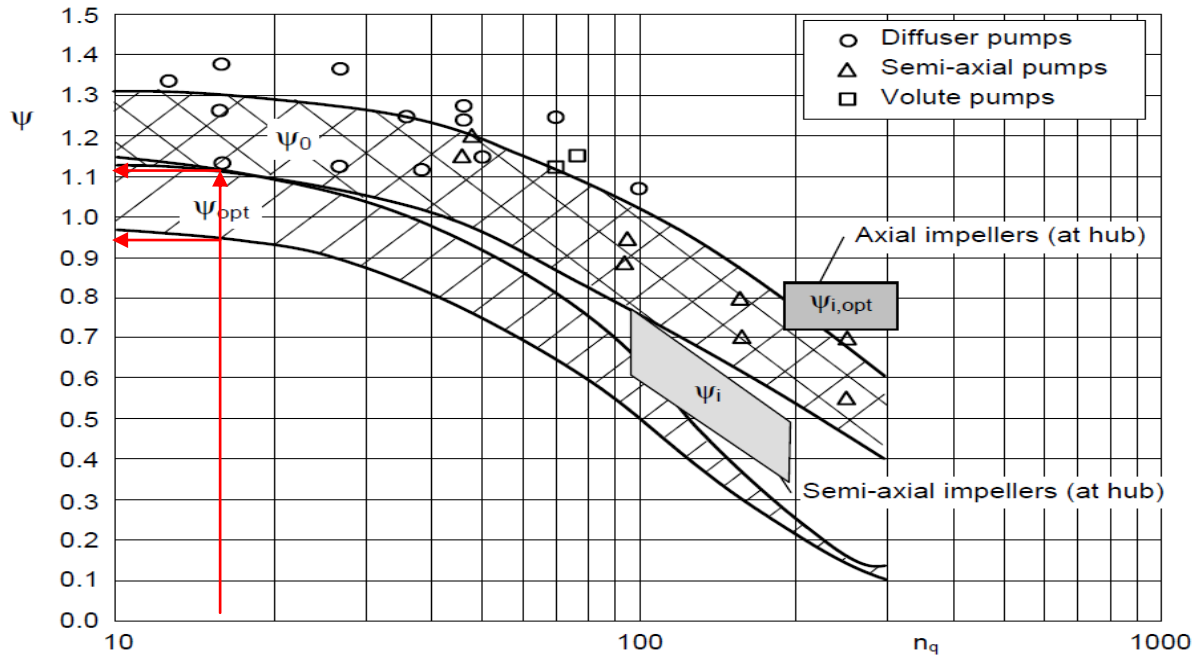


Figure 41: Head coefficient range for different n_q numbers. [9]

The number of blades that has to be chosen must be within the range of 5÷7 (according to [9]) for this kind of machines. Values out of this range can be chosen in consideration of particular situations but have generally to be avoided because of the high blade load (less than 5 blades) or because of the higher friction losses and instability of the curve (more than 7 blades). As will be later explained, the excessive load is one of the main problems of this pump and therefore it is better to go for a 7 blades design.

The inlet external diameter D_{1ext} is generally related with the cavitation requirements but in this particular situation this is not an issue and more stress can be put on the reduction of the relative speed at the blade inlet. The following experimental formula has to be applied:

$$D_{1ext} = D_2 * f_{1d} * \sqrt{D_n^2 * D_2^2 * \frac{1,48}{10^3} * \Psi_{opt} * \frac{n_q^{1,33}}{(\eta_{vol})^{0,67}}}$$

Where the coefficient f_{1d} has a value of 1,15 for n_q numbers lower than 20.

The inlet internal diameter is the lower limit of the blade intake angle. Its lower value is limited by the presence of the shaft. This dimension can be chosen in order to fit well the drawn blade geometry and to create the smoothest possible variations; this is done without a specific formula but two considerations have to be remembered: a low value of D_{1ext} improves the stability of the curve but force to build more tangential blades.

The knowledge of the impeller inlet geometry allows us to determine the **intake angles** using the following procedure. In order to have a sufficient accuracy, it is required to repeat the calculation for at least three different streamlines.

With the passage area we could calculate the meridian component of the relative velocity (C_m that is the absolute velocity) while the circumferential one comes from the rotational speed and the radial position of the stream line that we are considering. The two elements are composed to calculate the total relative velocity that is also the hypotenuse of the velocity triangle.

$$A_1 = \frac{4}{\pi} * (D_{1ext} - D_n)^2$$

$$C_{1m} = \frac{Q}{A_1}$$

$$u_{1i} = \pi * \frac{n}{60} * D_i$$

$$W_{1i} = \sqrt{u_{1i}^2 + C_{1m}^2}$$

$$\beta_{1i} = \arctg\left(\frac{C_{1m}}{u_{1i}}\right)$$

The presence of the blades causes a reduction of the free cross section and the increase in speed of the flow. This effect is summarized in the blocking factor that permits to calculate a new flow angle with blockage. The reduction of the passage area (expressed by the term τ_1) causes an increase in the axial component of the total speed.

$$\beta_{1i}' = \arctg\left(\frac{C_{1m} * \tau_1}{u_{1i}}\right)$$

$$\tau_1 = \frac{1}{1 - \frac{N_{blade} * e}{\pi * D_1 * \sin\beta_{1gi} * \sin\lambda_{LA}}}$$

Where the value of “e” is the thickness of the blade, chosen to be equal to the original value of 2,6 [mm]. λ_{LA} is the angle of relative inclination between the hub and the leading edge of the blade. The second value can be determined after the actual drawing of the impeller; the operation is clearly iterative.

A certain amount of incidence (0-4 [°]) should be added to the calculated value, in this way the flow rate of shock-less entry is slightly above the BEP. The same effect could be obtained through an exaggeration of the angle. The new value is the geometrical intake angle:

$$\beta_{1gi} = \arctg\left(1,1 * \arctg\left(\frac{C_{1m} * \tau_1}{u_{1i}}\right)\right)$$

Since the leading edge is spread across growing radial positions, the tangential velocity will grow from the most internal stream line to the one placed at bigger radius, as a result β_{1gi} becomes smaller. From the difference between the two extreme values follows the usual distribution of the angles across the blade that is decreasing (radial-wise) for the internal lines and increasing for the external.

The outlet width has to be chosen considering its effects on the acceleration inside the channel, for this reason it must always be that $b_2 < b_1$. Higher value of outlet angle produce a more stable characteristic curve but increase the non-uniformity of the flow and the turbulent dissipation losses. Since the above effects are difficult to be quantified, it is common to select $b_2^* = b_2/d_2a$ from empirical data, for example using the graph in figure 42. The resulting value for the considered situation is supposed to be smaller than 10 [mm].

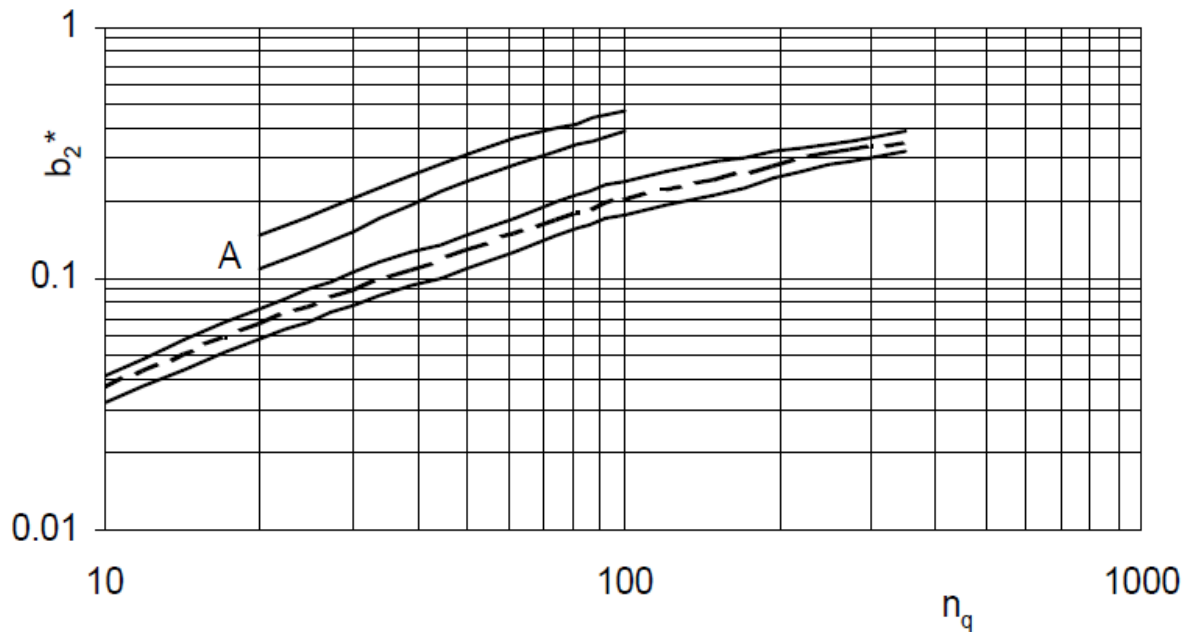


Figure 42: Head coefficient range for different nq numbers. [9]

The outlet geometrical angle (β_{2g}) is now calculated to produce the head value that was defined in the beginning of the process. For nq numbers lower than 40 it is common to keep the angle constant along all the blade high, this does not compromise the effectiveness and simplifies the project. Once again the calculation involves many of the previously defined variables (external diameter, number of blades, outlet width) that can all influence the stability of the curve, this must be eventually checked and the process iterated.

The head comes from the definition of the generic eulerian work exchanged by a stadium [13] considering the reduction of area due to the blocking factor and the linear reduction of the work exchanged due to the slip factor, this happens because the real angle of the outgoing flow is lower than the geometrical angle of the blade. It must be clear that the slip factor does not cause a loss but only a reduction of the specific energy absorbed by the pump.

In the formula it is also present the hydraulic efficiency because the hydraulic losses diminish the real head produced. The angle is initially assumed (in most of the real projects it is inside a range of 20-27[°]) to perform the following calculations:

At first the slip factor (γ) is calculated using the following formula suggested by [9]. According to the author: "This is the most accurate formula known in literature. [...] Other attempts to improve the accuracy of the correlation through additional parameters [...] have failed so far. Although these parameters have some influence, it is not sufficiently systematic and, consequently, obscured through additional 3D-effects of the flow."

$$\varepsilon_{lim} = \exp \left\{ -\frac{8,16 * \sin \beta_{2g}}{N_{blades}} \right\}$$

$$k_w = 1 - \left\{ \frac{(D_{1m} * D_2) - \varepsilon_{lim}}{1 - \varepsilon_{lim}} \right\}^3$$

$$\gamma = 0,98 * \left(1 - \frac{\sqrt{\sin \beta_{2g}}}{N_{blades}^{0,7}} \right) * k_w$$

If $(D_{1m} * D_2) \leq \varepsilon_{lim}$, then kw must be equal to 1.

The value of outlet cross section and the outlet blocking factors are calculated as follows.

$$A_2 = \pi * b_2 * D_2$$

$$\tau_2 = \frac{1}{1 - \frac{N_{blade} * e}{\pi * D_2 * \sin\beta_{2g} * \sin\lambda_{LA}}}$$

Here $\lambda_{LA} = 90 [^\circ]$ because the blade is supposed to be perpendicular to the hub shroud.

Now the head can be calculated.

$$H = \frac{\eta_h * u_2^2}{g} * \left\{ \gamma - \frac{Q}{A_2 * u_2 * \tan\beta_{2g}} * \left[\tau_2 + \frac{(A_2 * (D_{1m} * D_2) * \tan\beta_{2g})}{A_1 * \tan\alpha_1} \right] \right\}$$

β_{2g} must be changed until the searched head is attained. In this process it is also preferable to pay attention for the limit of $\frac{W_2}{W_{1internal}} > 0,7$ to be respected, this “De Hallen criterion” controls the risk of premature stall and efficiency losses. W_2 can be calculated in the following way:

$$W_2 = \frac{\frac{Q_{tot}}{A_2}}{\sin\beta_{2g}}$$

The blade thickness “e” is limited by the structural stresses and the production system. The lower limit for cast impellers blade is considered to be 3÷5 [mm], and, in general, structural considerations impose a minimum value of $e_{min} = 0,016 * D_2 = 2,5 [mm]$. In the current situation the blade has a thickness of 2,6 [mm] and since no structural nor productive problems have ever been noticed, there is no point in changing it.

The leading edge profile is semi-circular in the current project, this shape is the simplest one but it does not create ideal inflow conditions. The simple round shape could be chosen only for low demanding applications but in all the other cases an elliptical geometry is preferred. Long wedge like profiles perform their best only in a narrow range around the BEP where the flow is almost chock-less, far from it the jump of pressure behind the blade rises too much. In figure 43 the three possible shapes are shown.

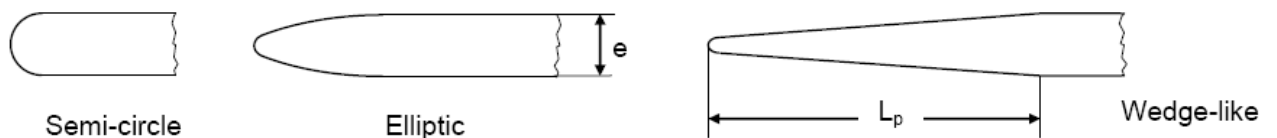


Figure 43: Possible shapes of the leading edge.

The trailing edge profile must undergo to some considerations about the productive simplicity and the further operations on the impeller. The most common feature for small machines is to conserve the full blade thickness up to the trailing edge; here the blade is cut as the circumference is. This geometry is equal to the one of the smaller models that is obtained by the reduction of the external diameter. For this reason and for simplicity-wise, the simple cut trailing edge will be used.

The blade load is calculated using most of the previous dimensions. A simple load criteria that is mainly influenced by the number and length of the blades, permits a more consistent approach and a verification of the quality of the design. This is calculated as follows and can must be inferior to 0,9.

$$\xi = \frac{\pi * \Psi_{opt}}{N_{blades} * L_{blade} * D_2 * \sqrt{\varphi_2^2 + \left(1 - \frac{\Psi_{opt}}{4} * \left(1 - \frac{\sin \varepsilon_{MS}}{N_{blades}}\right)\right)^2}} < 0,9$$

$$\varphi_2 = \frac{W_{2m}}{u_2}$$

The value of ε_{MS} is the angle between the axial direction and the mean direction of the meridian channel, it is equal to 0 [°] for axial machines and 90 [°] for perfect radial machines. It comes on its own that the length of the blade can only be determined after the 3D model is drawn. The process has to be iterated till an acceptable value of the coefficient is attained.

Throat area A_{1q} is the cross section at the inlet of the blade channel, it is closely related to the acceleration of the flow that enters the channel. This acceleration must be kept both over a certain limit to prevent an early recirculation and under another limit to reduce cavitation problems at high flow. The throat area must be selected so that the following limit is respected:

$$0,75 < \frac{W_{1q}}{W_{1m}} < 0,85$$

Where W_{1q} and W_{1m} are the mean relative velocities before and after entering in the blade channel.

The width of the outlet blade channel “ a_2 ” is the smaller distance between the trailing edge of a blade and the previous blade. To obtain a certain slip factor (and hence the volute head) the a_2 value should match the β_{2g} . In the practical experience, this is ensured if the following limit is respected

(with $\beta_{2a} = \arcsin\left(\frac{a_2}{\pi * \frac{D_2}{N_{blades}}}\right)$):

$$0,70 < \frac{\sin \beta_{2a}}{\sin \beta_{2g}} < 0,9$$

The main dimensions of the meridian section are shown in fig.44 and can be calculated using the following expressions:

The axial extension Z_e can be calculated as:

$$Z_e = (d_2 - d_1) * \left(\frac{n_q}{74}\right)^2$$

The internal curvature radius can be calculated as:

$$R_{Ds} = (0,6 \div 0,8) * b_1$$

Where

$$b_1 = \frac{d_1 - d_n}{2}$$

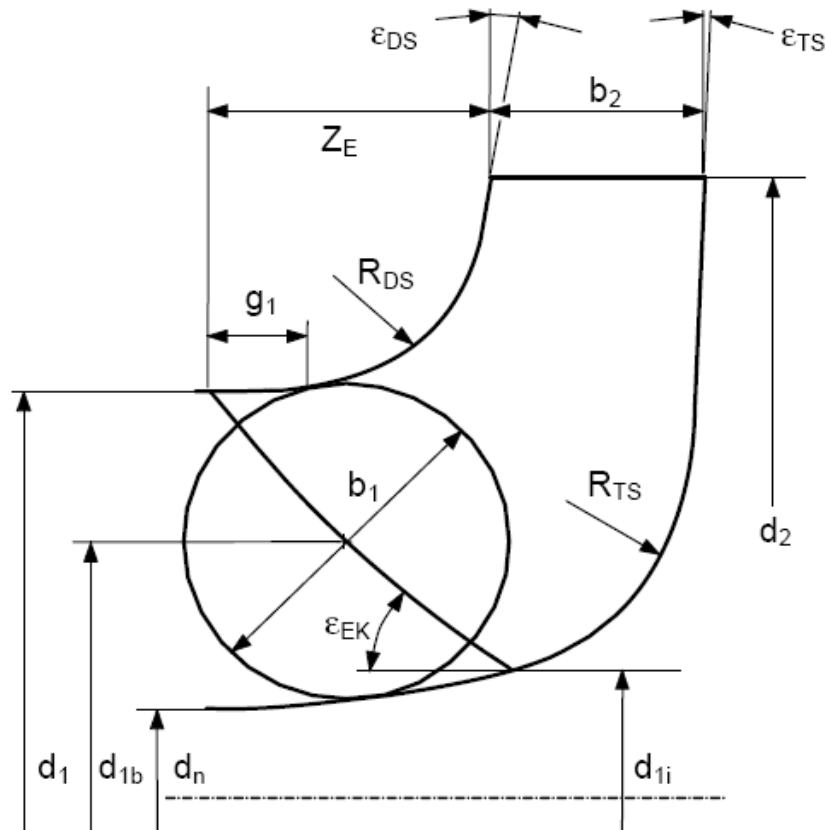


Figure 44: Meridian section and main dimensions.

The leading edge should be located inside the eye of the impeller to create more favorable flow conditions. The first stream line, the one near the front shroud, should be located at a minimal distance "g" from the curved region.

$$g = (0,2 \div 0,3) * b_1$$

The angles ϵ_{DS} and ϵ_{TS} define the shape of the front and rear shroud near the outlet section. These dimensions affect the velocity distribution inside the channel. For pumps with a nq number of less than 20 it is common to have $\epsilon_{DS} = 0 [^\circ]$ and $\epsilon_{TS} = 0 [^\circ]$. For bigger machines, the two values can grow up to 20 [°], with $\epsilon_{DS} > \epsilon_{TS}$.

The procedure seen till now helps in the design of a new pump and the limits are suggested to have a better predictability of the hydraulic performances.

4.2.2 Definition of the impeller

The drawn of the impeller should follow some principles relative to both the blade channel and the blade itself. The meridian section is linked with the flow distribution across the blade high and a lot of effort must be put to ensure that all the variations are as smooth as possible. An eye must be kept on inner and outer stream lines and passage section.

The high of the channel must change continuously from b_1 to b_2 following a law that helps avoiding sudden changes. As a general rule the value of “ b ” should diminish from the inlet to the outlet to contrast the radial deceleration of the flow.

The shape of the leading edge has some influence on the part-load behavior and can be modified according to the particular working conditions. For a single stage, overhung pump with an axial entry, it is suggested an ε_{EK} angle within the range of 30-40 [°], a bigger value would force to chose a high β_{1g} internal angle while a low value causes stability problems in the head characteristic curve.

The design of the blades determines the geometry of the blade along the stream lines so that the inlet and outlet angles are obtained. This geometry is defined trough the evolution of the tangential angle (β) as function of the radial position. The tool used for doing this is the ANSYS tool called Blade Gen, it allows defining at first all the geometrical dimensions and then to change the shape of the blade acting directly on the β curve that is a Bezier curve which number of nodes can be defined by the user. The Bezier curve is particularly useful for this job because it automatically imposes the congruence of the derivate in every node that is considered. When the β curve is changed, the program also automatically changes the θ curve. The angle θ is the one (with respect to the center of the impeller) between the beginning of the blade and the considered element.

The same operation has to be repeated for more streamlines, in our situation, as it is common for smaller machines, just two of them are considered, the most internal one that lies on the hub shroud and the most external one that lies on the front shroud. Bigger machine can also refer to more stream lines. The program also does automatically the next step that is, for every radial position, the linear connection between the two extreme part of the blade high. The three dimensional geometry of the blade is now completely determined. In fig. 45 are shown the β and θ curves for both the stream lines that define the blade. It is also possible to see the already mentioned difference in distribution of the β angles that is growing or decreasing according to the position of the considered stream-line. The most common range for the θ angle in 7 bladed machines is 100÷130 [°].

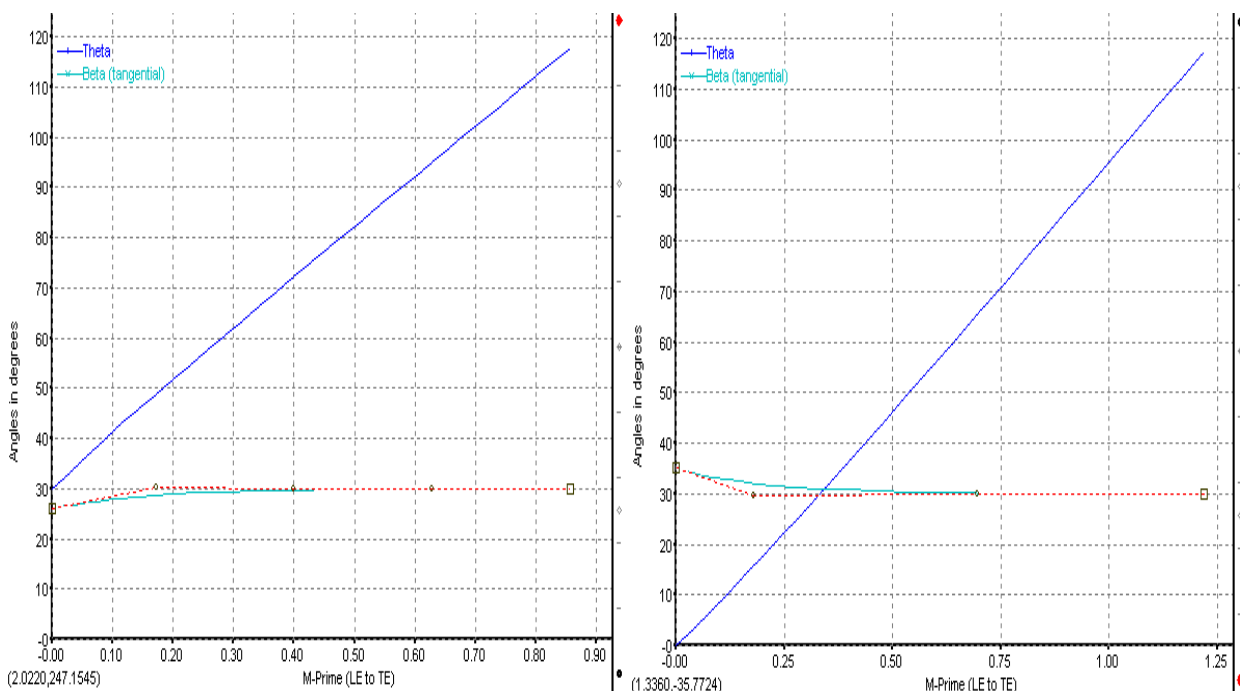


Figure 45: Internal (right) and external (left) blade angles distribution in a version of the pump.

4.3 Application of the procedure to the original impeller

Once the procedure is known, it can be applied to define the optimal geometry during the design of a new machine. This is supposed to be a first step of a subsequent numerical analysis rather than a fully geometrically defined new version. In other words, it is more a direction to follow than a precise indication. But there is another possible application of this procedure: by starting from the data of the original design it is possible to calculate the optimal geometry for those particular conditions. In this way the old value can be confronted with the new and some considerations could be derived from the comparison.

The calculations are here done using the following input data coming from the measure on the original model: flow rate of maximum efficiency QBEP=5,5 [l/s]; head of maximum efficiency HBEP=29 [m]; rotational speed 2900 [rpm]; external diameter D2=155 [mm]; inlet hub diameter Dn=30,2 [mm]; number of blades Nblades=7. The leading edge geometry is maintained constant and only the angles are changed in order to show the difference between them and the optimal value.

Geometrical value	Measurement unit	Original project value	Suggested value	Difference [%]
n	[rpm]	2900	2900	-
Qopt	[l/s]	5,5	5,5	-
Hopt	[m]	29	29	-
nq	[-]	17,3	17,3	-
Dw shaft diameter	[mm]	18,0	18,0	-
N blades	[-]	7	7	-
Dn hub diameter	[mm]	30,2	30,2	-
D1ext	[mm]	57,5	67,8	17,9
D1int	[mm]	55,0	55,0	0,0
β_{1gi}	[deg]	30,0	17,7	69,5
β_{1gm}	[deg]	29,0	16,0	81,8
β_{1ga}	[deg]	28,0	14,5	93,0
b2	[mm]	8,2	7,0	17,1
β_{2g}	[deg]	33,0	20,0	65,0
e blade thickness	[mm]	2,6	2,6	-
inlet geometry	[-]	semi-circle	elliptic	-
Trailing edge	[-]	e=cost	e=cost	-
Lblade	[mm]	145	85	70,6
blade load	[-]	0,54	0,93	72,2
a2 outlet width section	[mm]	28,0	-	value too high
Ze	[mm]	4,0	18,4	360,1
b1	[mm]	13,0	18,8	44,8
Rds	[mm]	5,5	12,2	122,4
g	[mm]	-5,0	3,8	232,9
ξ_{ds}	[deg]	10,0	10,0	-
ξ_{ts}	[deg]	0,0	0,0	-

Table 46: Comparison between original value and ideal ones.

Table 46 shows the results of the calculation done following the above explanation. The biggest difference between the original project and the suggested one lies in the angles of the blade. Those in the inlet part are too axial causing high incidence not only at the best efficiency point but, most important of all, at part load operations where the flow is more tangential. The outlet angle is too high and out of the suggested range, this causes the shortening of the blades and therefore the increase of the blade load.

In the meridian view, the channel results to be smaller than what is suggested, not only the inlet and outlet area are smaller but also the radial extension is strongly limited and the front shroud curvature radius is supposed to be way bigger.

It can be concluded that: the blade inlet angles are designed for higher specific speed while the meridian channel is optimized for a lower one. The outlet angles and the length of the blade cause an unacceptable rise of the load.

4.4 Conclusions

The first step in the design of a new geometry is to calculate its main dimensions through the use of a simple method that is based both on sturdy theoretical bases and on the experience. The second element is obtained by applying semi empirical correlations or statistical data (often summarized in graphs). From this values, the impeller can be drawn with a three dimensional designing tool.

In the present chapter a simple method was shown to produce an optimized geometry. The model requires as input the characteristics of head and flow rate in the best efficiency point and from here all the main dimensions are determined, leaving little freedom to the user. The current design-method will be used later in the optimization stage as a generator of first-try optimized geometry.

Another application of the calculation model is to compare its results to the current impeller to see the diversities between the ideal geometry and the current one. From this analysis, it results that some features are not optimized for the specific working conditions: the inlet and outlet angles are too high, the blade is too short and the blade channel has a low axial extension with consequent sharp bends. These differences could cause some additional losses and a new design must consider the suggestions coming from this chapter.

The effectiveness of the method is here only proved by the literature references but its results will be then compared with other methods to have a complete view on the problems of the machine.

Chapter 5: CFD model.

In this chapter will be described the procedure used to obtain the CFD model used to analyze the pump. Results will be discussed in the end.

5.1 Introduction

To optimize the pump we will use an iterative process in which the pump is manually modified after every step of a CFD analysis. Every time the model will be changed on account of the results. To do this it is important to have a CFD model yielding results close to reality, this is the reason why a comparison with the measured data is required.

After the model is developed it must prove results close enough to the real values to be considered a valid instrument for understanding the complex phenomena that occur inside the impeller. This knowledge is important to determine what has to be changed, how and how much. The relative enhance of the efficiency characteristics will be considered as an index of the optimization, while the absolute value have less importance.

The use of a CFD model was carried out in cooperation with the technical staff of Institute for Hydraulic Fluid machinery of Graz University of technology. For what concerns this work, the CFD model will be considered just as a tool, a black box in which the geometry is entered and from which come the result files; therefore this work won't go too much into the theoretical background and details of the numerical simulations of the CFD program.

A general presentation of the software is anyway necessary to understand the main passages of the work that have been done.

The commercial software **ANSYS-CFX**[®] is a powerful CFD code commonly used both in the academic and in the commercial field. It is composed of four different components:

- **CFX-Turbogrid**[®], is the tool used to generate the calculation domain and the mesh in which the equations are solved.
- **CFX-Pre**[®]. Here the domains can be created along with the boundary and initial conditions. Also the type of fluid and turbulence models can be selected here.
- **CFX-Solve**[®], starts the calculation and allows the user to follow the evolution of the main variables.
- **CFX-Post**[®], permits the visualization of the results and some successive operations on the measured quantities.

This program guides the user step by step in the definition and solution of the cases. Although it permits the solution of even complicate problems, it always requires a good basic knowledge of fluid dynamics.

5.2 CFD Theory

5.2.1 Balance equations

The finite volumes method is the base for solving fluid dynamic problems in a numerical way. It is based on the time and space discretization of the balance equations of mass, energy and momentum:

$$\frac{\partial \rho}{\partial t} + \nabla \cdot (\rho \mathbf{V}) = 0$$

$$\frac{\partial(\rho e_T)}{\partial t} + \nabla \cdot (\rho e_T \mathbf{V}) = \rho \bar{g} \cdot \mathbf{V} - \nabla \cdot q + \nabla \cdot (\bar{\tau} \mathbf{V}) - \nabla \cdot (p \mathbf{V})$$

$$\frac{\partial(\rho h_T)}{\partial t} + \nabla \cdot (\rho h_T \mathbf{V}) = \rho \bar{g} \cdot \mathbf{V} - \nabla \cdot q + \mathbf{V} \nabla \cdot \bar{\tau} + \bar{\tau} : \nabla \mathbf{V}$$

Where the term $\bar{\tau} : \nabla \mathbf{V}$ represents the dissipation function and takes account of the conversion of the kinetic into internal energy.

For a Newtonian fluid, the viscosity shear stress tensor is known to be:

$$\bar{\tau} = 2\mu \bar{d} - \frac{2}{3}\mu \bar{I} \nabla \cdot \mathbf{V} = \mu(\nabla \mathbf{V} + (\nabla \mathbf{V})^T) - \frac{2}{3}\mu \bar{I} \nabla \cdot \mathbf{V}$$

5.2.2 Reynolds average and “closure” of the problem

The turbulence is a fluctuation in the variables (speed, pressure, temperature...) of a three-dimensionally moving fluid. It is caused by the non linearity of the Navier-Stokes equations and it is triggered by fluid dynamic instabilities that, in certain conditions, can cause the creation of non stationary vortexes; these cause a viscous dissipation inside the smaller vortexes [11].

If all the scale of turbulence has to be analyzed, then the only possibility is to use a direct numerical simulation (DNS) that requires a practically non affordable computational cost.

When the aim is to understand the mean characteristics of the turbulent flow, a statistical (and much less time consuming) approach can be followed; this is the RANS (Reynolds Average Navier-Stokes). Following this approach, every variable of the flow is considered to be the sum of two terms, the mean value and the fluctuation around the mean: $f = \bar{f} + f'$.

When the mass conservation equation is averaged over the time, it results in a new equation formally equal to the former. This does not happen for the momentum conservation equation because of the non linear terms. The fluctuation terms (that are different from zero even is averaged) takes the name of Reynolds stresses and have to be modeled somehow in order to close the problem. This thinking, which can also be done in the same way for the energy conservation equations, leads to the formulation of new equations to balance the presence of these new variables.

The trace of the Reynolds stresses tensor is:

$$tr(\bar{\bar{r}}) = -\rho(\overline{u^2} + \overline{v^2} + \overline{w^2}) = -2\rho k.$$

Where the term k is the turbulent kinetic energy. For this value a balance equation can be written:

$$\frac{\partial(\rho k)}{\partial t} + \nabla \cdot (\rho k \bar{\mathbf{V}}) = \bar{\bar{r}} : \nabla \bar{\mathbf{V}} - 2\mu(\overline{\overline{\overline{d}} : \overline{\overline{\overline{d}}}}) + \nabla \cdot (-\overline{P' \mathbf{v}} + 2\mu \overline{\overline{\overline{d}} \mathbf{v}} + \frac{1}{2} \overline{\mathbf{v}^2 \mathbf{v}}).$$

The variable that has to be modeled is the dissipation term, $\varepsilon = \mu(\overline{\overline{\overline{d}} : \overline{\overline{\overline{d}}}})$.

When the k- ε model is used, the flow cannot be solved on the surfaces because there the term ε is singular. For this reason it has been introduced a new parameter: the turbulent frequency ω ($\omega = \frac{\varepsilon}{C_{\mu}^* k}$) that is connected to the dimension k. For this term can be written a conservation equation that has a solution on the wall but is not very accurate in the far flow [15].

This leads to the construction of the SST (shear stress transport) model that behaves like the k-omega model near the wall but then it gradually becomes a k-epsilon one.

The effective viscosity is defined to be the sum of two terms: the flow viscosity (μ) and the turbulent viscosity (μ_t). The SST model uses the two following balance equations for the values of k and ω :

$$\begin{aligned} \frac{\partial(\rho k)}{\partial t} + \nabla \cdot (\rho \mathbf{V} k) &= \nabla \cdot \left[\left(\mu + \frac{\mu_t}{\sigma_{k3}} \right) \nabla k \right] + P_k - \beta' \rho k \omega + P_{kb} \\ \frac{\partial(\rho \omega)}{\partial t} + \nabla \cdot (\rho \mathbf{V} \omega) &= \nabla \cdot \left[\left(\mu + \frac{\mu_t}{\sigma_{\omega 3}} \right) \nabla \omega \right] + \\ &+ \alpha_3 \frac{\omega}{k} P_k - \beta_3 \rho \omega^3 + P_{\omega b} + (1 - F_1) 2\rho \frac{1}{\sigma_{\omega 2 \omega}} \nabla k \nabla \omega. \end{aligned}$$

This model comes from the one of Menter but a so called blending factor is also used to limit the maximum value of turbulent viscosity:

$$\mu_t = \rho \frac{\alpha_1 k}{\max(\alpha_1 \omega, SF_2)}$$

Here the value of F1 and F2 are two factors whose value is 1 close to the wall and slowly decreases till 0 in the end of the boundary layer, here the model becomes again a regular k- ε . The parameters β' β_1 β_2 α_1 α_2 σ_{k1} σ_{k2} $\sigma_{\omega 1}$ $\sigma_{\omega 2}$ are constants of the model. The terms P represent the production of turbulence due to viscosity and can be calculated [2].

This model is recommended in the user's guide of the software in the light of a big amount of comparison between experimental tests and numerical simulations. Also the experience of the Hydraulic Fluid Machinery Institute confirms the value of this model in situations similar to the one we are considering.

For the particular problem treated in this work, a default inlet relative intensity of the turbulence is chosen; this represents a value of $I = \frac{u}{U} = 0,037$ and permits to define the inlet turbulent conditions.

5.2.3 Boundary layer: the y^+ factor

The universal velocity profile of the flow near the surface is described in figure 47. There is possible to recognize:

- a viscous laminar sub-layer where the velocity profile is linear
- an intermediate region called buffer layer
- a logarithmic region where the speed has a logarithmic evolution

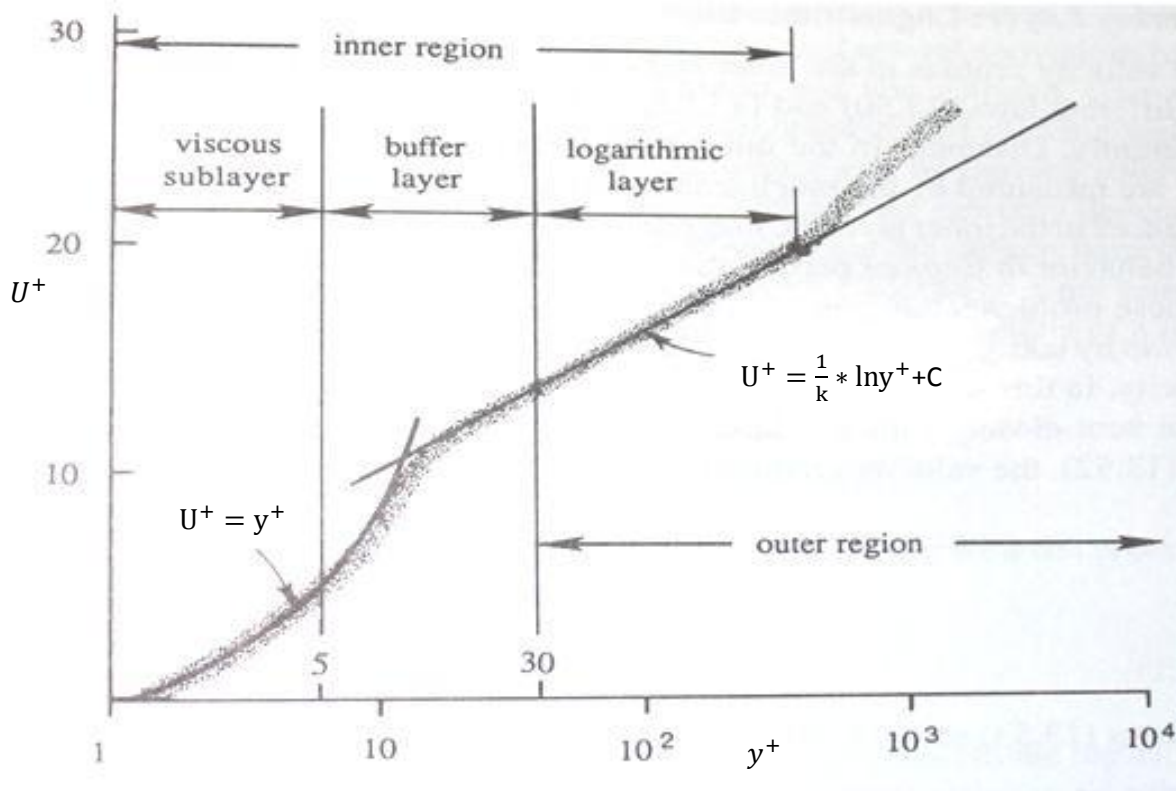


Figure 47: Velocity profile of the flow near the surface. Elaborated from [10]

When the analysis is focused on the 2D turbulent flow, the concept of mixing length “ l_T ” can be introduced: a vortex of the dimension l_T causes the fluctuation of the velocity that is proportional to $\frac{\partial u}{\partial y}$

and to l_T . Two dimensional scale are introduced: the shear velocity: $u_\tau = \sqrt{\frac{\tau_w}{\rho}}$ and the viscosity length $\delta_w = \frac{\mu}{\rho * u_\tau}$. By defining the terms $y^+ = \frac{y}{\delta_w}$ and the $U^+ = \frac{u}{u_\tau}$ and by assuming that near the wall the mixing length is proportional to the distance from the wall $l_T = k * y$ and therefore $l_T^+ = k * y^+$, then the 2D equation of momentum conservation can be written in the following way:

$$\left(1 + k^2 (y_T^+)^2 \frac{\partial U^+}{\partial y^+}\right) \frac{\partial U^+}{\partial y^+} = 1$$

Close to the wall, in the laminar sub-layer, the molecular diffusion is way bigger than the turbulent mixing, there the Reynolds stresses can be neglected causing $U^+ = y^+$: this means a linear increase in the speed with the perpendicular distance from the wall.

At a bigger distance from the wall the Reynolds stresses are the most important and therefore it can be written: $U^+ = \frac{1}{k} * \ln y^+ + C$ that is the logarithmic wall function where k and C are the constants related to the external pressure gradient.

The importance of the parameter y^+ can be understood in the light of the following explanation: it gives a scale of the velocity profile close to the wall: if $y^+ < 5$ then we are in the laminar sub-layer; if $5 < y^+ < 30$ then we are in the buffer-layer; if $30 < y^+ < 300$ (or more if Re gets bigger) then we are in the logarithmic zone. [10]

For solving the problem close to the wall, the grid must have a value of $y^+ < 1$ in the first cell and $y^+ < 10$ in the first 10 cells to produce a smooth transition to the central part of the flow. When a wall function is used to model the behavior near the wall, it solves the turbulence up to a certain distance. In this situation the use a smaller mesh could cause an error.

5.2.4 The finite volumes method

ANSYS-CFX[®] exploits the finite volume method; this uses the subdivision of the space through the mesh. The mesh produces smaller volumes on which the balance equations are integrated. As an example, it will be explained the 2D method of modeling. The balance equations are written in a conservative way for every volume of the domain:

$$\frac{d}{dt} \int_V \rho dV + \oint_{\partial V} \rho \mathbf{V} \cdot \mathbf{n} dS = 0$$

$$\frac{d}{dt} \int_V \rho \mathbf{V} dV + \oint_{\partial V} \rho \mathbf{V} (\mathbf{V} \cdot \mathbf{n}) dS = \oint_{\partial V} (-p \bar{\mathbf{I}} + \bar{\boldsymbol{\tau}}) \mathbf{n} dS$$

$$\frac{d}{dt} \int_V \rho e_T dV + \oint_{\partial V} \rho h_T (\mathbf{V} \cdot \mathbf{n}) dS = \oint_{\partial V} (K \nabla T + \bar{\boldsymbol{\tau}} \bar{\mathbf{V}}) \cdot \mathbf{n} dS$$

The volume integrals represent the storage terms while the surface integrals represent the flow through the surfaces of the control volume. The surface integrals are calculated in the so called integration knots that are the centers of the surfaces. This discretization process leads to the re-write of the integral equations:

$$V \left(\frac{\rho - \rho^\circ}{\Delta t} \right) + \sum_{ip} \dot{m}_{ip} = 0$$

$$V \left(\frac{\rho U_i - \rho^\circ U_i^\circ}{\Delta t} \right) + \sum_{ip} \dot{m}_{ip} (U_i)_{ip} = \sum_{ip} (P \Delta n_i)_{ip} + \sum_{ip} \left(\mu_{eff} \left(\frac{\partial U_i}{\partial x_j} + \frac{\partial U_j}{\partial x_i} \right) \Delta n_j \right) + \bar{S}_{U_i}$$

$$V \left(\frac{\rho \phi_i - \rho^\circ \phi_i^\circ}{\Delta t} \right) + \sum_{ip} \dot{m}_{ip} \phi_{ip} = \sum_i p \left(\Gamma_{eff} \frac{\partial \phi}{\partial x_j} \Delta n_j \right)_{ip} + \bar{S}_\phi V$$

Here $\dot{m}_{ip} = (\rho * U_j * \Delta n_j)_{ip}$; V is the control volume and Δt is the time step in the stationary situation; Δn_j is the outgoing vector perpendicular to the surface; "ip" is the integration point; the superscript $^\circ$ is the parameter that is considered.

This system of algebraic equations is non-linear (there are products of different variables) and has to be solved in an iterative way doing a linearization every time around the previous try solution and starting from the boundary conditions.

When the system of equations is linearized, it is solved numerically with a Multi-grid Accelerated Incomplete Lower Upper factorization technique [2].

5.2.5 Domain, grid and boundary conditions

Mesh generation is one of the most critical aspects of fluid dynamic simulation. Too many cells may result in long solver runs, and too few may lead to inaccurate results. ANSYS provides a technology able to balance these requirements and to obtain the right mesh for each simulation in an almost automated way.

The meshing environment makes it possible to generate the following mesh types: Tetrahedral; Hexahedral; Prismatic inflation layer; Hexahedral inflation layer; Hexahedral core; Body fitted Cartesian; Cut cell Cartesian. Mesh connectivity is maintained automatically.

ANSYS TurboGrid® software provides designers with mesh creation tailored specifically to the needs of bladed geometries; this means that entering a blade geometry it is possible to automatically generate an appropriate mesh. The program automatically cares about the presence of high geometrical gradients. The software creates high-quality hexahedral meshes that are tuned to the demands of fluid dynamics analysis in rotating machinery. **ANSYS TurboGrid®** imports geometry definitions from blade design software like ANSYS BladeModeler. The software also provides an automatic check of the quality of the mesh to avoid the presence of volumes with an incorrect shape [2].

The treatment of the logarithmic region of the boundary layer is done by means of the relative wall function that has already been described. The linear (also known as near-wall) region is chosen to be treated with another wall function based on empirical formulas that impose suitable conditions without really solving the flow within the boundary layer. In this way a packed mesh is not required saving computational time. It also avoids the need to account for viscous effects in the turbulence model. This model is widely used because of its simplicity and time saving characteristics and it is acknowledged as a reliable method.

In this work it is not of primary interest to analyze the field of motion inside the boundary layer and this is the reason why it is possible to choose the simplest wall function that permits to use the already discussed automatically generated mesh.

The mesh is then changed to have smaller volumes and therefore more accuracy in some important points such as the leading and trailing edge of the blade and the cutwater component of the volute. Also the y^+ factor will be different in these regions.

5.3 Modeling the pump for CFD

The first step in the creation of a CFD model is to design the impeller geometry that has to be investigated and to implement it into the **CFX-Turbogrid**[®] component in order to create the mesh. This is easily archived through to the use of another component of the ANSYS software: **BLADE-GEN**[®]. Using this tool a new impeller geometry is reconstructed with just the knowledge of the main dimensions and the blade angles.

The most important step is the construction of the impeller. The different points of view are by the meridian section (blade channel) and by the blade to blade view. Since there were no accurate drawings available from the company, the geometry of the impeller had to be measured by using a caliper and a radius gauge.

To measure the blade channel, the impeller was opened by taking the front shroud off. The result of the hand measure of the blade channel can be seen in fig.48.

For what concerns the blade, the evaluation of the dimensions was done by printing the section of the

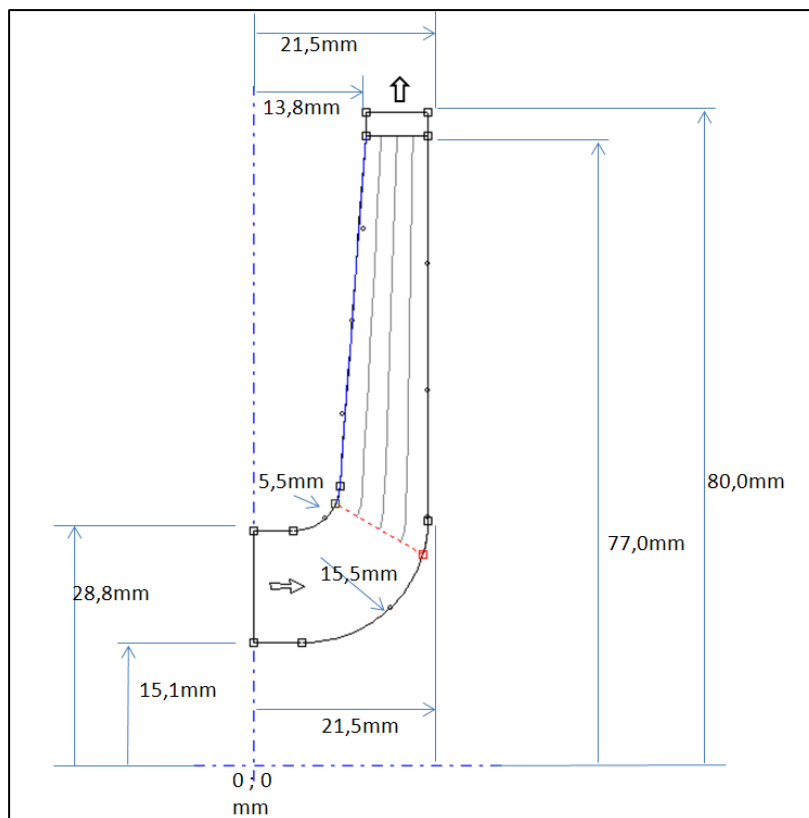


Figure 48: Meridian view of the original impeller.

impeller on a paper and then measuring the angles. The two dimensional geometry of the blade was of great help during this procedure. To improve the accuracy, the angles were not only measured with a protractor but also by means of the software “**WINDIG**” that permits to evaluate the exact position of the points in a picture. From this analysis it results that the outlet angle has a value of 33°, the inlet angles have a value of 27° and 40° (the blade starts in two separate points and the one on the hub shroud is placed to a lower radius (from which the bigger inlet angle), the back blades have inlet and outlet angles of the same value, equal to 45°.

These data are not enough to reproduce the blade in **BLADE-GEN**[®], it is also required to change the law

with which the angle changes along the radius. This law is difficult to measure and the way to proceed is through trial and errors. The software allows defining the geometry of the blade as a Bézier curve in which the control point can be moved to obtain the desired shape. Since it is a Bézier curve, the changing in the angle is always very smooth. Fig.49 shows the result of this iterative process.

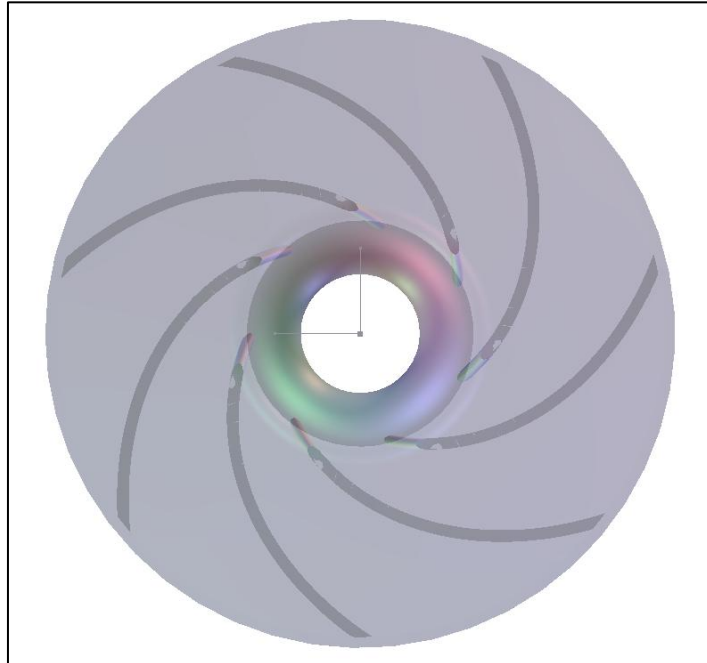


Figure 49: Frontal view of the original impeller reconstructed with Blade Gen.

Fig.50 shows the overlap between this model and an ink print of the original impeller section. The superposition is not perfect but the angles are respected, the overall length is almost equal and the angular extension of the blades is the same. This is the best of a long series of previous versions and is the most similar to the real machine.

The differences will certainly cause an imperfect reproduction of the flow conditions but the deviation is supposed to be very small if not even negligible.

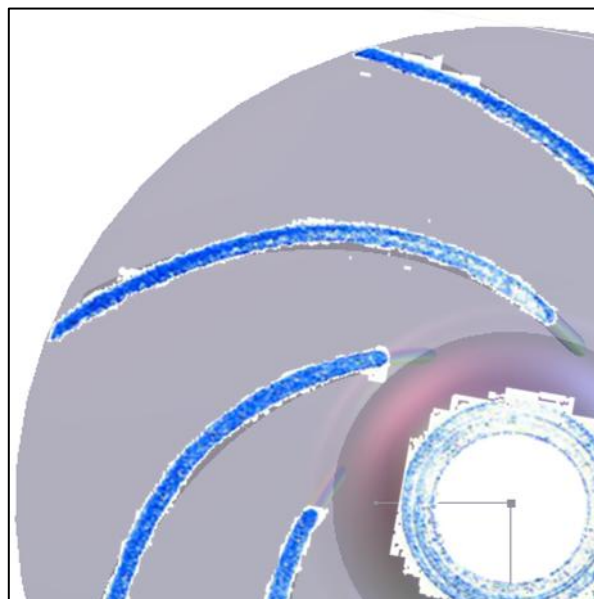


Figure 50: Comparison of original impeller and reconstructed one.

The volute was reconstructed using the drawings provided by the company which are shown in fig.51. This operation was done using a software called "Pro/ENGINEERING". Once more, the dimensions of the CFD model could not be exactly the same of the real object but the difference is minimal and should not cause problems during the simulations.

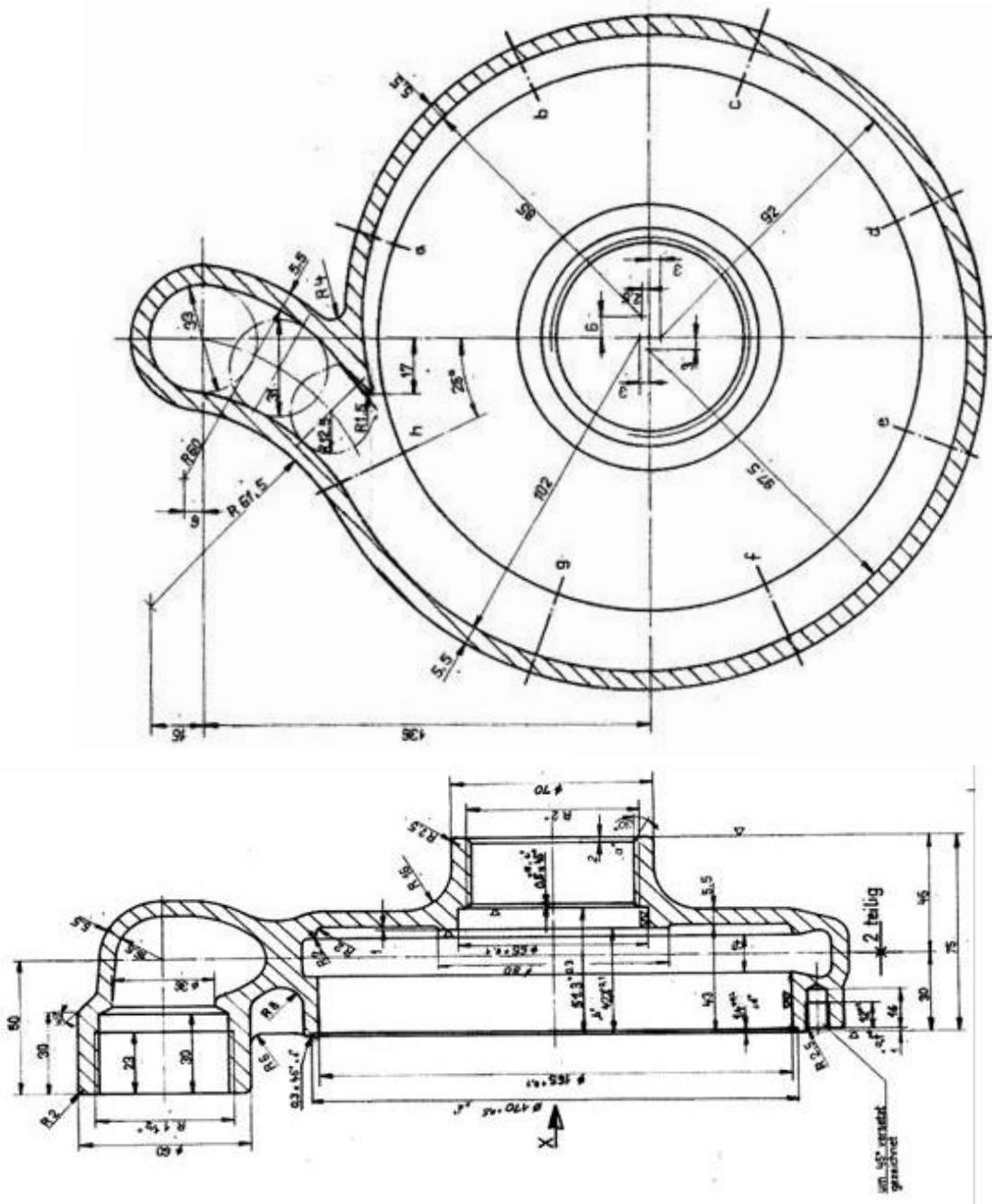


Figure 51: Drawings of the volute.

The final 3-D model is the sum of the single parts: volute, impeller, outlet tube, inlet fluid section, back shroud and frontal shroud.

All of these components are connected in the **CFX-Pre**[®] so that the flow can virtually pass through. To reduce the computational effort, the impeller is represented just by a single blade channel. Periodic boundary conditions on the side faces allow a realistic simulation of the flow inside a pump.

Fig. 52 is shows the 3-D model without the rear and frontal blades, to make it visible the space around the blade. The figure also shows the annulus from which the flow enters and the outlet section placed on top of the outlet tube, after the bend. The blade actually consists of an empty space but the flow cannot trespass that border. The blade channels tip is smaller than the gap inside the volute and it is placed symmetrically inside it.

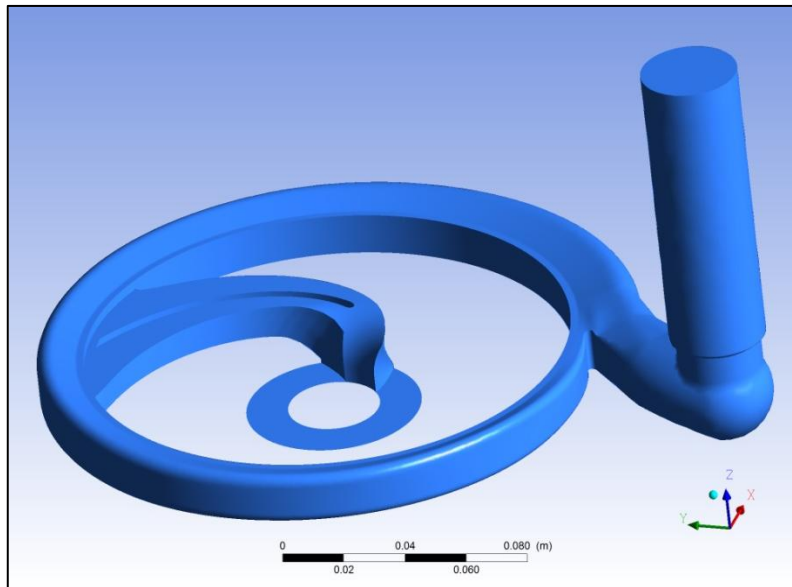


Figure 52: Three dimensional view of the complete model.

With the closer snap of fig.53 it is possible to notice the end of the blade and the interaction with the volute. The walls corresponding to the front and rear shroud have been removed to show the height of the blade. In the outlet of the impeller it is possible to notice a small space of around 4 [mm] caused by the smaller dimension of the impeller with respect to the volute. In that region it was necessary to define an additional volume in which the equation will be solved.

The wire frame makes evident the symmetrical position of the blade in the volute gap.

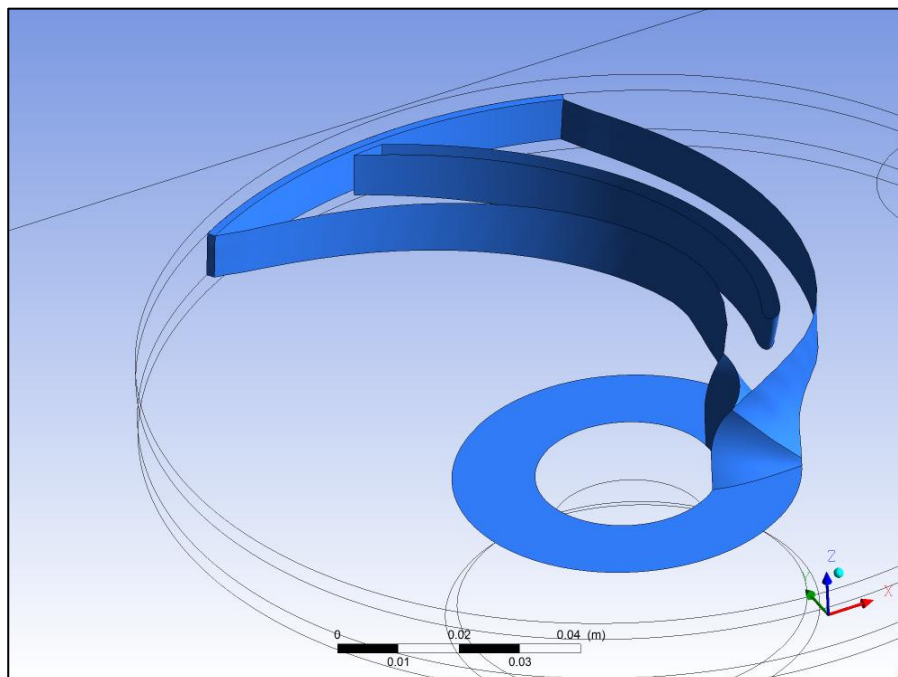


Figure 53: Three dimensional view of the detail of the blade.

The mesh was created using a **CFX-Turbogrid**[®] tool that automatically creates a mesh on the Blade Gen model.

The investigated mesh has the characteristics shown in table 54:

Mesh-part	Grid-type	Mesh-quality	Number of nodes	Max. y+ for optimum
Intake part	Hexaeder	Medium	570.000	35
Impeller	Hexaeder	Coarse	69.800	110* / 25**
	Hexaeder	Medium	130.000	95* / 20**
	Hexaeder	Fine	190.000	90* / 15**
Volute casing	Hexaeder	Very-fine	470.000	65* / 12**
	Tetraeder	Medium	615.000	90° / 60°°
	Tetraeder	Fine	1.000.000	90° / 50°°
	Tetraeder	Very-fine	1.500.000	

Table 54: Characteristics of the investigated mesh.

Comments:

- * ... Lowest y+: only at the trimmed outlet part of the blade
- ** ... Averaged y+: valid for the rest of the blade channel
- ° ... Lowest y+: only at the cutwater-region
- °° ... Averaged y+: valid for the rest of the walls

It was noticed that there were no observable changes in the values of efficiency and head of the of the solution when the quality of the mesh changed between “fine” and “very-fine”, both in the impeller and in the volute. For this reason the models used from now on will all have a “fine” mesh with a y+ parameter of 90* / 15** for what concerns the impeller and 90° / 50°° for the volute.

5.4 Creation of the CFD model

After the creation of the different parts of the pump, the domains and the boundary conditions have to be defined. Particular attention should be paid to the wall conditions, the turbulence model and the interfaces between rotating and static domains. The software used to complete this part of the procedure is **CFX-Pre**[®]. Here the domains can be created along with the boundary and initial conditions. Also the type of fluid and turbulence models can be selected here. An important passage is the assembly of the single parts that were discussed in the previous paragraph; this step requires the definition of the interfaces, of the flow conditions and of the relative movement of the parts. For simulating in the most realistic way the entering conditions, it was created an inflow domain that is a square with the side of 50 [cm], whose walls are defined with the “opening” conditions and perpendicular flow. This means that the water can flow in and out of the same surface. The possibility from the flow to adapt itself to the real entrance of the machine is the best way to reproduce this phenomenon.

The turbulence model that was used in all the cases is the shear stress transport (SST) turbulence model. This is an alternative choice to the classical k-ε model but it is better for near wall treatments and to describe separated flows and adverse pressure gradients; at the same time it is as computationally economical as the k-ε method. An automatic wall treatment was used for the near wall flow.

The wall conditions require the definition of the surface roughness condition because the interference between the flow and the walls affects the behavior of the boundary layers. Different possibilities can be faced for what concerns the roughness of the walls: since a measure of this value is not available, the

only possibility is to try different realistic values and to analyze the influence on the final result. For the walls inside the blade channels, a value of $\epsilon < 0,002 \div 0,001$ [mm] is likely to be the real one [9]. From the theoretical loss analysis it is clear that this value is negligible and a hydraulically smooth wall can be chosen as well. The roughness of the volute, as opposite, is all but negligible: not only the velocity inside this component is high, it is also made of cast iron, a procedure that lets the surface far less uniform and smooth. For these reasons, different models have to be tested in order to find a value of roughness that permits good results. This value will be inside the range of $\epsilon = 0 \div 0,5$ [mm].

The analysis done is a Steady State one, since it can produce good results (as proved by the experience of the technical staff of the Fluid machinery department and by [3]) and it would have been too much time expensive the use of a transient simulation.

The interaction between the rotor and the (asymmetric) volute is modeled thank to the use of a frozen rotor approach: the rotor consists of a single blade with the conditions of periodicity on the sides, the simulation is stationary with the relative position between the components kept constant. This method is time saving and proved good results [2] but fails in the description of the transient phenomena of the periodic interaction with the volute.

The simulation has to be repeated in multiple flow conditions in order to get a complete view over the behavior of the pump. The points examined are at the following flow rate: $Q = 1; 2; 3; 4; 5; 6$ [l/s]. It is useless to study higher flow rate conditions because they are out of the real operating field of the machine. The rotating speed is always 2900 [rpm].

Different models

The procedure to find a model that is close enough to the real behavior of the machine is described here.

Many different models are created with small differences in the superficial roughness. These models are tested in 5 different flow conditions to reproduce the characteristics curves in the range of flow that is of the greatest interest for the company. The characteristic curves will be compared to each other and to the measured values to determine which CFD model is the most realistic and can be used for a successive optimization.

The following different models were tested:

-Model "A" has a hydraulically smooth volute and does not have the back and front side vanes. The volumetric losses are then neglected and so are the disk friction losses. This model is the most simple and easiest to calculate. Even if it is not accurate at all, it permits to keep the focus on the flow inside the two main components: the volute and the impeller.

-Model "B" is a model comprehensive of the back and front side vanes. This permits us to analyze the effects of the flow in the side vanes and the volumetric losses. The volute has a roughness of $\epsilon = 0,3$ [mm]. This value is on the border of the range that is suggested for this kind of applications and could be referred to old or rusty pipes. This model is expected to produce the worst performances in term of head and efficiency.

-Model "C" is a model comprehensive of the back and front side vanes. The volute has a roughness of $\epsilon = 0,1$ [mm] that is intermediate between a hydraulically smooth component and a very rough one. This value is probably more close to the real characteristic of the pump.

-Model "D" is a model comprehensive of the back and front side vanes. The volute is hydraulically smooth.

All the models are tested according to what already explained and their characteristic curves of head and efficiency are reported in fig. 55 and 56. With this graphs it is possible to compare the calculated curves with the measured ones to derive some conclusions about the accuracy of each model.

The characteristic curves of the model "A" are clearly unrealistic both for the value of head and for the efficiency that is the 22% higher than in the current best efficiency model.

Model B is the one with the worst characteristics and the difference in the head values are too high to consider this model as a good reference for a successive optimization.

The two models that produce values closer to the reality are the model "D" and "C". The model "C" is the most similar and both the geometry and the roughness seem to be close to the real pump. The head calculated by the model C is inside the 5% of measured values, except for the last two points at 5 and 6 [l/s] of flow rate. The efficiency is inside a range of 6,5%.

The Model "D" has less physical meaning because of the lack of roughness but it could be considered as an extreme limit of a range in which the measured characteristics are always contained. Its values are all in all not so far from the measure especially for what concerns the head.

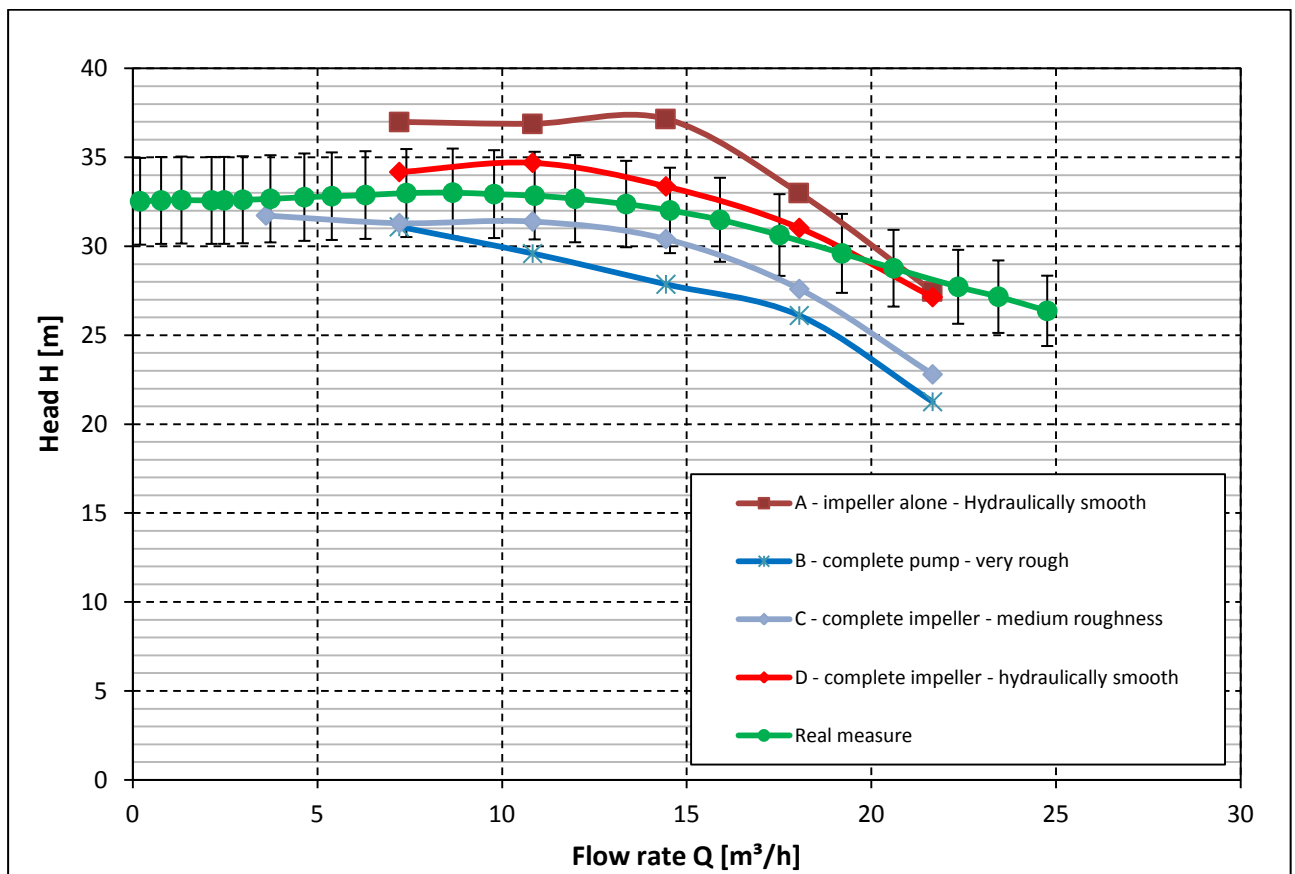


Figure 55: Characteristics of head of some of the simulated models.

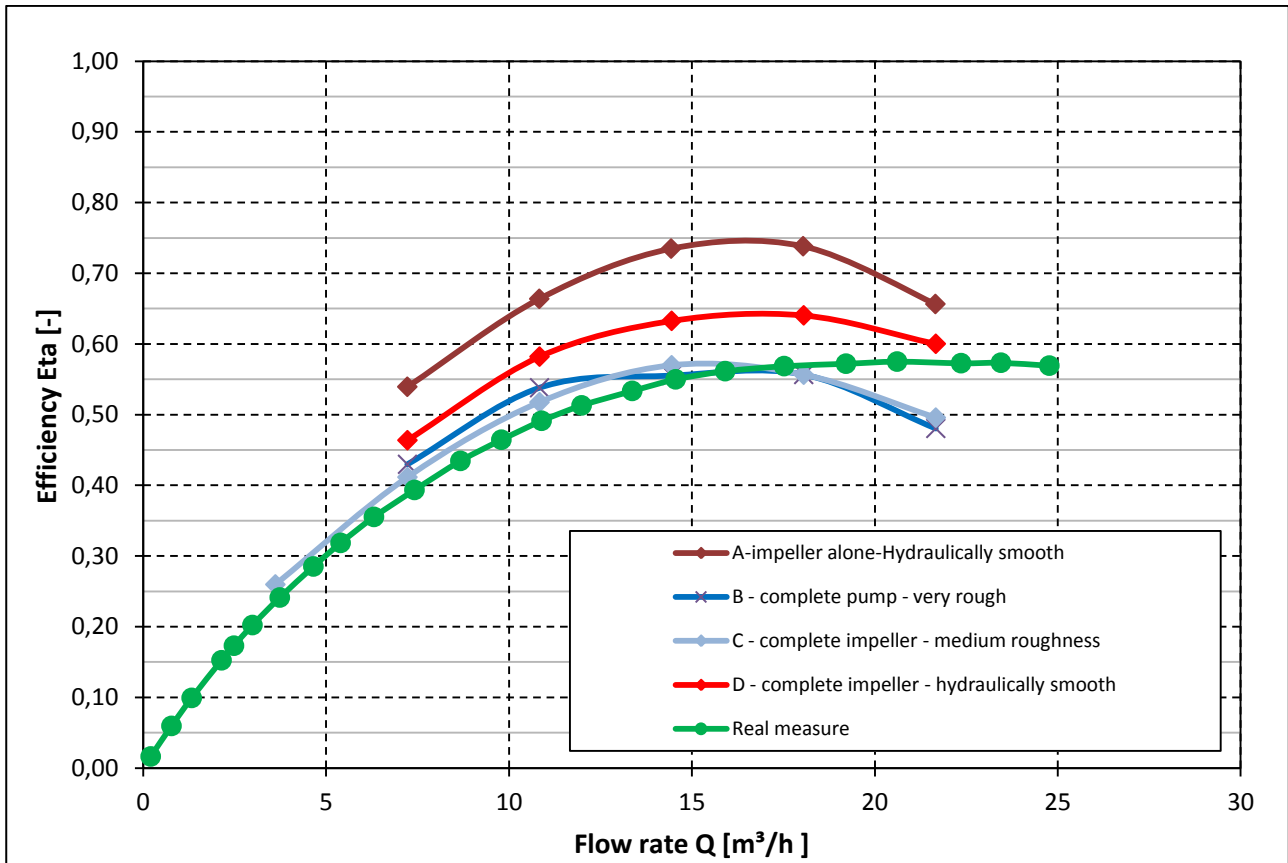


Figure 56: Characteristics of efficiency of some of the simulated models.

All the models show a drop of the values at the operation points of 5 and 6 [l/s] of flow rate, this causes a deviation between the measured values and the calculation. The shape of the curves is similar in the first part but then it becomes different. The systematic difference suggests the presence of an error that could be in the geometrical model or in the simulation.

One possible cause of error could lie in the details that could not be reproduced perfectly due to the use of too simple drawings that lack of information to cope with the complexity of the three dimensional geometry. Another reason may be that the simulation is stationary, meaning that the calculation is done in a precise position of the blade while, during the rotation, the characteristics should show a pulsation. As a result, the calculated value could be slightly distant from the mean value of efficiency.

Looking at the results of the calculation, it must always be remembered that small differences between the real model and the CFD geometry can occur. It is not surprising that even the best model always shows a deviation from the real values. The differences are anyway very small and the found model could be considered appropriate for the simulation of the pump.

To summarize what has been done in this chapter, we look back over the major steps. The physical model of the pump was reconstructed component after component and the interactions between these components defined according to the real flow conditions. Different CFD-models have been created with small differences in the roughness and in the construction. All these models have been tested and their characteristic curves drawn. From the comparison with the measured values, it is possible to identify the models that behave in the more realistic way. Actually the real results should be something between the model "C" (volute with roughness $\epsilon=0,1$ [mm]) and the model "D" (hydraulically smooth volute).

Summary for the CFD-models:

The followings is a summary of all the characteristics common to all of the models discussed above:

Analysis Type:	Steady State
Turbulence Model:	SST-model (with automatic wall treatment)
Domains:	-Stationary: Intake part, Volute casing -Rotating (n=2900rpm): Impeller, front and back cavity
Boundary Conditions:	-Side walls of intake box: Opening with a relative pressure of 0bar -Outlet of the spiral casing: Outlet with definition of mass flow rate -Outlet at back cavity (leakage): Opening with a relative pressure of 0bar
Interfaces:	Frozen-Rotor interfaces between stationary and rotating parts
1-channel-model:	Definition of periodic interfaces between the side surfaces of the blade channel
Advection Scheme:	High resolution (method for the spatial discretization)
Convergence criteria:	10^{-6} for the RMS*-values
Timescale Control:	Physical timescale with $\Delta t=1/\omega$
Maximum number of iterations:	ca. 400

(*)The RMS (Root Mean Square) residual can be considered as an index of how well the solution is converged. It is obtained by taking the mean of the square of all of the residuals from all of the equations throughout the domain, then taking the square root of the mean. This value is an index of a typical magnitude of the residuals at each time step of the simulation.

5.5 Analysis of the flow by use of CFD simulations

Now is available a CFD model that is appropriate for what concerns the geometry and the physical reproduction of the pump; its reliability is also proved. The results of the calculated flow inside the components should therefore be close to the reality. This means that now it is possible to use this instrument to study the phenomena that occur in order to better understand them. This can eventually provide guidance for the optimization process.

The program **CFX-Post**[®] is the ideal tool for this job because it permits to visualize the flow field in many different and useful ways. It is possible to show the changes of every variable considered inside the three dimensional spaces of the machine by means of displaying the stream lines, or the vectors projection on a certain plane. One other interesting possibility is to initialize the “Turbo mode” that allows to see the variables representation in the meridian or in the so called blade to blade planes.

The meridional section represents the projection of the velocity vectors on a chosen axial-radial plane. This plane is therefore perpendicular to the front and rear shrouds and shows the evolution of the variables across the meridian section. In all the meridian plots that will be showed in this work the horizontal axis shows axial distance (X) while vertical axis shows the radius (R).

The blade to blade view is composed by: the horizontal axis that shows the stream wise location (S) and the vertical axis that shows theta. The streamwise location is the dimensionless distance between the inlet and the outlet of a certain stream line placed at a chosen blade height. Theta angle is the angular coordinate in the plane perpendicular to the rotation axis; the right hand rule is always followed. [2] As an example, the axis will be showed only in figure 57 and 58 but then they will be always ignored.

5.5.1 Flow at Best Efficiency point

Skipping through the blade to blade representation of the vectors (see APPENDIX 2) it is clear that the condition in which the flow is less separated is the one obtained at around 5 or 6 [l/s] of flow rate. This is clearly the point in which the hydraulic losses in the impeller are minimal. In agreement with what experimentally verified, these can be considered as a surroundings of the BEP ($Q_{BEP} \pm 10\%$).

The first variable analyzed is the pressure. As it is typical for centrifugal pumps, the pressure rises with the radius and this effect is strongly dependent on the centrifugal effect (as can be seen in fig. 57 for 6 [l/s]). The effect that causes the transfer of work to the water is the difference of pressure between the pressure side and the suction (visible in fig.58 for 6 [l/s]). This causes a load on the blade that is almost uniform and is contained in a range of difference of pressure of 50÷70 [KPa] (see fig.59 for 6 [l/s]). The load curves rise in a smooth way causing a homogeneous transfer of work.

It is also possible to notice a low pressure region close to the entrance of the blade channel, behind the leading edge of the blade. This is caused by the imperfect incidence of the flow that is then forced to get faster around the nose of the blade.

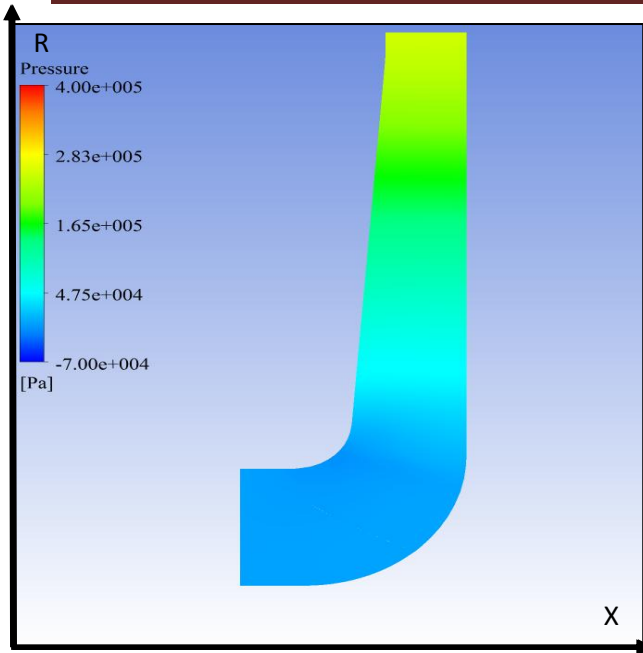


Figure 57: Pressure distribution in meridian view.

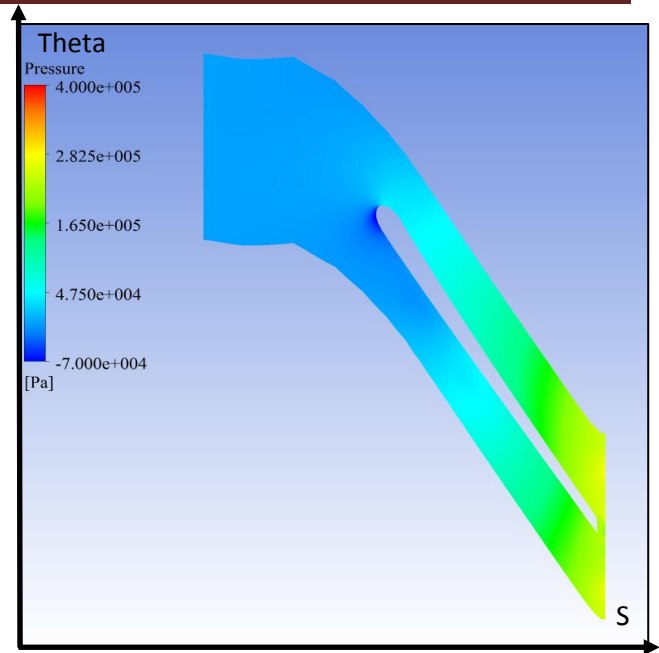


Figure 58: Pressure distribution in blade to blade view.

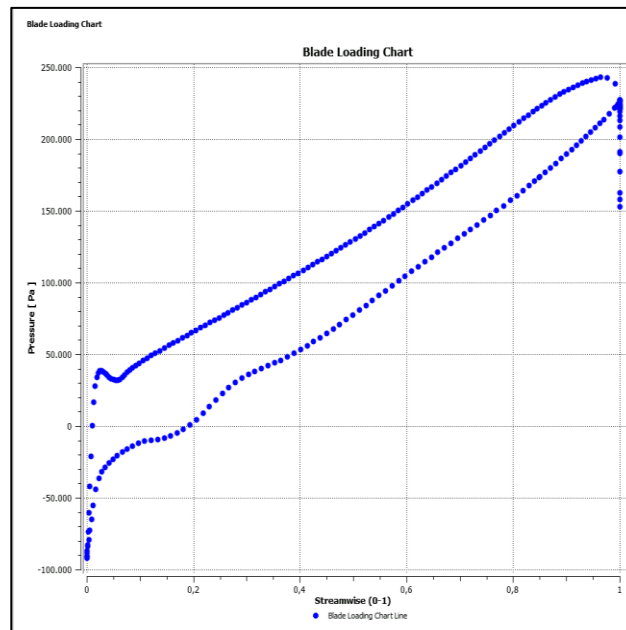


Figure 59: Load of the blade.

To study the development of the relative speed variable, is possible to display it both as a continuous variable and by vectors, each of them is representative of the variable in the surroundings. The snaps in the meridian section show a speed inside the channel of up to 10 [m/s] and some interesting non-uniformities. First of all it is interesting to notice a general decrease of the speed after the bend, inside the blade channel. A growing radius means a greater passage section and this effect is only partially balanced by the reduction of the height of the blades along the radius. Another localized reduction of speed is behind the bend of the shroud. There the change of direction of the flow is too sudden and the water has to accelerate. This causes a high gradient and a region of almost stagnant water. The last slow flow region is in the entrance, close to the hub shroud. Here the flow has a lower centrifugal speed.

Although this reductions of speed do not help in avoiding the development of the turbulences, they don't cause the vein separation across the hub and frontal shrouds.

It is anyway clear that the meridian section presents a too sharp bend, a poor axial extension and a limited cross section reduction with the radius.

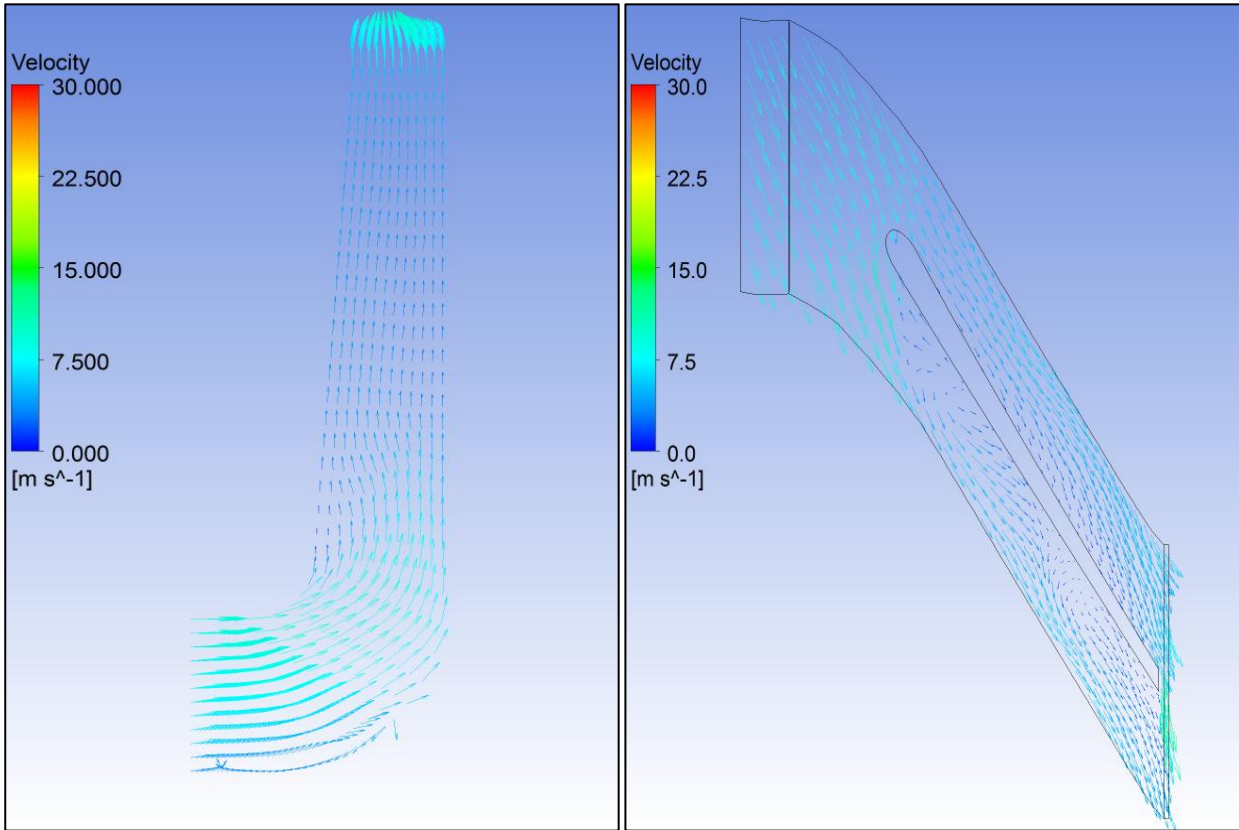


Figure 60: Speed distribution inside the meridian channel and inside the blade to blade plane.

Switching to blade to blade view it is possible to visualize the flow separation at different blade heights. From a general prospective, the flow is almost uniform in the channel (from which the consideration of being in the BEP) but a zone of separation is present on the suction side. This separation gets closer and closer to the leading edge with the height of the blade (see figure 60 left). Fig. 60 also shows a blade to blade plane section placed at 80% of the blade (this means close to the front shroud). Here it is possible to see the separated region very close to the leading edge. Placing the section at lower height (farer from the front shroud), causes the separation point to move further as well. This effect could be caused by the interference with the slow velocity point that is placed after the bend, on the front shroud, as already explained.

A closer look to the flow around the leading edge helps to understand the effects of the geometry in this region. Fig 61 refers to the velocity vectors in this region, for 5 [l/s] flow rate. The stagnation point is on the pressure side of the blade, this means a positive incidence. While this does not cause cavitation problems (see appendix 4), the drop of pressure behind the blade causes strong dis-uniformities of the flow that eventually cause separation. This is particularly true close to the front shroud.

This is also true for the 6 l/s calculation where the inlet flow is slightly more axial and the incidence minor. As a result the separation point is shifted towards further blade positions. (APPENDIX 3).

Separation in the blade channel causes losses and may be a reason for the comparable loss of efficiency. The operation of optimization should consider this and try to reduce the separation.

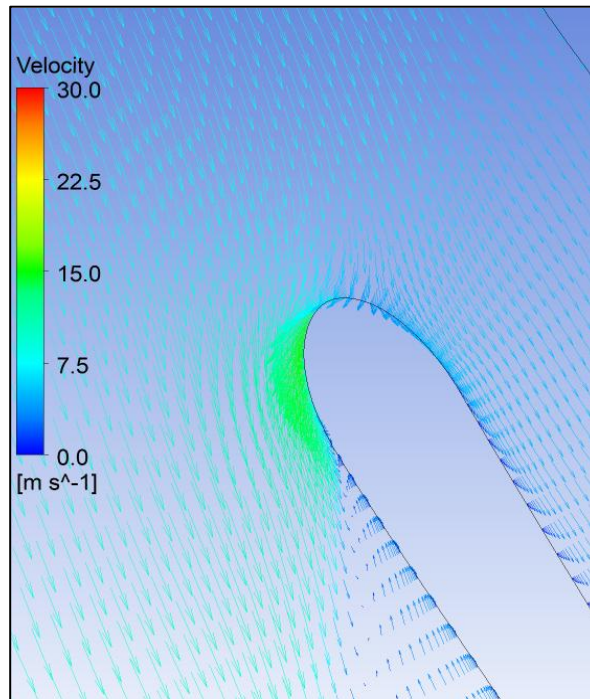


Figure 61: Velocity vectors inside the blade to blade channel, around the leading edge.

The quality of the simulation results is also proved by some details in the reproduction of the flow in accordance with a theoretical explanation. One example of this is the reproduction of the secondary flow inside the volute. In fig.62 is confronted the calculated flow at 6 [l/s] with the expected one. The presence of this vortex is caused by the secondary flows and is not different from the one that can be observed in a curved tube. This behavior can be observed only around the BEP but not at part-load where the volute cross section does not match the flow rate, creating a different flow pattern.

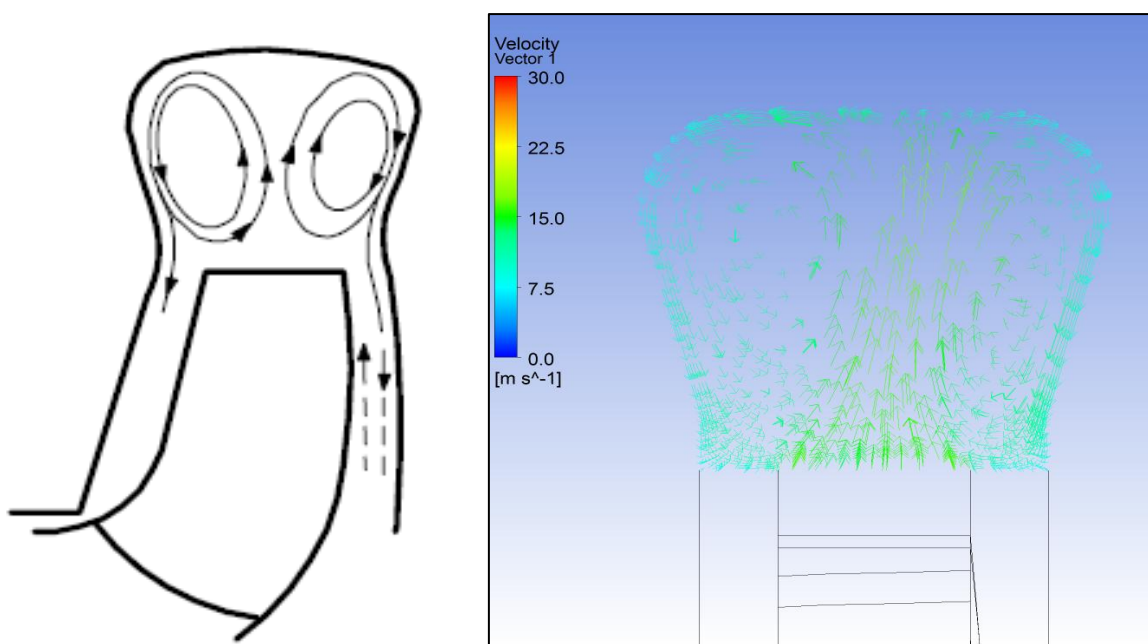


Figure 62: Detail of secondary flow inside the volute.

5.5.1 Part-load operation flow

The behavior of the machine at part load is of a great importance because this is the condition where the pump is most likely to work.

The pressure distribution is mostly similar to the one in the BEP but the difference of pressure between pressure and suction side decreases with the flow rate, and so does the load on the blade. This reflects the presence of vortex and recirculation flows. In fig. 63 it is possible to see the load of the blade gradually reducing from 30-40 [KPA] of difference of pressure for $Q=4$ [l/s] to 10 [KPa] of difference of pressure for $Q=1$ [l/s]. In these conditions the transfer of work to the water is mainly up to the centrifugal effect. With a flow rate of 2 and 1 [l/s] the pressure does not rise anymore gradually but shows a peak close to the trailing edge, there most of the work is transferred.

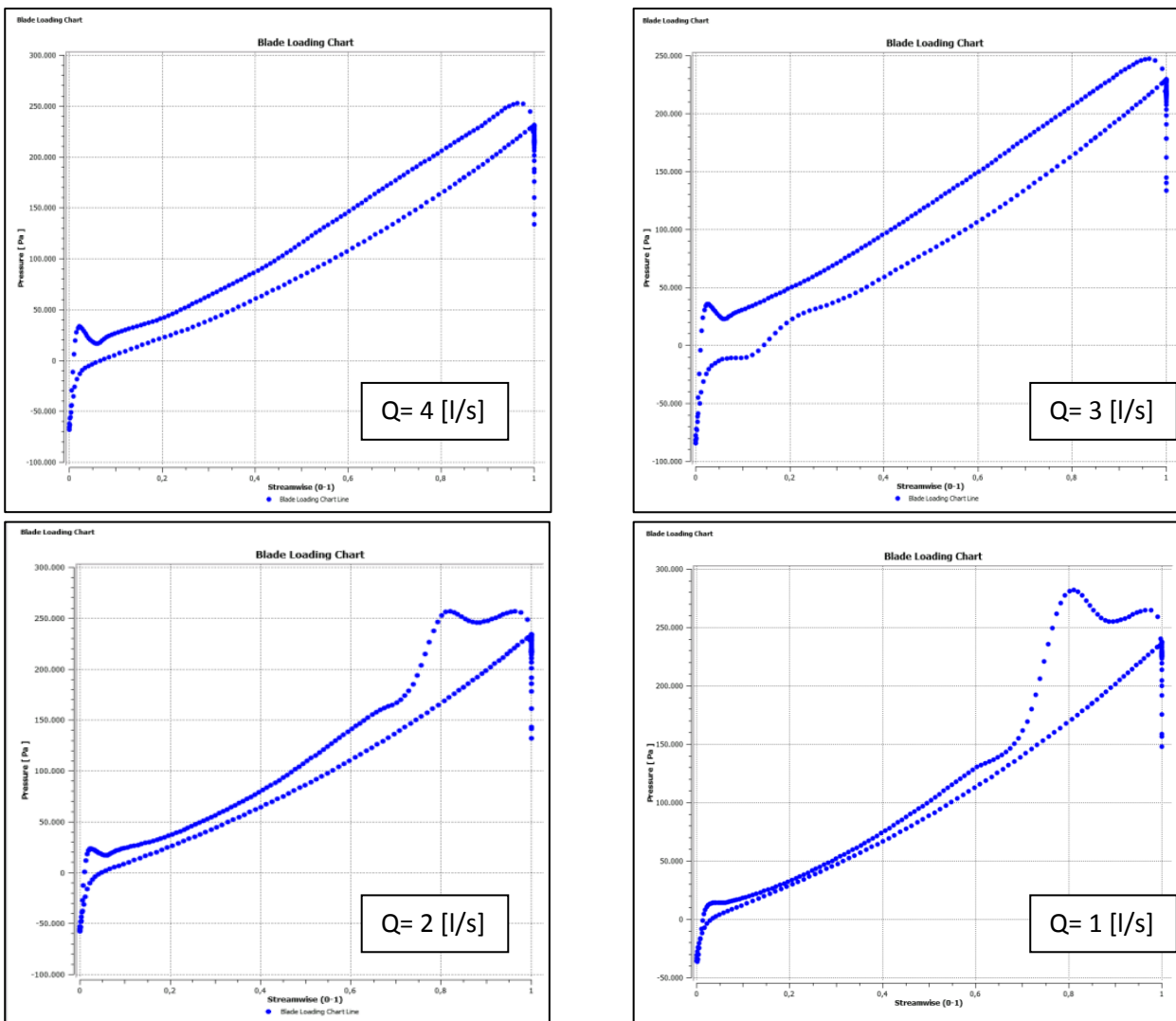


Figure 63: Load of the blades at decreasing flow rate.

The velocity distribution in the meridian plane does not offer big differences with respect to the BEP. The conditions of flow are slightly more uniform, proving that the blade channel has a design that works well at part-load conditions: a reduced axial component of the speed causes less trouble when the flow is bent. This is also proved by the greater homogeneity of the flow in the first sections (before the

bending) where there is not any more the low speed region near the hub.

Despite the problems caused by a too small radius of the front shroud, this blade channel seems to behave quite well for low flow rates.

The blade to blade view clearly shows a separation of the flow that grows stronger and stronger with the reduction of the flow rate. At 3 [l/s] this takes the shape of a recirculation vortex placed closer to the suction side of the blade, where the flow is not well guided and therefore separates. This vortex gets stronger at 2[l/s] and 1 [l/s] when the recirculation flow is bigger. Here it affects almost the entire blade channel. This behavior is natural and is caused by the fact that the flow that is pushed towards the tip of the blade is too much for the flow rate conditions and has to come back again. The phenomenon is possible in a separated flow and could be retarded (moved to lower flow rate) through the reduction of the BEP.

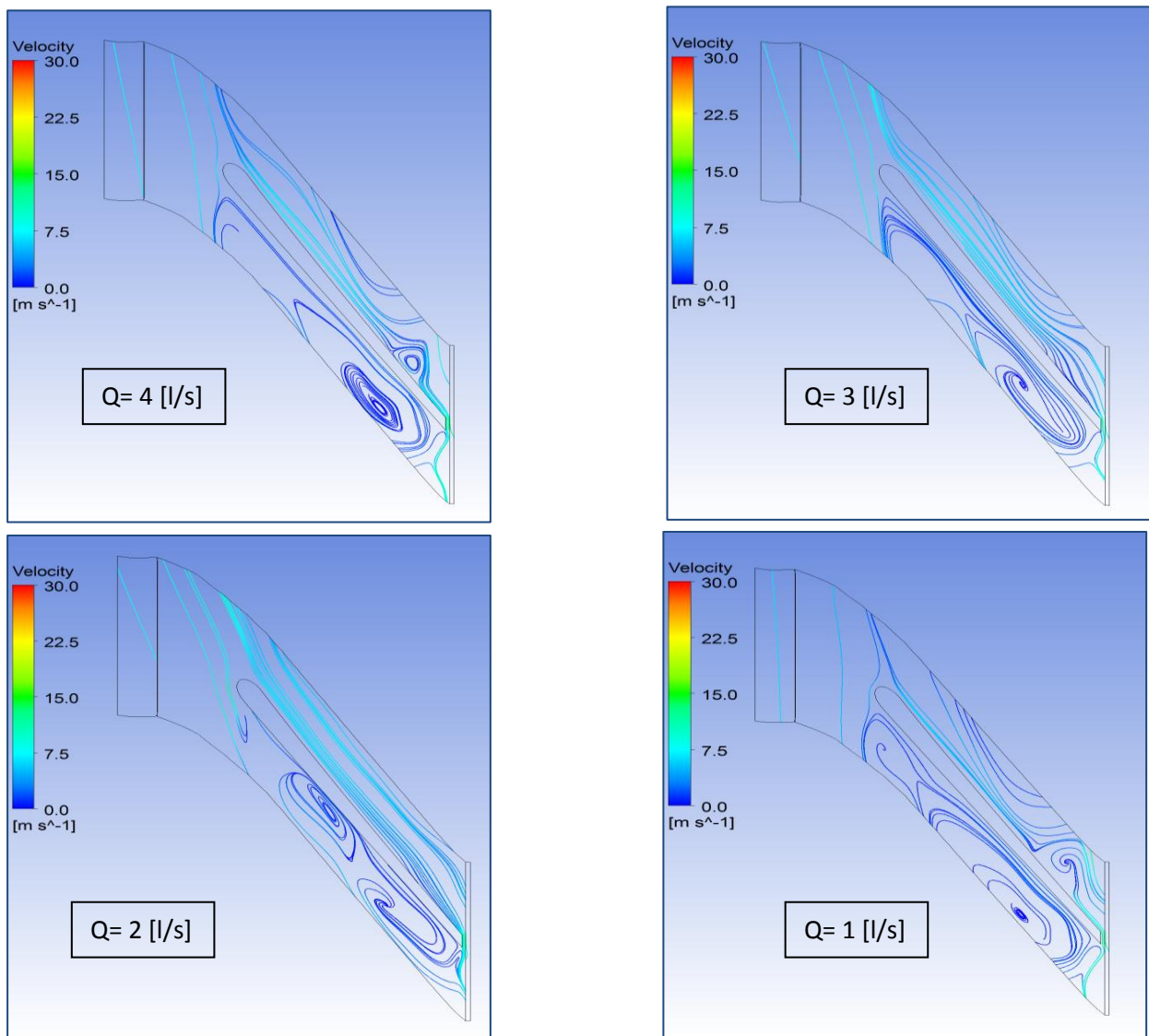


Figure 64: Stream lines inside the blade to blade channel at decreasing flow rate.

Fig.64 shows a view of the streamlines in the blade to blade plane placed at 50% of blade height. At first is only visible a generic separation on the suction side but this gradually takes the shape of a recirculation vortex that eventually affects the entire blade channel.

Focusing on the entrance of the blade channel we can see the flow getting more and more tangential with the reduction of the flow rate; also the stagnation point moves towards the pressure side of the leading edge (see fig. 56 relative to 80% of blade height). This causes earlier and stronger flow separation on the suction side. As it was for the BEP, the flow separation is closer to the edge at higher blade sections because of the influence of the sharply bended front shroud.

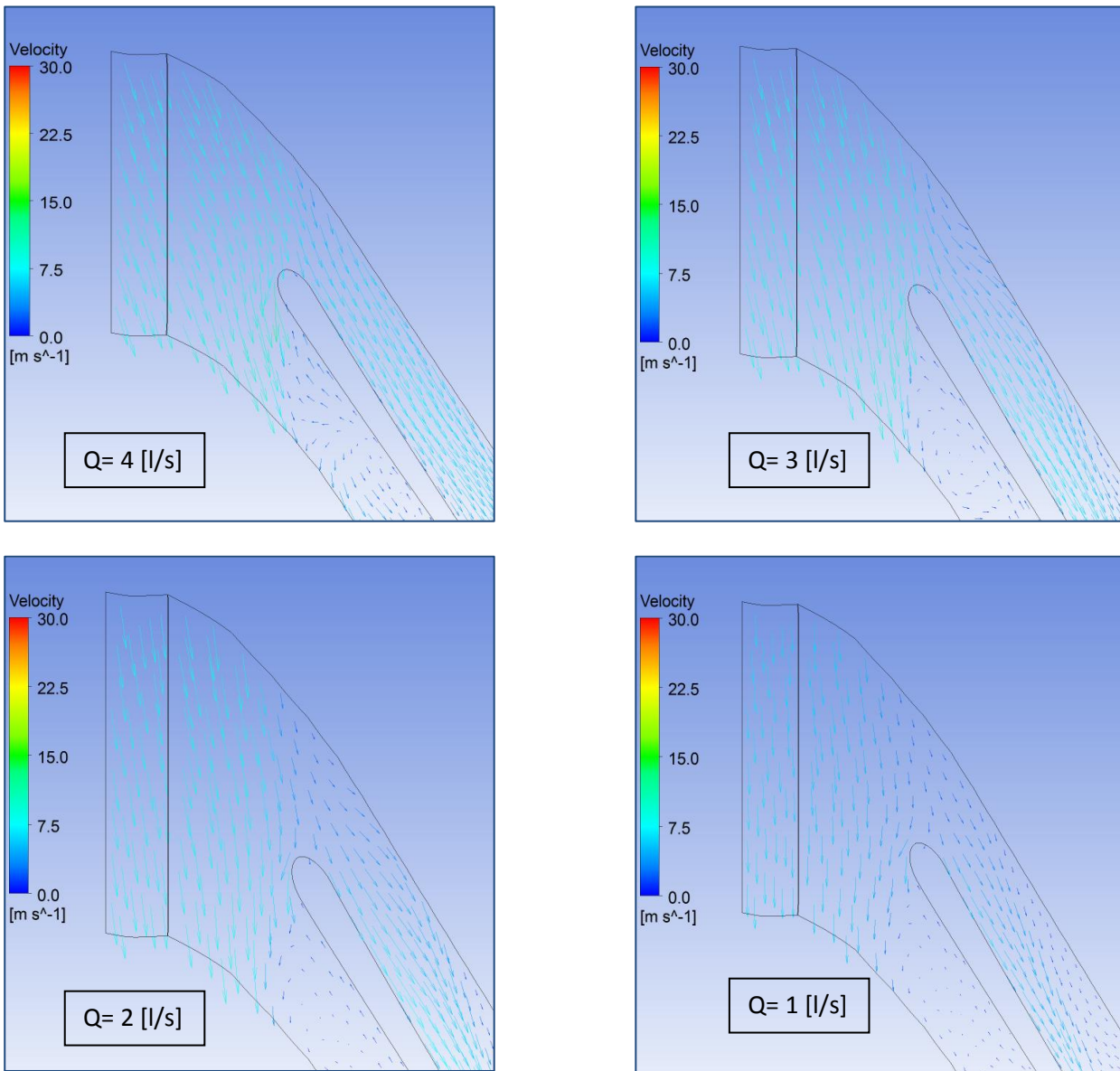


Figure 65: Speed distribution in blade to blade channel around the leading edge.

Unlike what happens around the BEP, at part-load operations, the outlet flow is much less uniform for what concerns pressure and velocity distribution between one blade and the following. In particular a recirculation of the flow and a low speed region behind the suction side trailing edge can be noticed. This region has less and less energy the closer it is to the front shroud, in accordance to the jet and wake theory [13]. For this theory, the motion field in the blade to blade is subject to a high non uniformity: in the pressure region the flow follows in the direction of the blade while there is a recirculation in the low pressure region; the pattern is shown in fig. 66.

The dis-uniformity grows of importance at lower flow rate where the separation begins at lower radius

and the recirculation is stronger. Here the mixing losses rise.

A more uniform flow at lower flow rate could help reducing the turbulent dissipation. As an example, in fig. 66 is represented the flow around the front trailing edge. Behind the blade, a region where the vectors are not pointed in a radial direction but have a radial component that is absent or negative (effect of the recirculation) is easily distinguished; this is the wake region.

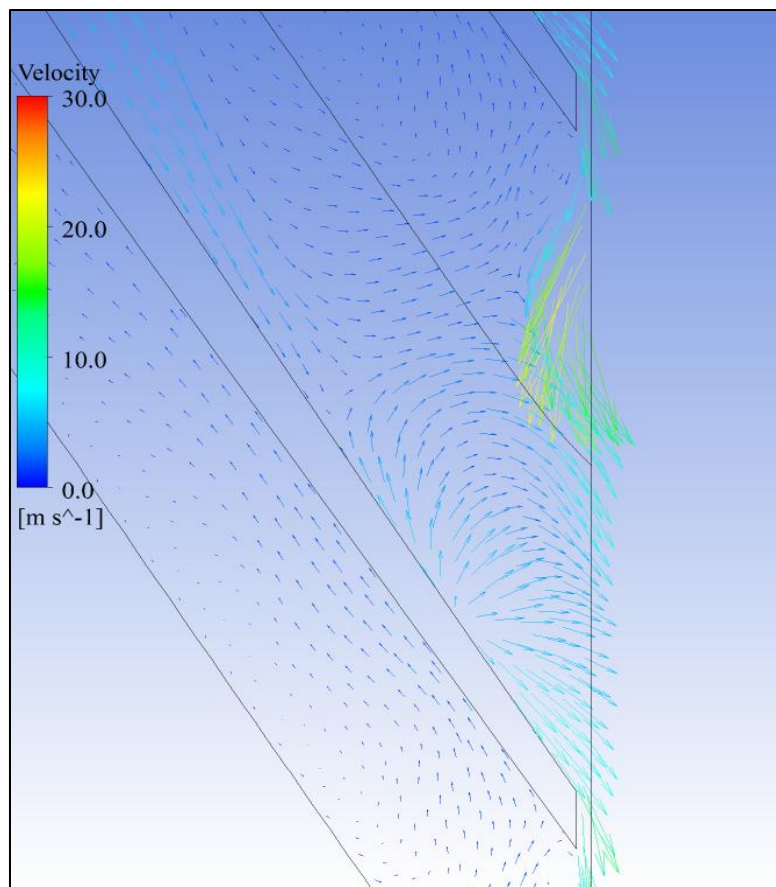
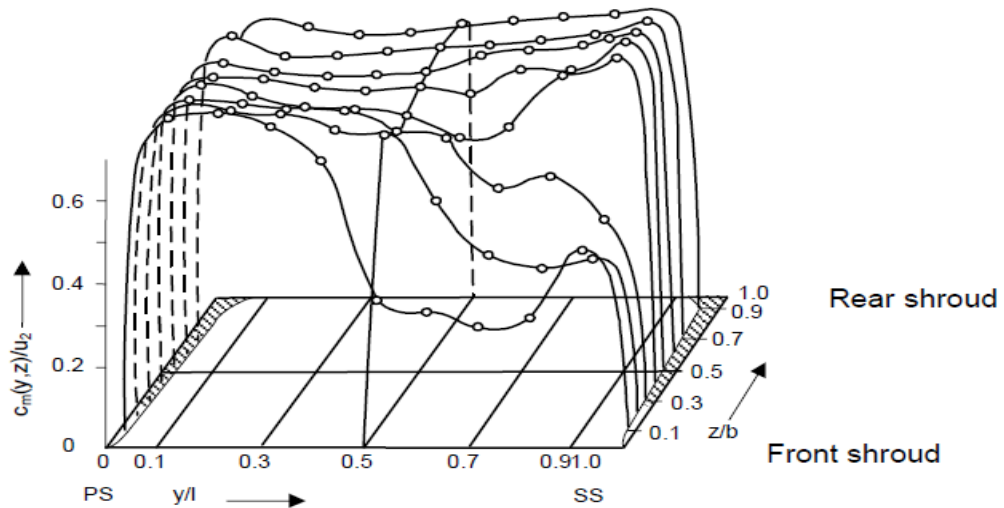


Figure 66: Confrontation between expected Jet and wake behavior [13] and blade to blade distribution of velocity.

5.6 Conclusions

The use of a sophisticated CFD calculation allows us see inside the machine to better understand the physical phenomena. Although the thrust in this tool comes from the confrontation with the measured characteristic curves, the results must always be regarded with a critical eye and confronted with a simple theoretical description of the effects.

The analysis of the results allows for some general conclusions that could help drawing the line for the optimization process.

The flow around the BEP is overall good and uniform but could still be improved. A certain quantity of separation is still present and can be reduced with the use of less loaded blades and with better inflow conditions. In particular the intake angles should be reduced to minimize the shock loss and to prevent the flow to separate. Also the influence of the sharp outline of the frontal shroud works against the uniformity of the flow. Its effect should be reduced using a bigger curvature.

Beside the value of the maximum efficiency itself, the position of the BEP is important because it could affect the behavior in the most common working point that is known to be at around 4 [l/s] or even less. To have a BEP placed at higher flow rate means that the pump is not strictly optimized to work in that point and most of the times it will work with too tangential flows, bigger vortexes and a beginning of recirculation; this means bigger flow dis-uniformities and vortex dissipations. At the same time it must be remembered that a pump designed for a higher nq number has, as a general rule, a higher efficiency.

The meridian channel has a low axial extension and a too sudden bend on the front shroud; this contributes to increase the presence of vortexes and the separation.

The inlet flow is characterized by high (i.e. very axial) inlet angles that cause the stagnation point to move far on the pressure side of the blade causing big drops of pressure and causes a sudden separation behind the blade. A good idea could be to reduce the inlet angle in order to reduce the incidence and to move the BEP to a lower flow rate.

The use of optimized inlet angles, less loaded blades, more gentle curvature, could reduce the intensity of recirculation and Jet and Wake phenomena. These could also be moved away from the working point when the whole pump is designed to work in the BEP.

Chapter 6: Comparison of the results.

In this chapter the previous results will be discussed and compared to each other to provide a complete understanding of the problems of the investigated pump and to suggest the way to cope with them.

6.1 Introduction

The comparison of the different analysis done till now is of a particular importance because it permits to check the quality of them. In this way we can have a better perception of the reliability of the results and of the tools that will be used for a successive optimization.

The pump has been studied using different approaches: empirical formulas, experimental and numerical (CFD). Now these results have to be compared to end up having a single, unified view on the problems. Based on this procedure we can define the main points on which the optimization process should focus. This does not only concern a qualitative view but also a numerical one. The different characteristics will be confronted to see how much they are similar and to try to understand the causes of deviation.

The instruments used for acquiring information on the behavior of the machine can also be used in the following step of optimization. For doing this, the results must be trusted and it must be proven that they are in agreement with the physical meaning. This point was actually accomplished in the previous chapters where the exposition of results was supported by their theoretical interpretation.

6.2 Comparison between the real characteristic curves and the ones provided by the company

The Purpose of this operation is to evaluate the reliability of the dates supplied by the pump manufacturer.

The characteristic curves that are provided by the company are referred to the head and power consumption. All of these have to be compared with the experimentally measured data. The efficiency curves are not part of the information that the company presents when the pump is sold, nevertheless the power consumption curves seen on the data sheet indirectly represent the efficiency of the pump. In this sense, improving the efficiency means to reduce the power consumption.

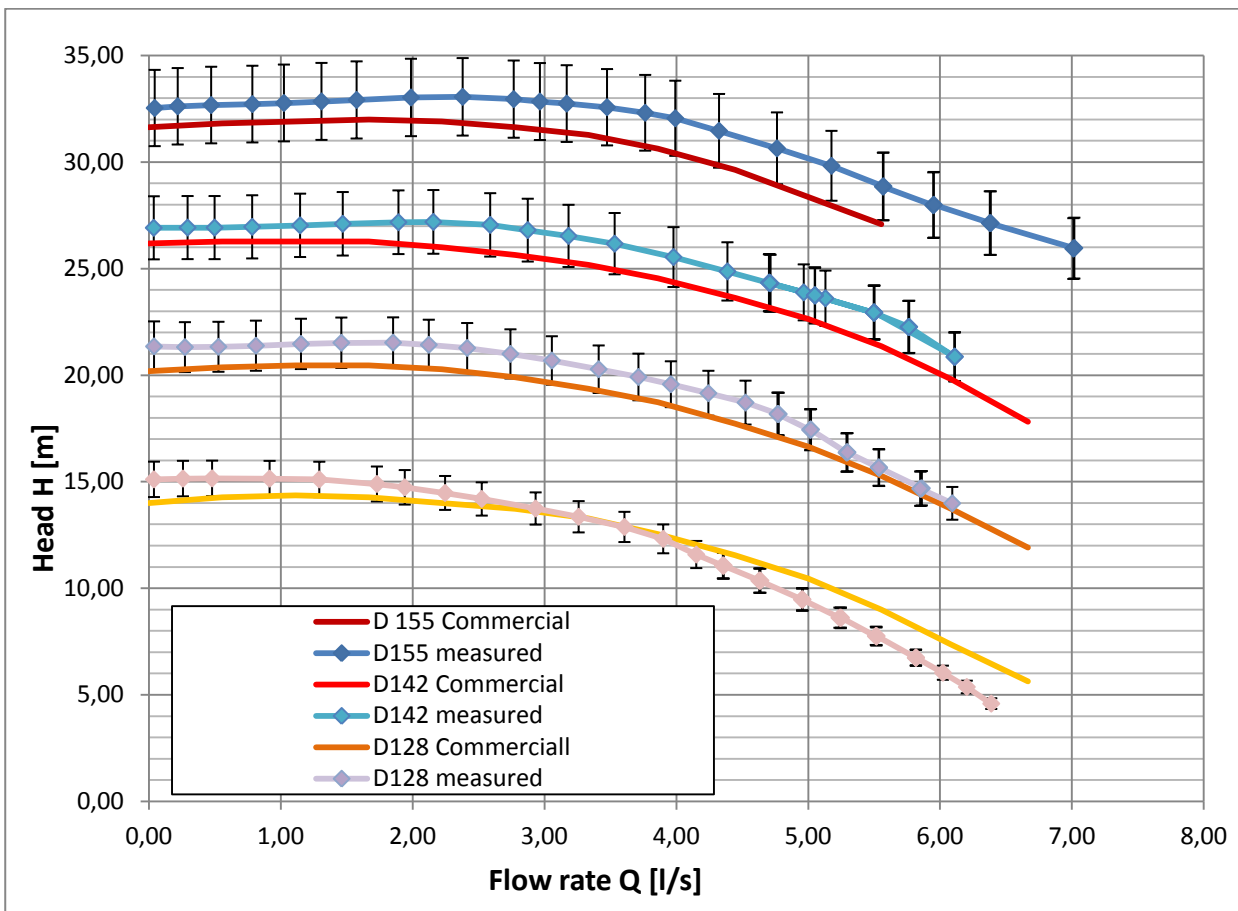


Figure 67: Confrontation between commercial and measured head curves.

Fig. 67 shows the head curves of different diameters; they are only referred to plastic impellers. It turns out that the commercial curves are generally below the measured ones. For the D155 model (the one that has to be optimized), this distance is between 1 and 1,5 [m]. Once more we see that the value of head is probably not so important for a commercial purpose and there will certainly be a range of accepted value around it. As have been already noticed for the cast iron impellers, under the same name are sold machines with values of head far from the declared one.

Additionally the curves shows the error bar corresponding to a 5,5% error. This value comes from the ISO 9906 guide lines and is the acceptable value of head for a degree of accuracy 2. It is interesting to notice that the commercial curves are generally inside the admissible range and, from this prospective, true.

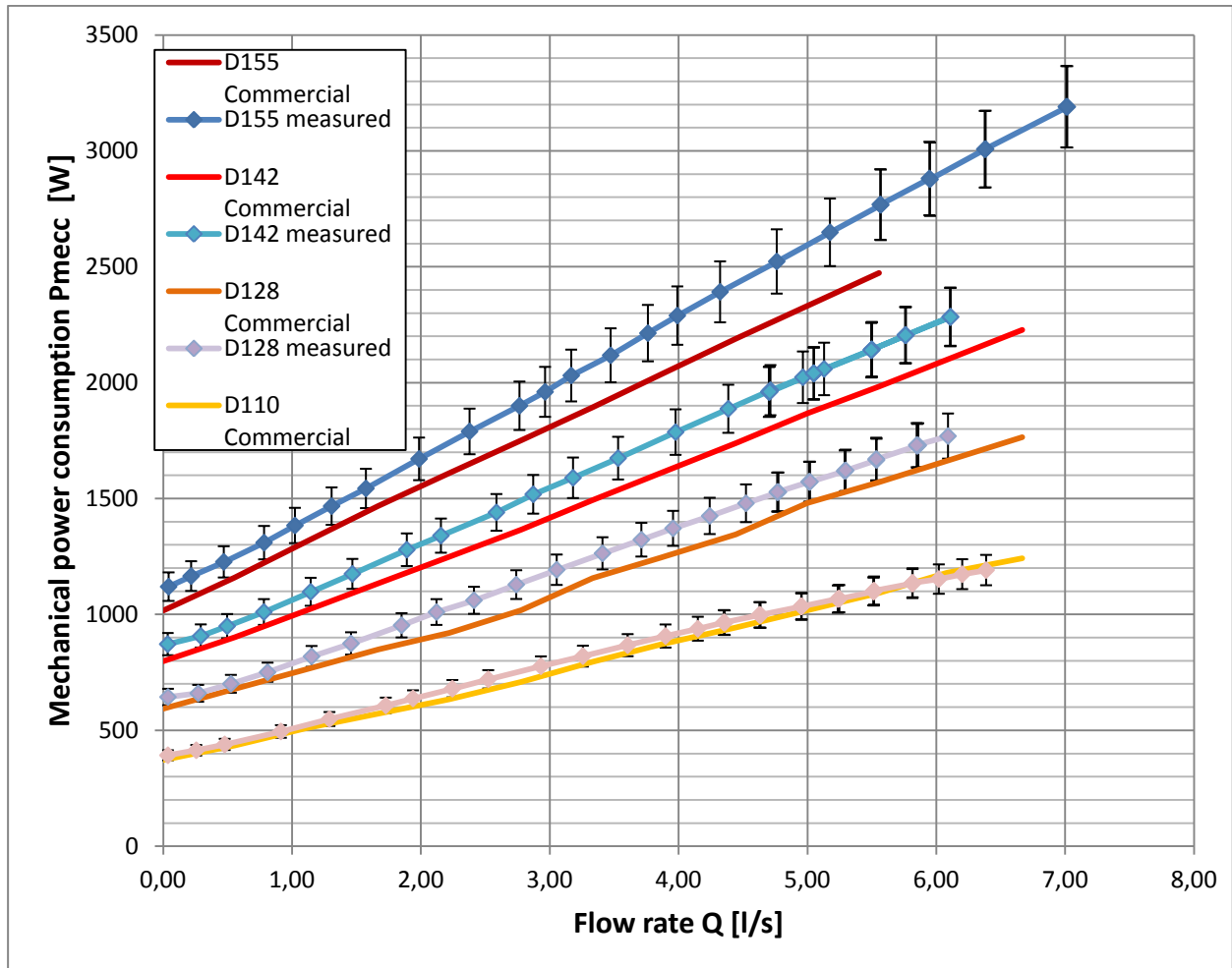


Figure 68: Confrontation between commercial and measured power consumption curves.

The commercial curves of power consumption are shown in fig. 68 along with the measured values. The reference is always to the overall mechanical power that the machine requires, comprehensive of the efficiency of the engine. The values have been cleaned from the power consumption of the additional bearing that was required for the tests and does not exist in the real machine.

As we see, the commercial curves are always lower than the measured, and are not even inside the accepted measurement error range. These curves are definitely wrong and should be changed by the company.

The efficiency curves are derived from the power and head curves assuming an efficiency of the electrical engine of 85%. This value is the commercial nominal efficiency of the motor and it is also the approximate value that was measured during the tests. Smaller impellers require less power and the motor operates far from the rated power value and with lower efficiency. Because of this it was necessary to use the calculated engine efficiency (always between 80% and 85%) for lower power outputs.

The commercial curves are higher than the measured, showing a behavior better than the real. It is also important to notice that the impellers analyzed are the plastic versions that have a higher efficiency than the cast iron versions. This causes an additional distance between the real and the commercial data.

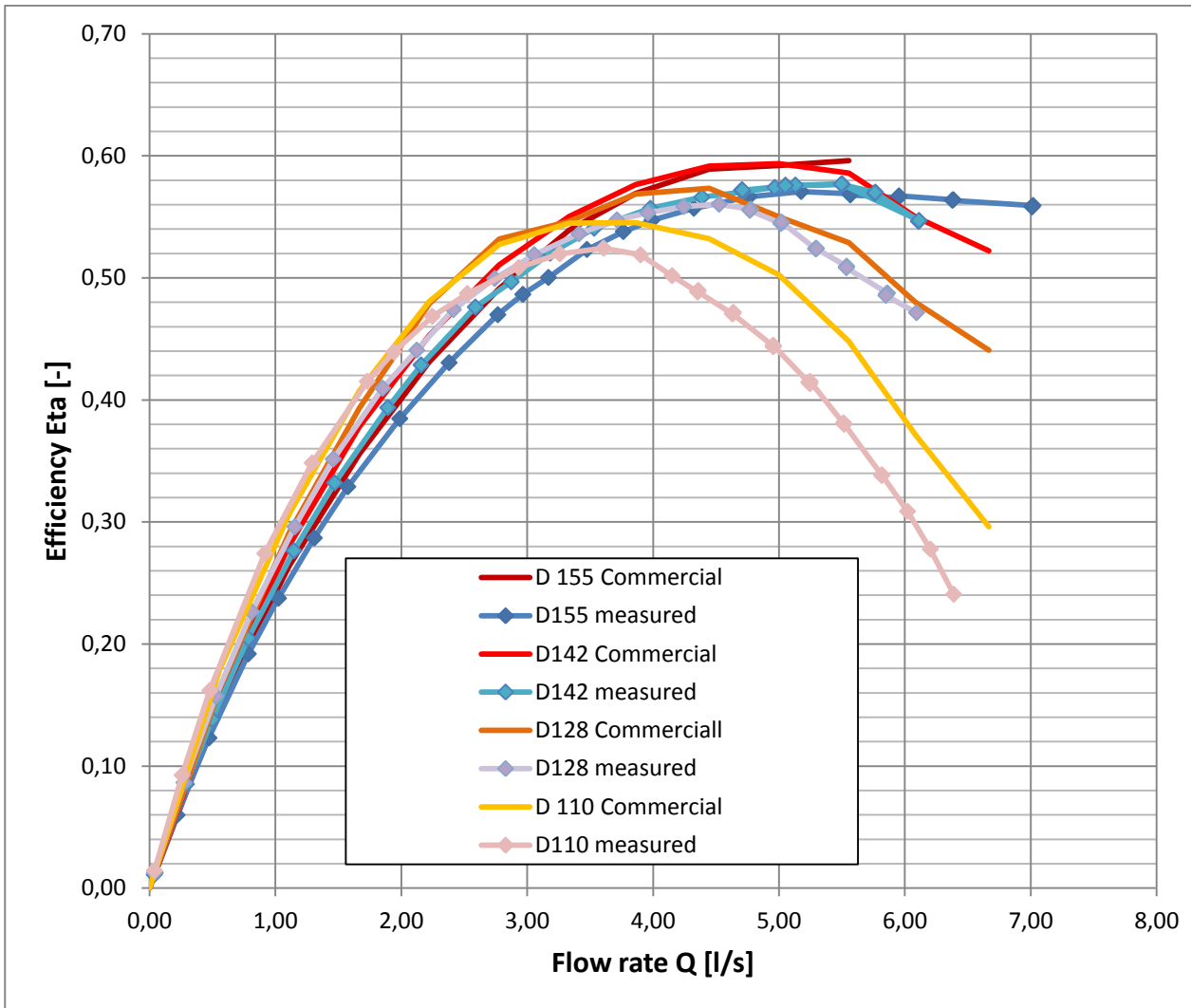


Figure 69: Confrontation between commercial and measured efficiency curves.

All in all the curves provided by the company cannot be taken into account for a detailed analysis of the pump and this could wrong foot us in the validation of the CFD model.

From the above comparison graphs it results that the data given by the data sheet are most probably referred to the cast iron impellers.

6.3 Comparison between CFD and semi-empirical loss analysis

The semi-empirical models were able to tell us something general about the losses and their reciprocal proportion. Now it is possible to use the CFD calculation as a confront term to compare the absolute value and the relation between them. An accordance of the trend will support the quality of the CFD model.

The first observation could be done by dividing the components of the total efficiency in three parts: The volumetric efficiency, the impeller efficiency and the volute efficiency. In fig. 70 it is possible to see the result this division.

The total efficiency is here defined to be the product of three different components:

$$\eta_{tot} = \eta_{vol} * \eta_{impeller} * \eta_{volute}$$

On the other hand, the single efficiency-values taken from the CFD-calculation can be defined as follows:

$$\eta_{vol} = \frac{Q}{Q + Q_{leakage\ front} + Q_{leakage\ back}}$$

$$\eta_{impeller} = \frac{\rho g (Q + Q_{leakage\ front} + Q_{leakage\ back}) H_{imp}}{M_{tot} \omega}$$

Where

$$H_{imp} = \frac{(P_{tot\ 2} - P_{tot\ 1})}{\rho g}$$

$$\eta_{volute} = 1 - \left(\frac{P_{tot\ 2} - P_{tot\ 3}}{P_{tot\ 2}} \right)$$

With P_{tot} is indicated the total pressure at different interfaces: the interface number 1 is the one at the entrance of the impeller, the number 2 is the interface between the impeller and the volute while the interface number 3 represents the last section of the outlet pipe (the volute is considered to end there). The value of Q is the useful flow rate, the one that actually flows into the pipe and can then be measured. M_{tot} is the torque that enters the pump through the shaft. It is comprehensive of all the losses of the machine but not of the losses of the electrical engine.

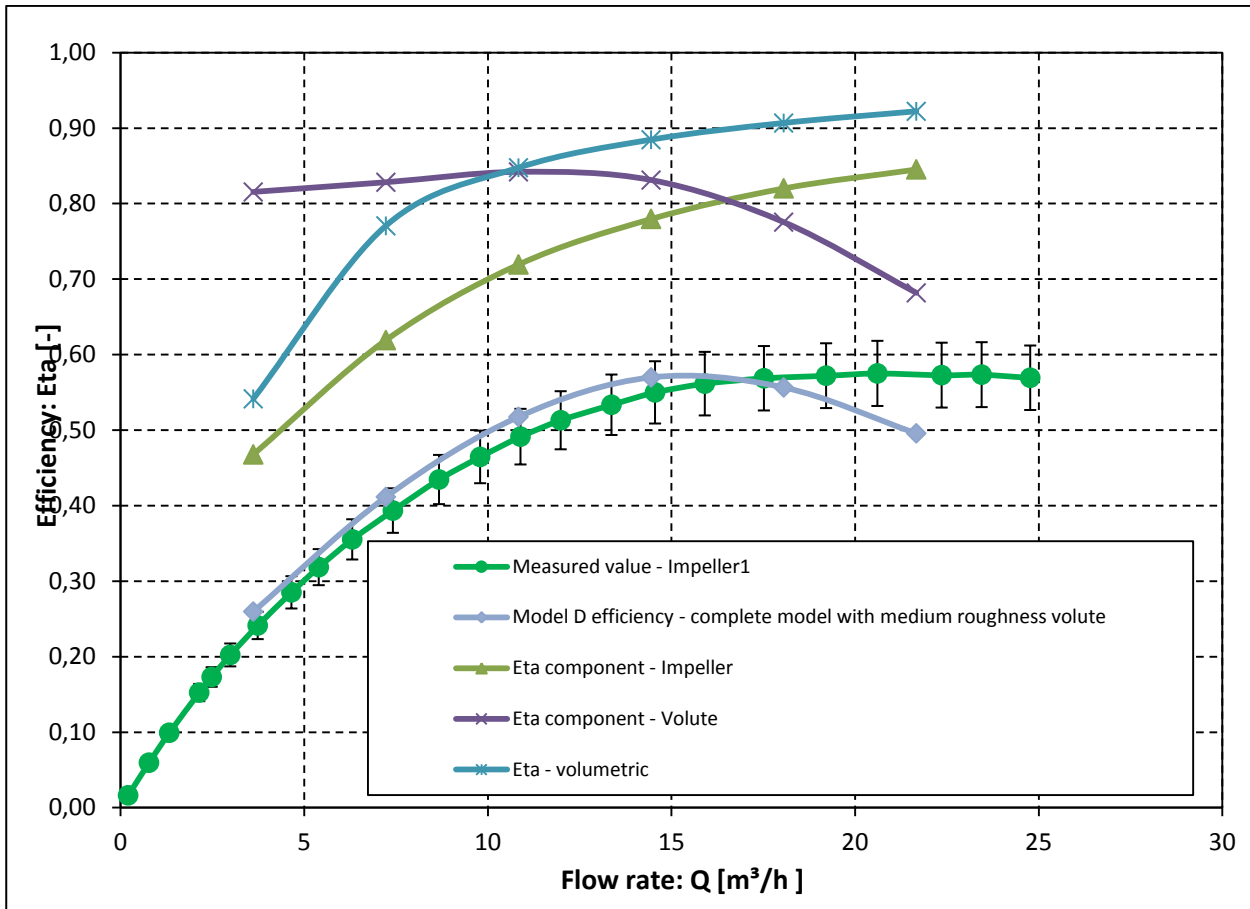


Figure 70: Efficiency split curves of a numerically simulated model.

The volute component of the efficiency is clearly responsible for the final drop of the total efficiency curve with respect to the real values. This can be explained with an error in the geometrical reproduction of the chasing based on simple 2D drawings: a too small cross section causes excessive speed inside the component and a strong rise in the friction losses especially at high flow rate.

The ratio between the different components was not completely expected: while the volute provides the biggest amount of losses, the impeller losses are not negligible as well. This is in contrast to what suggested by the simple analysis done in Cap. 3. Anyway the losses caused by the impeller are a small fraction around the BEP but become the main cause for efficiency loss at part-load operations.

The shape of the impeller efficiency curve suggests that it is optimized for a higher flow rate than what it is really used. A new design should take into account this and hopefully increase the curve in the central part, around 15 [m³/h] (corresponding to 4,2 [l/s]).

The consequences of these considerations are that if we want to improve the efficiency at high flow rate we should focus on the volute, while for the part-load behavior the optimization of the impeller is the main goal.

The volute

The velocity distribution inside the volute is similar to the one used for the calculations in chapter 3, having a range of value between 10 and 20 [m/s]. The peaks of velocity found with the CFD are lower than 25 [m/s] while the simplified calculation suggests a speed higher than 35 [m/s] in the first sections. This could cause an over estimation of the loss in this component. This consideration diminishes the importance of the volute as a source of loss.

The meridian channel

The simplified loss analysis does not stress the importance of the losses inside the impeller but some features may have other effects: in example the increase in outlet blade height could reduce the speed of the flow inside the volute. The literature suggestions for the main dimensions tell us to improve the axial extension, radius of curvature, outlet height of blade and inlet section area (chapter 4). In agreement with this, the CFD calculation shows a high velocity in the suction chamber, a beginning of separation after the sharp bend, an excessive velocity in the volute.

In other words, all of the three analyses tell us that the blade channel has not enough axial extension for the actual nq number of the machine.

The possibility of reducing the BEP flow rate has already been proposed and its effects on the blade channel are interesting: the geometry seems not any more so bad. The table 71 shows the real value of the geometry, compared with the suggestions for nq of 17. Beside this, the suggestions for a nq=13 corresponding to an optimal flow rate of 3,6 [l/s] or 13 [m³/h] are presented. These are closer to the optimal value especially for what concerns “b2”.

	Actual geometry	Suggestions for nq=17	Suggestions for nq=13
Ze [mm]	4,0	20,6	16,3
b1 [mm]	13,0	13,7	13,7
Rds [mm]	5,5	8,9	8,2
g [mm]	-5,0	2,7	2,7
b2 [mm]	7,7	8,4	7,9
ξ ds [deg]	0,0	0,0	0,0
ξ ts [deg]	0,0	0,0	0,0

Table 71: Suggested meridian geometry for various nq numbers. Based on literature suggestions [9].

CFD calculation confirms that the behavior becomes better at a lower flow rate of 3÷4 [l/s].

The blade

The intake angles, the length of the blade and the outlet angle seem not to be optimized, causing a high load on the blade that results in excessive non-homogeneity of the flow and separations. This is at first showed in the theoretical calculation and much more underlined in the results of the CFD simulation. A solution that could help to enhance these characteristic is the use of a three dimensional blade that enters inside the eye of the impeller meeting the flow where it is more uniform. This feature is essential in bigger machines where even small improvements of efficiency are important achievements and where the costs of production are less concerning.

6.4 Conclusions

The first consideration of this chapter is about the reliability of the data furnished by the pump manufacturer. The characteristic curves used for a commercial purpose are wrong and cannot be used for a following study. This also raises questions regarding the accuracy of other data like the drawings of the volute.

The final CFD model proved to be close enough to the experimental results of the pump and its results are in agreement with the physical explanation of lots of phenomena. Also the theoretical calculation and the simplified loss analysis agree on the results.

The comparison between the three different calculation results produces a unified view on the problem that is summarized as follows:

- The BEP is placed at too high flow rate with respect to the working point. The machine spends most of the time not working at maximal efficiency. At the same time a reduction of the optimum flow rate causes a reduction of the n_q number and a drop in the maximum efficiency. The equilibrium point between these two effects must be found.
- The intake angles should be more tangential to produce better inflow conditions for the incoming flow and to move the separation point towards more radial positions. This will increase the uniformity of the flow at lower flow rate. In this way the impeller will operate with less vortices and recirculation for a longer time.
- The blade should enter in the eye of the impeller and have a three dimensional shape.
- The outlet angle should be decreased to increase the length of the blade and to reduce its load.
- The volute cross section should be enlarged to reduce the speed of the flow and the friction losses.
- The axial extension of the machine should be bigger to permit a milder bend.
- The impeller outlet width (b_2) should be bigger unless we decide to lower the optimal flow rate to 3,5 [l/s], in this case the value of b_2 does not need to be changed.

Chapter 7: Optimization of the impeller with a CFD iterative process.

7.1 Introduction

Starting from the conclusions of the previous chapter 6, there are now the conceptual bases for the conclusive step of the project: the optimization of the impeller based on a validated CFD model. Before starting, it is better to summarize the conclusions that we previously draw and the hints that come from them, to light the way for a clearer and more linear procedure.

From a reasoned analysis of the experimental dates (chapter 2), from the theoretic analysis (chapter 3 and 4) and from the CFD results (chapter 5), the followings can be considered as guide lines for the improvement of the characteristics:

- Blades are too short and this leads to excessive loads and separation of the flow inside the blade channels.
- Outlet angle has a too high value and this implies having short blades.
- Inlet angles are too high causing higher pressure jumps behind the blade and excessive chock losses.
- the Geometry of the blades is 2-D and the shroud leading edge does not enter in the eye of the impeller as recommended by literature [9].
- the blade channel does not have appropriate characteristics: the bends have too low radius and the height of the channel is smaller of what is required (Chapter 5).
- the volute is the main cause of losses and the speed inside it is too high (chapters 3, 4 and 5).

Thus far is clear that some parameters have to be changed in order to obtain a higher efficiency but the range of possibilities is utterly wide. To reduce the enormous amount of possible directions to follow, it was necessary to ask the company which were the particular conditions of work to optimize. The discussion with the company ended in a set of additional considerations that are summarized here:

- The system must not be changed and determines the working conditions of the pump.
- The pump works almost only in a range of 5-20 m³/min that is a part-load type of operation (with the current machine).
- In these working conditions the head must not be too low with respect to the original project
- Blade channel and spiral chasing must remain unchanged because of the company decision.

These limitations reduce the range of possibilities of improving the existing machine. It is now possible to work out a route to be followed. The attempts will follow two main different directions concerning the geometry of the blade that could be two dimensional (reducing the manufacturing costs) or three dimensional. The parallel step is to optimize the inlet and outlet angles for the optimal flow rate (that could be changed) in order to obtain good inlet conditions and the required head performance.

Almost every parameter change causes both some good and some bad effects that have to be considered; the process has the aim to determine the best tradeoff between the two. This is true for the optimal flow rate that, if chosen too high, causes an increase of the maximum efficiency but in that way reduces the part load efficiency (that is the most important characteristic for our purpose). The same concept is valid for the outlet-angle that causes the increase of the blade length and thus the reduction

of the load and the pressure gradients along the blade but at the same times causes additional friction losses due to wider wet-surface.

The approach that is to be followed for the optimization is to change the influence variables one by one and to observe when their positive effects ends and the performances start to drop again. For doing this, the general rule of increasing each variable of a consistent amount was followed, in order to avoid the risk of too many unneeded steps. This means, for example, that the outlet angle was changed of almost 10° during the first try, instead of doing several minor steps. In this way it is possible to realize quite easily the changes produced by the alteration of a single parameter. To avoid confusion, in table 72 are shown the names of all the intermediate versions.

Models name	Geometry
Original model	2-D
Version 1	2-D
Version 3	2-D
Version 4	2-D
Version 6	2-D
Version 8	2-D
Version 2	3-D
Version 5	3-D
Version 7	3-D
Version 9	3-D

Table 72: intermediate versions.

The results will be discussed only for the final and optimized models.

7.2 Optimization of a two dimensional geometry

7.2.1 Version1

The process of optimization started from the analysis of a simple 2-D geometry with the hub and shroud leading edges completely overlapped and in parallel to the axis of rotation. The blade channel is the same as in the original project and so is the optimal flow rate. Repeating the calculation seen in chapter 4 it is possible to determine the optimal β_1 angle (in this case the value of β_{1a} and β_{1i} are the same). For what concerns the β_2 angle, a strong reduction is required to enter in the optimal range of 20-27°; in this way it is possible to attain an extension of the blade length and a reduction of the load.

Since the program “Blade Gen” allows to follow the rules of good blade construction through the use of Bezier curves, it is possible to use it for the development of the new geometry and to be sure that the angle variations will be as smooth as possible.

The drawing of the blade, according to the established angles produces, as expected, a longer blade. The shape of the leading edge will be elliptical from now on because (according to [9]) a sharper edge prevents big gradients of pressure on the blade when used around the best efficiency point. The changes can be summarized in the table 73.

Model	Blade channel	Geometry	Qopt [l/s]	β_{1gi} [grad]	β_{1ga} [grad]	β_2 [grad]	Lmin blade [mm]	Load factor (<0,9)
Original model	Original	2-D	5,5	30	28	33	85	0,96
Version 1	Original	2-Dpure	5,5	20	20	25	110	0,72

Table 73: Geometrical description of Version 1.

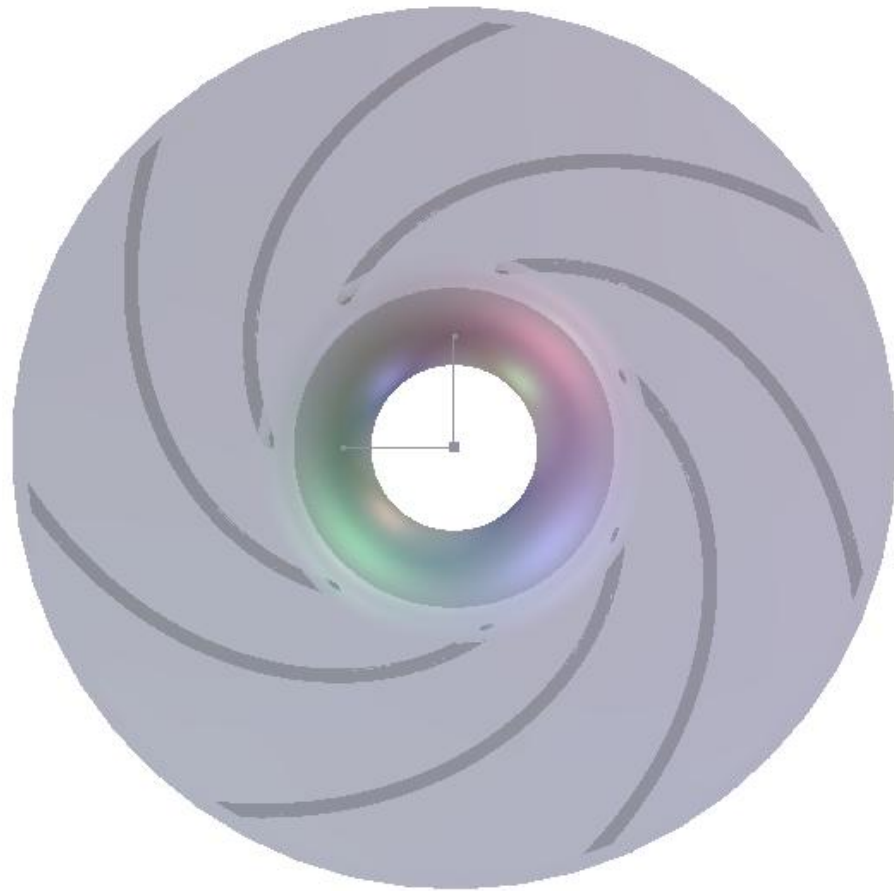


Figure 74: Frontal view of version 1.

Figure 75 shows the outlook of version 1, which also visualizes the complete superposition of the leading edges. It is clear that this kind of blades start from a point of the channel where it is not any more bended and, as a consequence, they are always perpendicular both to the front and to the rear shroud. This construction strongly simplifies the productive process.

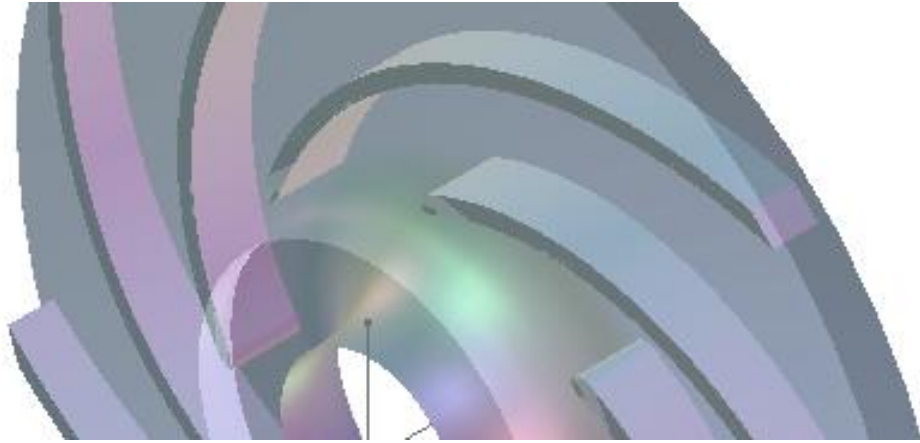


Figure 75: View of version 1.

Behavior of version 1

The expecting results are an improvement of the efficiency due to reduction of the load on the blade while the head should be the same; this is expected because not only the β_2 angle was reduced, but even the β_1 angle.

The CFD analysis of this model was done following the same approach seen for the development of the original model. As expected the characteristic of head is only slightly reduced while the efficiency has risen of around 7% in the BEP, while the rest of the curve doesn't show improvement. This has to be considered as a good result because the poor intake blade geometry meets the flow only after the bending while it is supposed to do it before.

The analysis of this paragraph proves that the use of appropriate angles is always important even for simple pumps with low n_q number.

Looking for more details into the fluid dynamic behavior of this impeller is possible to check that the separation point and consequently the re-circulating part have shifted to a further point with respect to the leading edge. Moreover the drop of pressure behind the leading edge is reduced causing better flow conditions and less shock losses.

The first is consequence of the improved blade length and the second is consequence of better intake angles.

The next logical step is to adopt a better geometry for the inlet, using the same trick seen in the original model: by moving the leading edge into the eye of the impeller is possible to make the blade meeting the flow in a condition that is closer to the ideal one but without compromising the simplicity of the blade that remains 2-D.

7.2.2 Version3

This version is strongly based on version1 but with the leading edge that enters the eye of the impeller. The intent is to investigate the effects of this geometrical feature. Since the two parts of the blade are in different positions they will be subject to different flow conditions and therefore must have different β_1 angles. The blade generating program allows us to determine the distribution of the angles across the length of the blade for two extreme lines corresponding one to the hub and one to the shroud, the values between them are interpolated in a linear way. The changes can be summarized in the table 76.

Model	Blade channel	Geometry	Qopt [l/s]	β_{1gi} [grad]	β_{1ga} [grad]	β_2 [grad]	Lmin blade [mm]	Load factor (<0,9)
Original model	Original	2-D	5,5	30	28	33	85	0,96
Version 3	Original	2-D	5,5	35	20	25	112	0,73

Table 76: Geometrical description of version 3.

The main values remain unchanged and so is the length of the blade and the load index. Even though, the expectation is for an improvement of the efficiency due to more favorable flow conditions in the first part of the blade. This is because the incoming fluid hits the profile in an earlier stage, where the cross section is bigger and the flow slower. Additionally, the curvature in that point is not completed and so is the stream lines distortion.

The lookout of the blade is shown in figure 77.

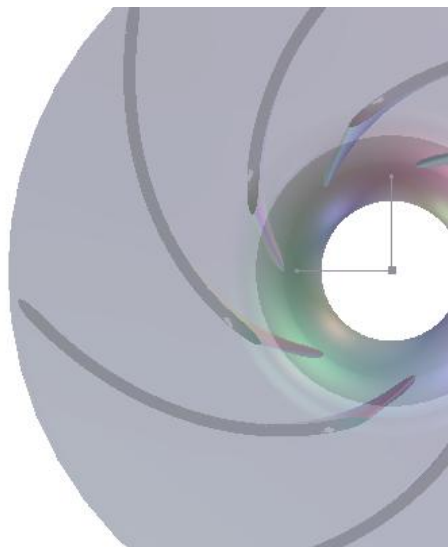


Figure 77: Frontal view of version3.

Behavior of version3

The expected effects of the new intake geometry can be recognized in higher part-load efficiency while the head and the maximum efficiency are not affected.

This geometry proved to cause smoother access into the channel, as a consequence the behavior with high incidence is better.

The flow separation is shifted by a small amount towards the trailing edge.

The efficiency characteristic is the same as the previous version1 around the BEP, but it is 6% higher at 2[l/s].

7.2.3 Version4

The next step of the optimization of a 2-D geometry is to detect the optimal flow rate the pump has to be optimized for. The main parameters have been recalculated to optimize a lower efficiency point. The reduction of the optimal flow rate results in a reduction of the β_1 angle in order to adapt this to the more tangential flow.

Along with this, the β_2 angle is reduced to produce longer and less loaded blades. The reduced flow rate should produce a shift of the efficiency curve and therefore higher efficiency value in the most interesting range of operation, while the longer blade should end up in a better efficiency as well but in a lower head.

The new parameters of this geometry are reported in the table 78.

Model	Blade channel	Geometry	Qopt [l/s]	β_{1gi} [grad]	β_{1ga} [grad]	β_2 [grad]	Lmin blade [mm]	Load factor (<0,9)
Original model	Original	2-D	5,5	30	28	33	85	0,96
Version 4	Original	2-D	4,5	27	14	20	132	0,65

Table 78: Geometrical description of version 4.

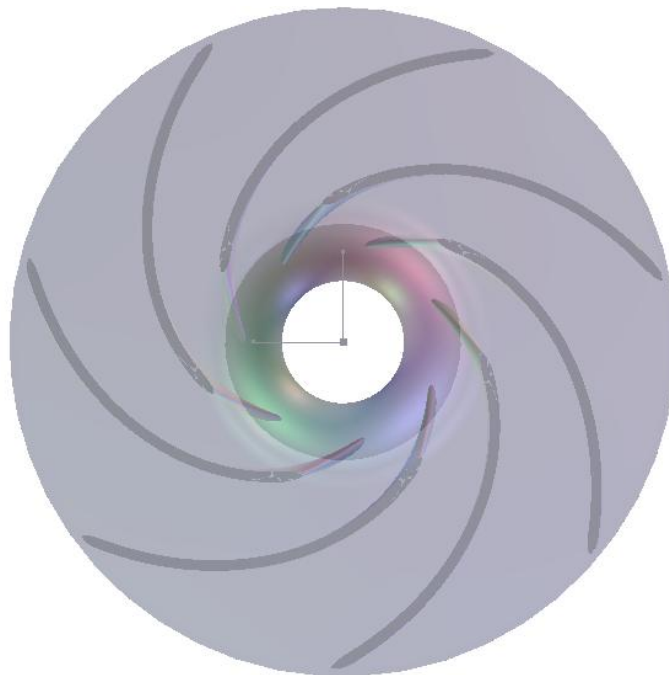


Figure79: Frontal view of version4.

From the picture 79 the longer extension of the blades can clearly be seen along with the reduction of the angles both on the leading and on the trailing edge.

Behavior of version4

As expected the efficiency curve calculated with the CFD is now shifted towards lower values of flow rate increasing the distance from the original curve in the part-load operations (+5% at 3 [l/s]). Additionally the efficiency in the BEP is not reduced, as it was expected from the displacement of the previous curve, but is slightly increased instead (+1% at 5[l/s]). This could be related to the use of a

longer and less loaded blade.

The head characteristic is reduced of around 2,5[m] as could be expected from a reduction of the eulerian work.

The observation of the CFD calculated flow shows that there is not any more a strong separation across the suction side. This is an important achievement because this kind of behavior of the flux is the one with fewer losses. Despite the absence of separation on the suction side, an incipient separation and recirculation can be noticed on the pressure side, this could be the consequence of a too developed boundary layer.

The β_2 angle is on the edge of the optimal range of values suggested by [9] whose experience, along with the two problems previously lighted, suggests to increase the value of the angle. This leads to the next version.

7.2.4 Version 6

In order to maintain the optimal flow characteristics of the previous version, to have a head not so low and a shortened blade that does not allow the boundary layer to grow so much, this version has a slightly higher β_2 angle. The value chosen is half way between the one of version3 and version4. The consequence of this choice is a smaller profile and a higher load.

The main parameters of geometry 6 are reported in the table 80.

Model	Blade channel	Geometry	Qopt [l/s]	β_{1gi} [grad]	β_{1ga} [grad]	β_2 [grad]	Lmin blade [mm]	Load factor (<0,9)
Original model	Original	2-D	5,5	30	28	33	85	0,96
Version 6	Original	2-D	4,5	27	14	22,5	120	0,71

Table 80: Geometrical description of version 6.

Behavior of version 6

As expected the head is increased with respect to the version 4 but is still 1,5 [m] below the original value. This was considered as acceptable.

With respect to the version4, the efficiency is raised of 2 more points at 3[l/s] and it is 1 point lower at 5[l/s]. Since the focus is on the part-load operation, this version is better than the previous one. Concerning the behavior of the fluid along the blades, with reference to the blade to blade view in the flow conditions of 4 [Kg/s] (that is now very close to the optimum point), can be observed the almost total absence of separation of the flow both on the pressure side and on the suction side. This means that excellent flow conditions have been achieved.

The variables optimized till now are: inlet and outlet angles, length of the blade, inlet geometry and flow rate.

One consideration is needed as far as it concerns the optimal flow rate: to lower it once again could be considered a good idea but in this way we would end up reducing too much the performances at higher flow rates and we would break the common sense rule for which the operation point should be a little bit lower than the best efficiency point [9].

Now the total gain in efficiency is of 4,3% at 3[l/s] and of 3,3% at 5[l/s].

7.2.5 Version8

Since the difference between version 4 and 6 is not so big, it is a good idea to decrease the outlet angle to clearly understand the trend of the efficiency.

Version 8 is therefore designed in the same way as version6 is but with $\beta_2=18^\circ$ in order to have bigger blades that are now 146 [mm] long. Nothing else is changed. The geometry 8 is summarized in the table 81.

Model	Blade channel	Geometry	Qopt [l/s]	β_{1gi} [grad]	β_{1ga} [grad]	β_2 [grad]	Lmin blade [mm]	Load factor (<0,9)
Original model	Original	2-D	5,5	30	28	33	85	0,96
Version 9	Original	2-D	4,5	27	14	18	146	0,59

Table 81: Geometrical description of version 8.

Behavior of version8

With respect to version6, the efficiency curve rises of 1% at 3 [l/s] but the rest of the curve is unchanged. The increase of efficiency is now of 4,5% and is uniform all over the useful range of the curve: between 3 and 5 [l/s].

Beside this, the head decreases by 1 [m] and reaches a value of 27,8 [m] at $Q=4$ [l/s]. This means a reduction of head by 2,5 [m] referred to the original impeller design. Such a low value of head could not be acceptable by the company but the decision of accepting it is up to them.

Figure 82 shows the steeper curve of version 8, the reduction of outlet angle causes the drop of head at higher flow rate. Figure 83 shows the efficiency curve. It is to be noticed the uniform rise on all the useful range (5-20 [m³/h]).

The efficiency splitting shows that the gain of efficiency is almost only caused by the rise of the efficiency of the impeller, while volute and volumetric losses are unchanged.

The improvement of impeller efficiency is caused by more favorable conditions of the inlet flow (as can be seen in fig. 85 left) and by the reduction of the blade load. The resulting effect is the disappear of separation along the blade as can be seen in fig.85 (right). Both the figures are related to a flow rate of 4[l/s] that is the most likely working point. These figures have to be compared with the number 64 and 65 of chapter 5, the separation is clearly disappeared and the flow is much more uniform; also the inlet conditions are far better and the stagnation point is rightfully placed on the leading edge.

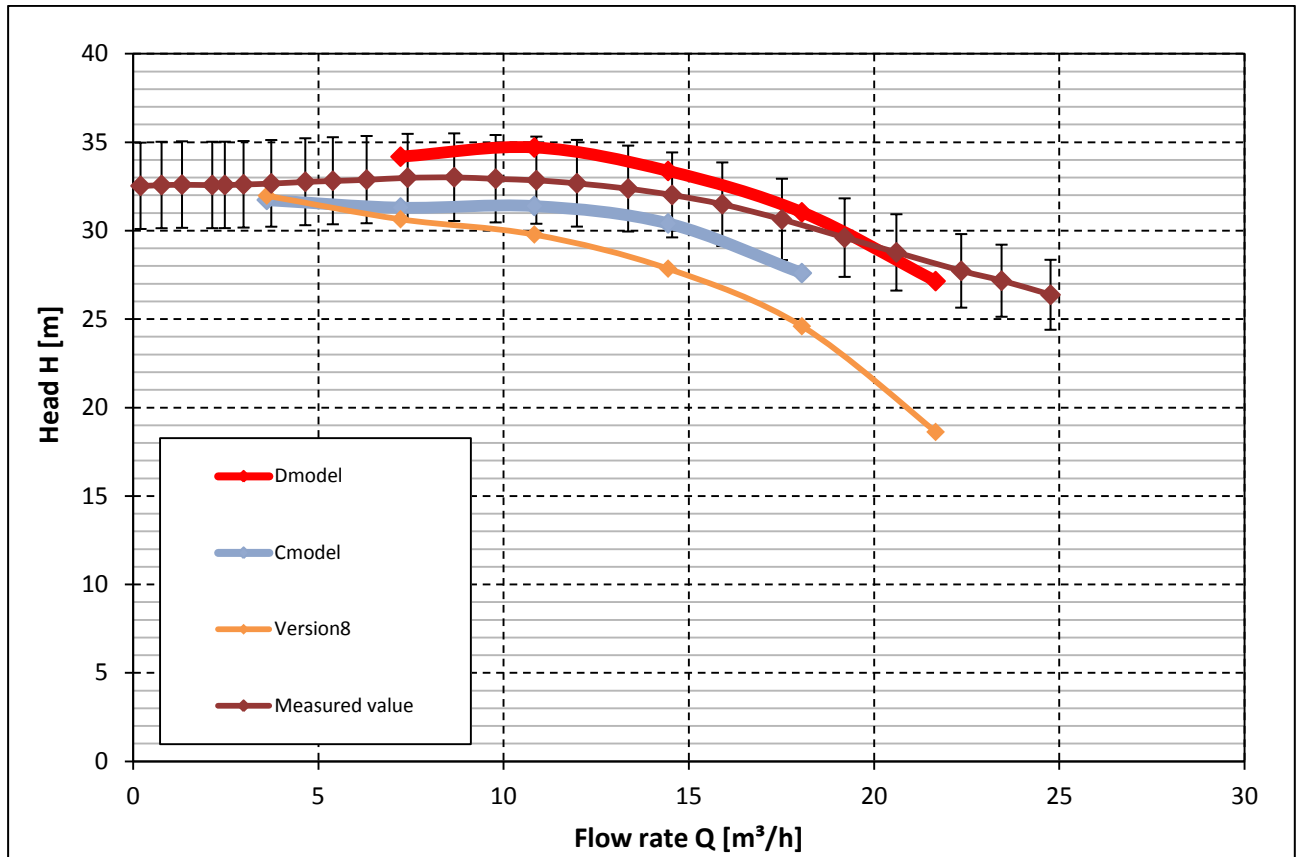


Figure 82: Calculated head curve of version 8.

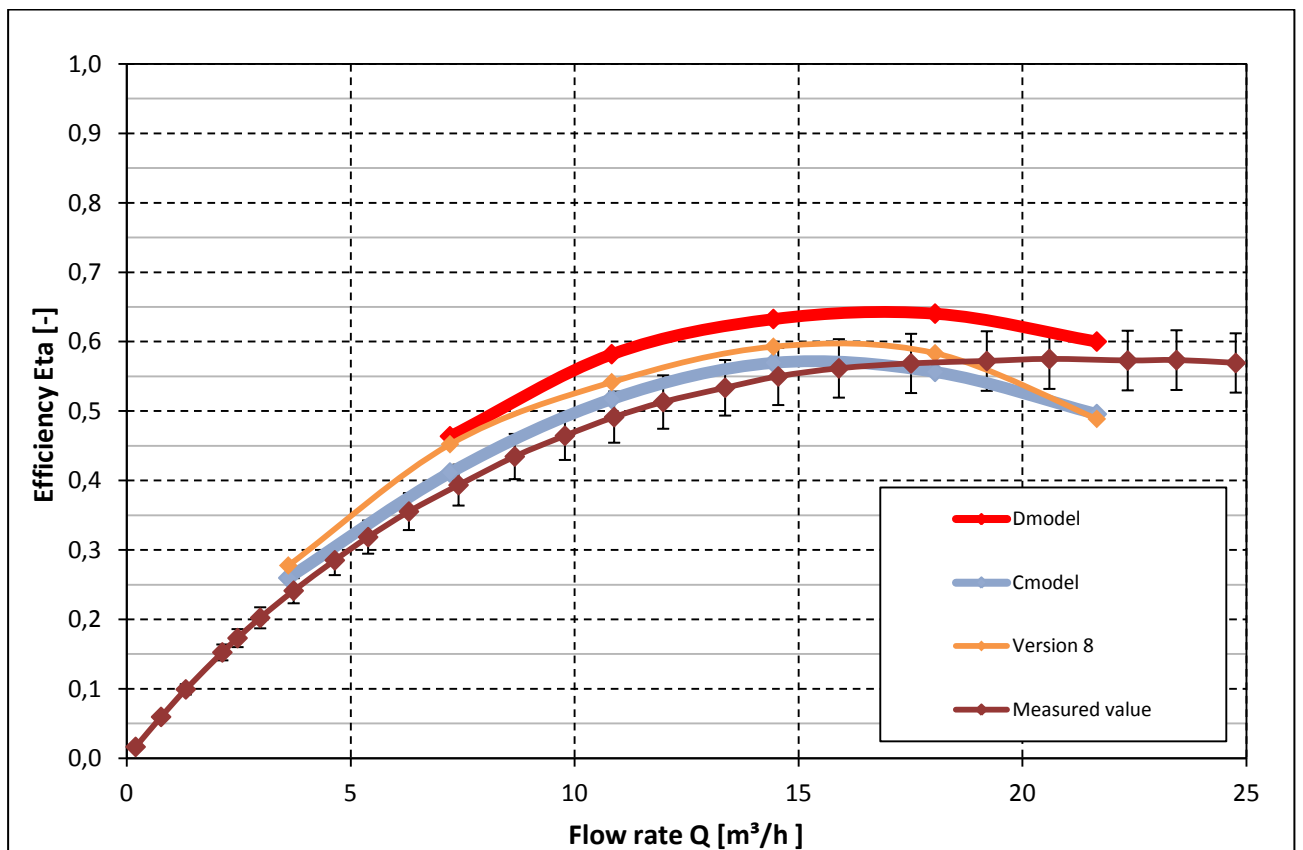


Figure 83: Calculated efficiency curve of version 8.

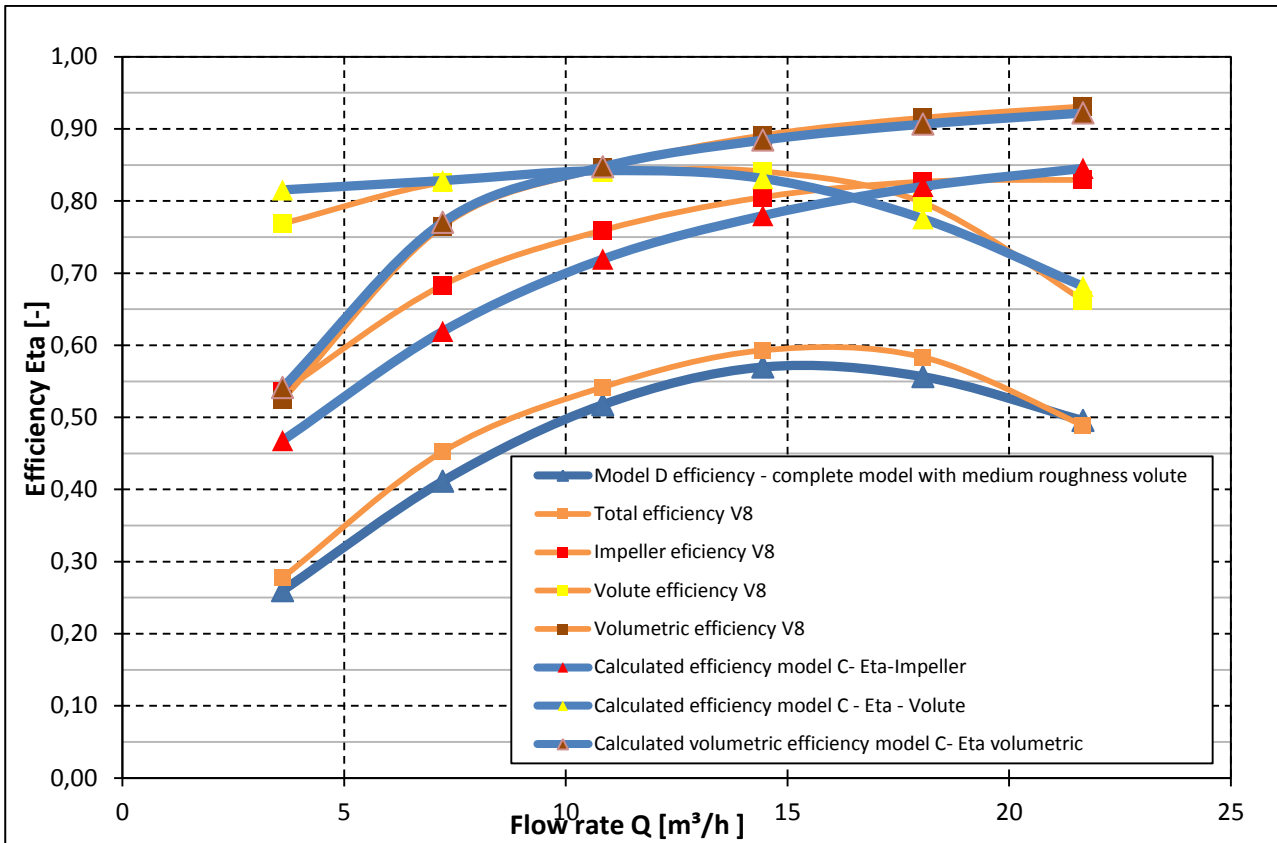


Figure 84: Splitting of efficiency components for original version and version 8.

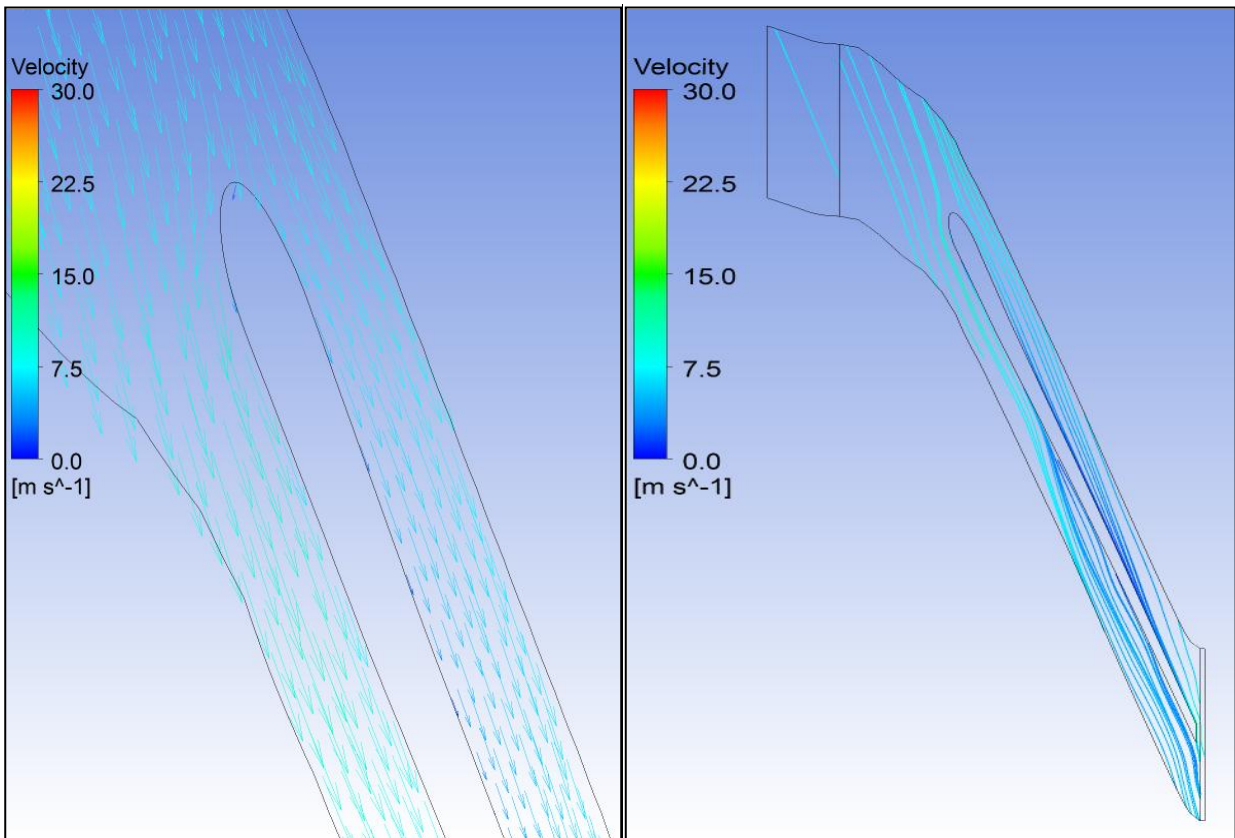


Figure 85: Version 8: Velocity distribution vectors (left) at 80% of blade height; stream lines (right) inside the blade channel at 50% of blade height.

7.2.6 Version9

The next step is to reduce the optimal flow rate to check the evolution of the characteristics. The position of the BEP flow rate is moved to 3,6 [Kg/s]. As a consequence the inlet angles are the one presented in tab.86.

Model	Blade channel	Geometry	Qopt [l/s]	β_{1gi} [grad]	β_{1ga} [grad]	β_2 [grad]	Lmin blade [mm]	Load factor (<0,9)
Original model	Original	2-D	5,5	30	28	33	85	0,96
Version 9	Original	2-D	3,6	24	23	20	132	0,65

Figure 86: Geometrical characteristics of version 9.

Behavior of version9

The efficiency curve shows a reduction (with respect to version6) of 0-2% all over the useful range and the drop, even if small, means that such a low optimal flow rate has jeopardized the maximum efficiency that can be reached. A flow rate of 4,5 [l/s] is the best one that we tried till now and is the best tradeoff between the optimal placement of the BEP and the reduction of nq number.

7.3 Optimization of a three dimensional geometry

7.3.1 Version2

A different approach for enhancing the performances of the pump is to provide that the leading edge of the blade enters in the eye of the impeller where the incoming flow is more homogeneous and slower. Eventually this operation causes an elongation of the blade that, as a consequence, is less loaded and less likely to face a flow separation and a drop of performances.

The downside of this construction is that the blade becomes three dimensional and more difficult to produce.

One particular expectation for this geometry is that the head curve rises when close to the zero flow rate operation, erasing every trace of instability. This is due to the bigger blade height in the first section that makes easier the recirculation process (compulsory at very low flow rate) by leaving more space for the fluid to recirculate. The recirculation forces the main flow on more internal stream lines that are subject to bigger centrifugal effect as can be seen from fig. 87.

According to these considerations, the version2 was built. The different radial position of the intake

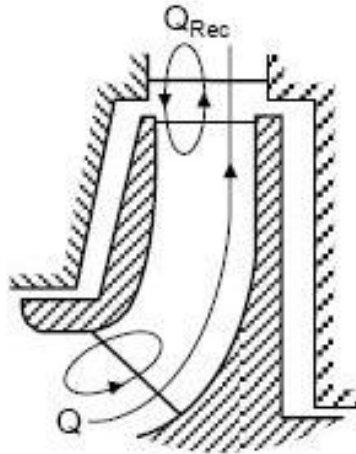


Figure 87: Representation of recirculating flow in the meridian channel. [9]

edge requires different angles that are calculated using the velocity triangles. One important detail is the distance between the shroud leading edge and beginning of the shroud bending. This distance should be of at least 3 [mm](according to [9]) to leave a little space for the fluid to regain pressure before starting to change direction; in this case the geometry does not allow this space so it is followed the rule of using the maximum value that is possible.

The β_2 angle is reduced to 25° based on the experiences with the two dimensional models. Blade channel and best efficiency flow rate are unchanged to better maintain the focus on the effects of the three-dimensionality.

The most important geometrical values are listed up in tab.88.

Model	Blade channel	Geometry	Q_{opt} [l/s]	β_{1gi} [grad]	β_{1ga} [grad]	β_2 [grad]	Lmin blade [mm]	Load factor (<0,9)
Original model	Original	2-D	5,5	30	28	33	85	0,96
Version 2	Original	3-D	5,5	39	27	25	120	0,66

Table 88: Geometrical characteristics of version 2.

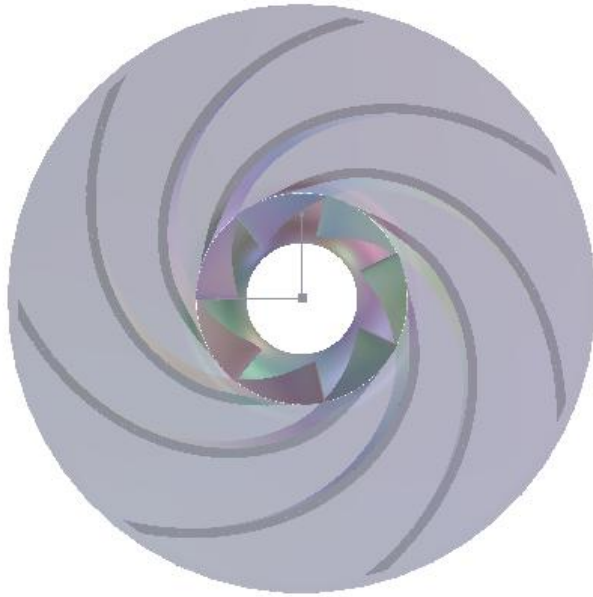


Figure 89: Frontal view of version 2.

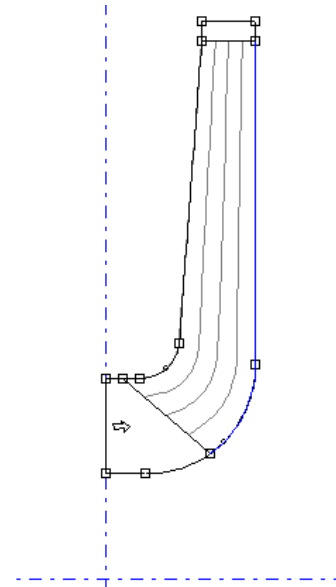


Figure 90: Meridian section of version 2.

Figure 89 shows the frontal view of the runner, showing the three dimensional characteristics. Figure 90 shows the position of the leading edge inside the channel in the meridian section.

Behavior of version2

The characteristics of head and efficiency were simulated with a CFD analysis on different flow rate conditions.

The efficiency curve is above the original in part-load region, the rise is around 5,3% for 3[l/s]. Around the BEP, the efficiency is 3% lower than before. The effectiveness of this geometry could be considered proved.

The head curve presents the expected shape with a higher value in the first part and a slightly lower one in the central part.

As it is always done in this work, the simulation is stopped at 6[Kg/s] because that is the upper limit of the exploited range and because this model didn't completely succeed in the modeling of the over load behavior.

Details of the flow across the blade to blade view show once more that the longer blade strongly reduced the separation on the blade by shifting its beginning to a further radial position, almost on the blade end. This is the reason for the better efficiency.

The stagnation point is not exactly in the tip but moved towards the pressure side on the hub stream line (β_1 too big) and moved towards the suction side on the shroud stream line (β_1 too small). Despite the non perfect flow conditions, this version has a better efficiency than most of the 2-D models.

The next logical step is to analyze the effect of a lower best efficiency flow rate and to try to find the best β_2 value.

7.3.2 Version5

This version has been developed with the aim of investigate the effects of an optimization for a reduced best efficiency flow rate of 3,6 [Kg/s]. This means that the intake angle has to be smaller to adapt to a more tangential optimal flow rate. The efficiency curve should result shifted from this operation. Along with this, it is tried a reduced β_2 of 23° to try to completely extinguish the flow separation but without increasing too much the length of the blade and the friction losses. This will reduce the head too.

The main parameters of the geometry 5 are summarized in the table 91.

Model	Blade channel	Geometry	Qopt [l/s]	β_{1gi} [grad]	β_{1ga} [grad]	β_2 [grad]	Lmin blade [mm]	Load factor (<0,9)
Original model	Original	2-D	5,5	30	28	33	85	0,96
Version 5	Original	3-D	3,6	29	22	23	133	0,63

Table 91: Geometrical characteristics of version 5.

Behavior of version5

The simulated characteristics of the pump are now better as far as it concerns the efficiency that has raised of around 7,2% in the part load field (3[l/s]) and of 3% around the BEP point (5[l/s]). As opposite, the head has now decreased and presents around 2[m] less than the original version at (5[l/s]). Ulterior reductions should be avoided.

The examination of the flow behavior shows no more signs of recirculation or flow separation. From a fluid dynamic point of view this is the optimal condition.

The stagnation point is now closer to the trim of the leading edge than before but β_{1hub} is still too big and must be corrected in a following version.

This version is the best seen till now both for fluid behavior and efficiency characteristic. The lack of instability in the head curve is another strong point of this model.

7.3.3 Version7

This version was developed based on the previous one but has the aim of investigating the effects of a further reduction of the β_2 angle. This is nonsense from the point of view of the head reduction but is important to understand whether the efficiency drops as well as the head does. For this reason the new impeller presents the dimensions shown in tab.92.

The β_1 angle near the hub has been lowered according to the considerations relative to version 5.

Model	Blade channel	Geometry	Qopt [l/s]	β_{1gi} [grad]	β_{1ga} [grad]	β_2 [grad]	Lmin blade [mm]	Load factor (<0,9)
Original model	Original	2-D	5,5	30	28	33	85	0,96
Version 7	Original	3-D	3,6	25	22	18	148	0,57

Table 92: Geometrical characteristics of version 7.

Behavior of version7

Despite the improvement of the intake geometry (that can now be considered optimal for what concerns the position of the stagnation point along all blade height), this version presents slightly lower characteristics of efficiency across all the considered range.

The interpretation of this phenomenon is that a too long blade causes at the same time a reduction of the load and an increase of the friction losses. The balance between these two effects gives the higher impeller efficiency. This point of best equilibrium has been found to be the one seen in version5.

7.3.4 Version10

The final version that should be the number 5 but, since it presented some problems in the inlet region (stagnation point moved on the pressure side), the model has to be adapted and, in particular, the β_1 near to the hub must be reduced.

The new intake hub angle has a value of 25°, in this way the stagnation point should be exactly on the edge of the blade avoiding big pressure drops on the suction side and reducing the impact chock losses. Everything else is equal to the version5.

The resulting geometry is summarized in tab.93.

Model	Blade channel	Geometry	Qopt [l/s]	β_{1gi} [grad]	β_{1ga} [grad]	β_2 [grad]	Lmin blade [mm]	Load factor (<0,9)
Original model	Original	2-D	5,5	30	28	33	85	0,96
Version 10	Original	3-D	3,6	25	22	23	133	0,63

Table 93: Geometrical characteristics of version 10.

Behavior of version10

As expected, this version presents the best characteristics of efficiency with an improvement of 3,3% at 5 [l/s] and 7,0% at 3[l/s]. The reduction in head is of 1,5 [m] at 5[l/s] and could be considered acceptable. From the analysis of the flow it can be seen that there is no more separation behind the leading edge, even in the most critical place: near the front shroud. This is visible from fig.94 (inlet flow conditions for the optimized version 10. The separation behind the blade is disappeared.).

The characteristic curves of head and efficiency are presented in fig. 95 and 96.

Fig. 97 shows the efficiency splitting. The total increase of efficiency is only caused by the impeller improvement while the components related to the volute and volumetric losses are mainly unchanged.

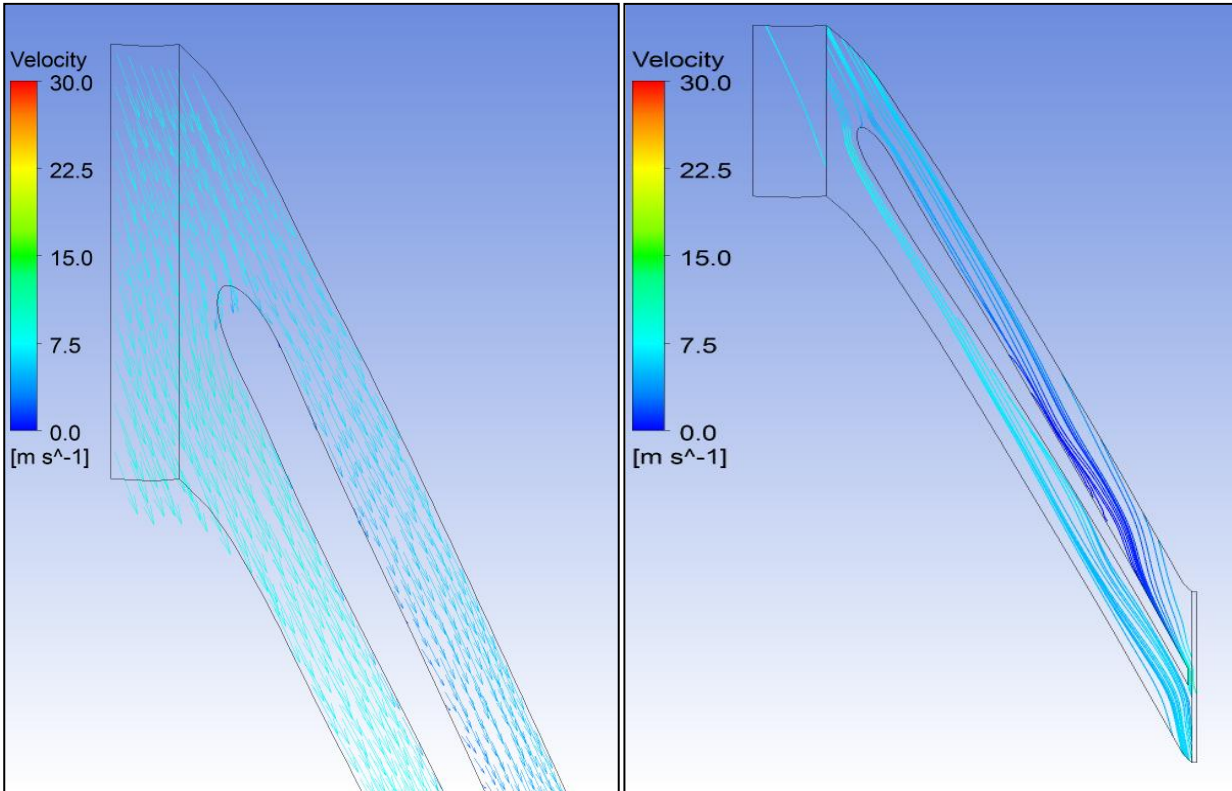


Figure 94: Version 10: Velocity distribution vectors (left) at 80% of blade height; stream lines (right) inside the blade channel at 50% of blade height.

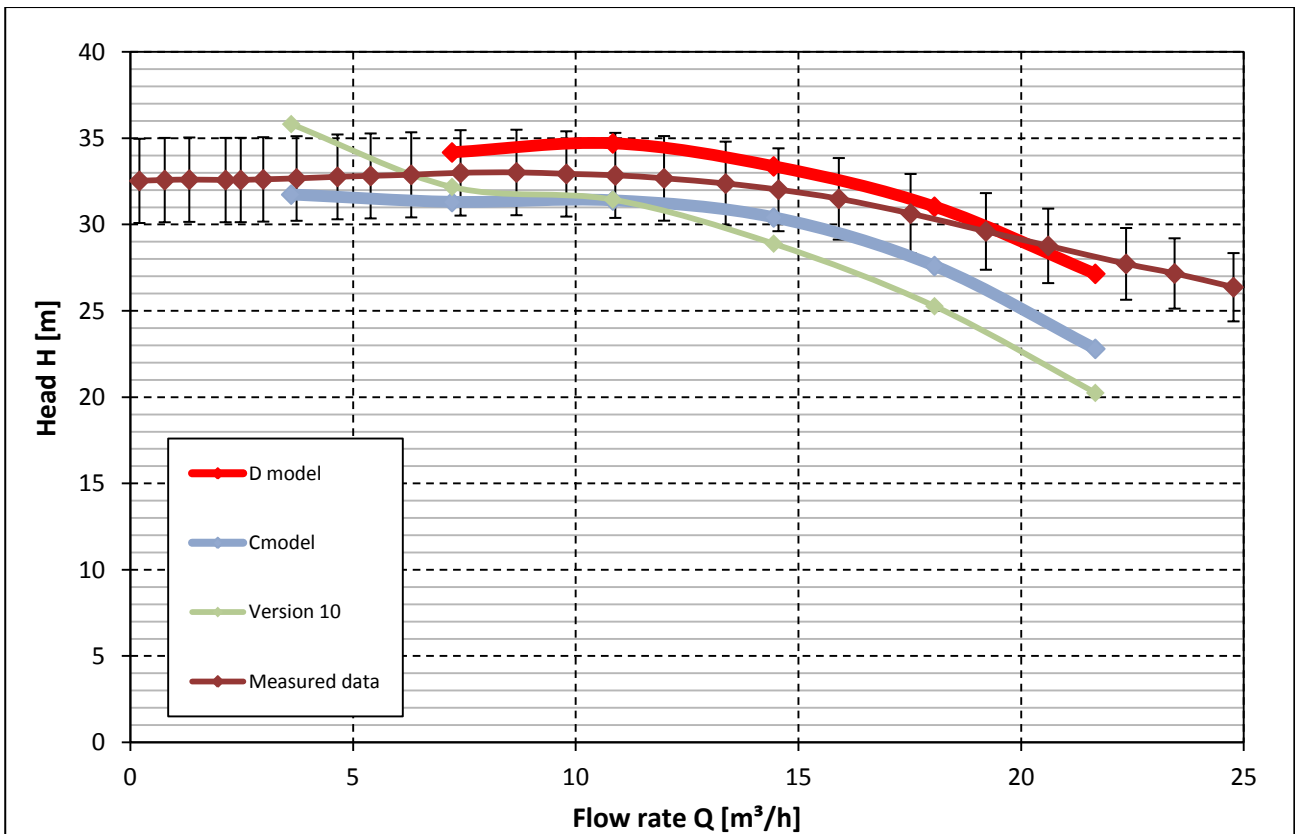


Figure 95: Calculated head curve of version10.

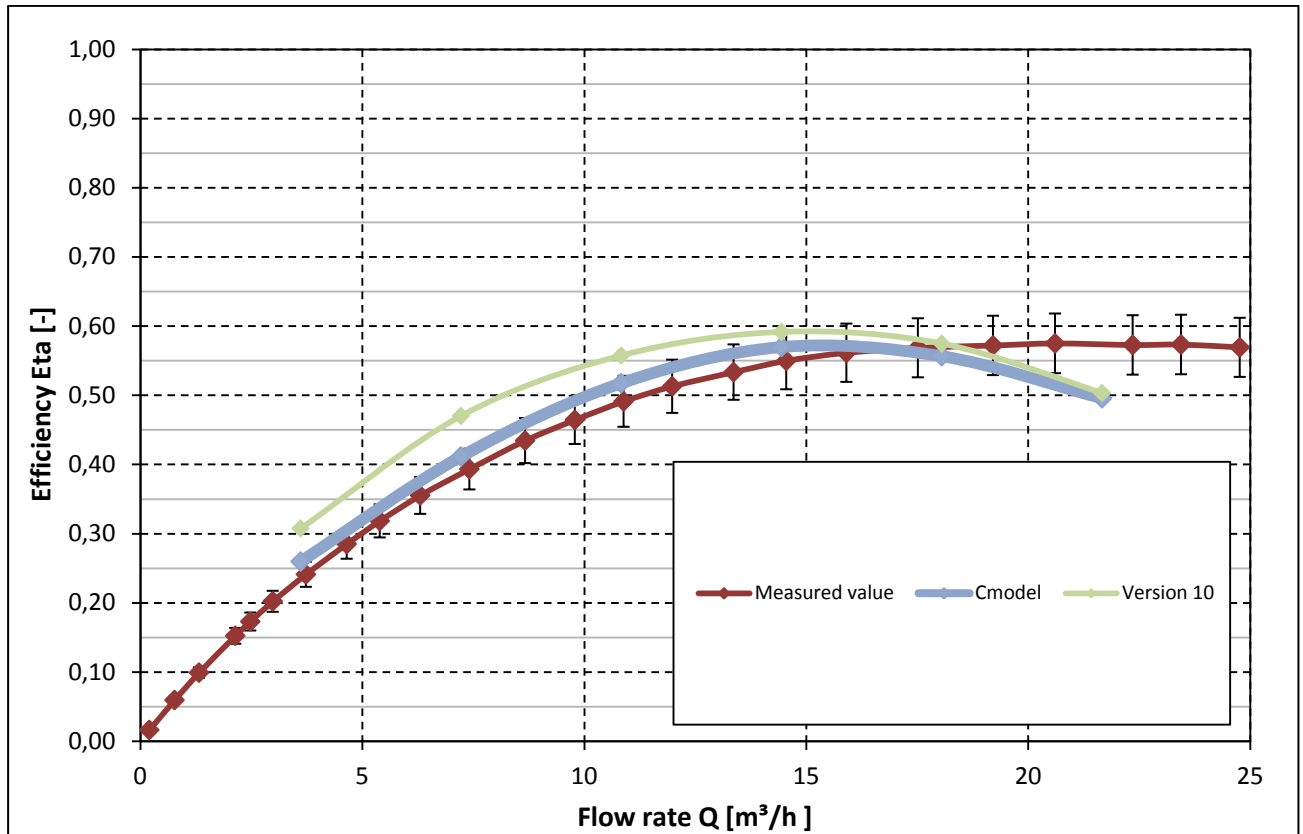


Figure 96: Calculated efficiency curve of version10.

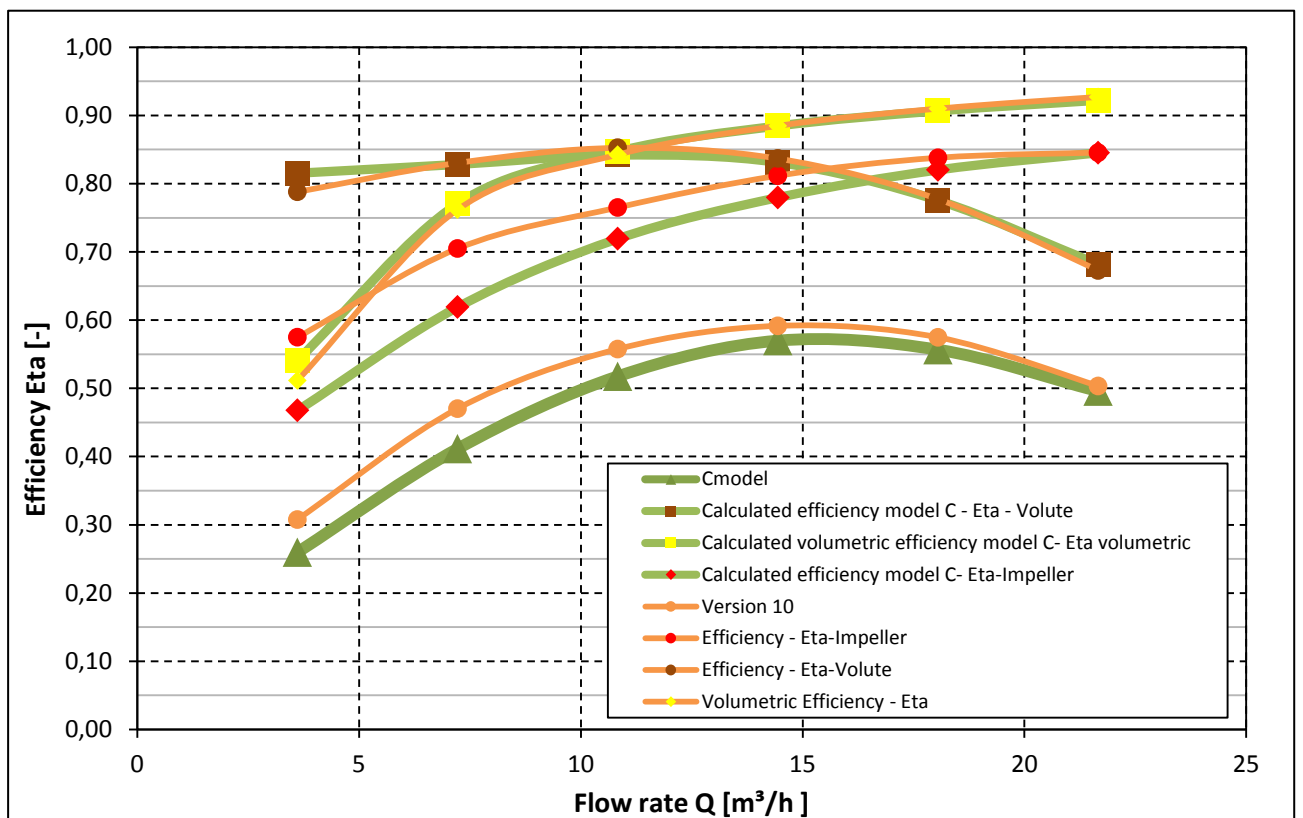


Figure 97: Splitting of components for original version c and version 10.

7.4 Conclusions

To work out a new improved geometry for the impeller, a CFD model was used that proved to give results close to the measured values in the considered flow rate range from 1 up to 6 [l/s]; these are conservative (meaning that the values of efficiency are slightly higher than the measured ones) so the value must be handled very carefully. For the purpose of this chapter, the calculated efficiency values are treated as an index of improvement. This means that we prefer to focus on the increment of efficiency rather than on its absolute value.

The ways followed for the optimization process are two: a two dimensional geometry (as the one of the original model) with the aim of obtaining blades easy to manufacture, and a three dimensional geometry that allows better flow conditions but requires a more complex manufacture process. The two geometries are shown in figure 98 both compared with the original version. The change in the angles is clearly visible and so is the extension of the blades.

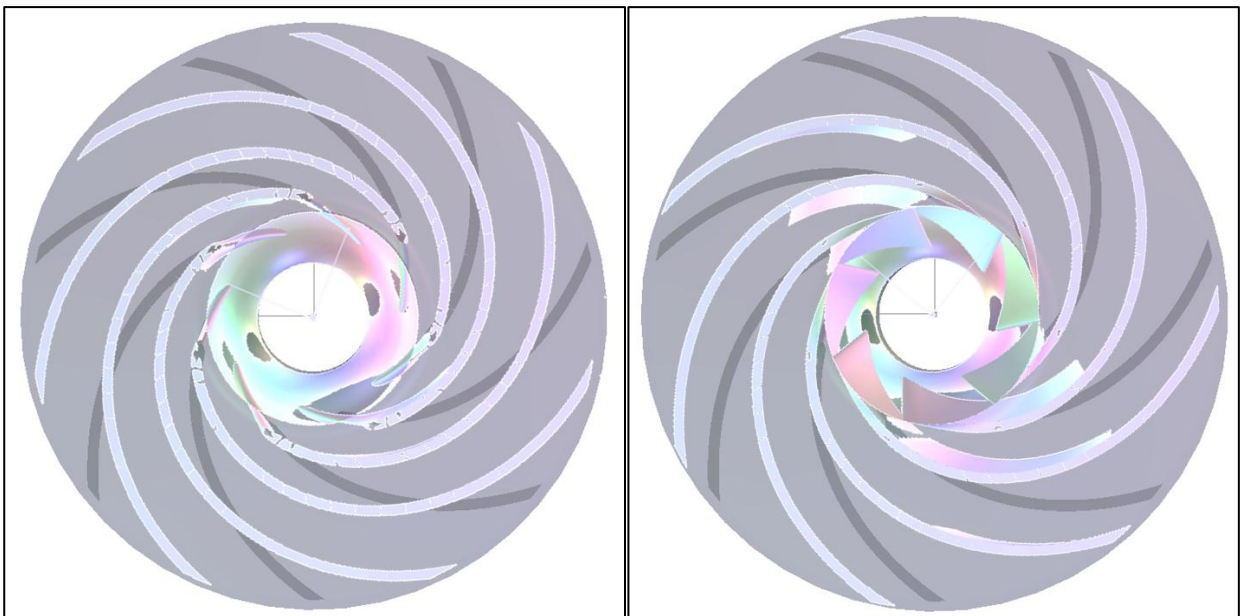


Figure 98: Geometry of impellers Version10 (left) and Version8 (right) confronted with the original impeller.

The two dimensional model proved to give the best results with version 8. This presents a leading edge that grows into the eye of the impeller, a β_2 angle of 18° , a blade with a length of 146 [mm] and a best efficiency point designed to be at a flow rate of around 4,5 [Kg/s].

In this way a rise of efficiency of almost 4,5% on all the useful range is attained.

The three dimensional model finds its best in the version 10 that has a β_2 angle of 23° , a blade with a length of 133 [mm] and a best efficiency point designed to be at a flow rate of around 3,5 [Kg/s]. This version provides a rise in part load efficiency of more than 7% and of 3% in the former best efficiency point.

Which version to choose between these two will be up to the company that has to take into account techno-economical knowledge of the productive process and of the market.

The increment of performances is very interesting if it is considered that every year several thousand of these pumps are sold and from this prospective also a small improvement makes sense. For what concerns the maximum value of efficiency that is actually reached, its value is around 60% for both the optimized models. When this is compared with the maximum value practically obtainable, it results that there is still room for further improvement. This should come from the optimization of the volute whose losses are the most important ones especially at higher flow rate ($Q > 15$ [m³/s]). The efficiency value of the impeller is lower at part-load because of the compulsory flow separation and recirculation. After a flow rate of 15 [m³/h], its value becomes more stable in all the versions analyzed, the maximum impeller efficiency stays around 85% and further improvement of this value since it is strongly constrained by the disk friction (the efficiency of impeller is in fact comprehensive of this loss).

Chapter 8: Final considerations.

In this chapter the main conclusions of the work will be drawn along with a brief summary of the procedure and with the suggestions for future works.

8.1 Overview on procedure and results

The pump had to be experimentally analyzed to validate the data sheets of the company and to have a trusted confrontation term for the numerical simulations. The numerical calculations based on literature models helped us in understanding the relative importance of different phenomena and to judge the plausibility of the CFD results. From these examinations we discovered that the main cause of losses are the disk friction and the volute, while the friction and turbulent losses inside the impeller acquire importance at part load operation. These considerations are in theoretical agreement with the small nq number of the machine ($nq=17$). The BEP resulted to be much higher than the real working point, forcing the pump to operate with non optimized flow conditions.

The main points on which the optimization process should focus on are:

- Reducing the load of the blade by using longer blade with a lower outlet angle.
- Improving the inflow conditions by reducing the inlet angles.
- Using a more axial impeller to avoid the current sharp bend on the front shroud.
- Using an optimized volute.

The company that manufactures the impeller proposed to focus the optimization only on the blades because they did not want to change the casing and the volute; as a consequence the blade channel of the pump had to remain unchanged.

The validated CFD model is used as a base for the optimization process and the new versions are derived from the change of this model. The relative improvements in efficiency are considered as an index of the quality of the process. The best results of the optimization are versions 8 and 10, the first has two-dimensional blades that develop only in the radial impeller, and the other version has three-dimensional blades whose leading edge enters inside the eye of the impeller: in short an inducer has been added. Both versions increased the efficiency at part load operation and in the BEP. The rise of efficiency is between 4,5 and 7 % at 3 [l/s]. This is also archived through the shift of the BEP to lower flow rates. The increase of efficiency at 5 and 6 [l/s] is caused by the better inflow conditions and by the reduction of the load of the blade.

Beside the better behavior at part-load, the maximum value of efficiency is now calculated to be higher than 60%. If compared with a maximum practically attainable efficiency of 67%, the upper limit it is still far. Nevertheless it must be kept in mind that the aim of optimizing the part-load behavior is in contrast with the increase of the maximum efficiency because the first process requires a reduction of the nq number and the second requires an increase of it. Moreover the imposition of not to change the volute and the blade channel prevents the pump from reaching higher efficiency.

Even a small increase of efficiency makes sense when several thousand pieces of the pump are sold every year.

8.2 Considerations

From the results of the work, some interesting conclusions can be found.

The original machine used to have an nq number of 17 that is considered low since the range for radial impellers is between 10 and 100 (Chapter 1). This peculiarity characterizes the behavior of the pump and the relevance of some aspects like the relative importance of some losses. The operations of optimization (considering the position of the actual working point) lead to the design of new versions with even lower nq number ($nq=13$); this is really close to the limit value of the range.

For this low value of nq , the importance of the impeller losses is reduced as confirmed in chapters 3 and 5. This leads some authors ([9]) to suggest not paying excessive attention to the blade design to the point that, for some applications, also straight radial blades can be suggested. Despite this, when the pump already shows a good behavior and the grow of efficiency is an issue, even small details of the blade become important. This is much truer in the present situation where the part-load operations are important: there the losses of the impeller become more relevant.

In the present situation it is worth focusing on the impeller for the purpose of optimization and the amount of pumps sold every year explains the importance of even small improvements.

8.3 Possible improvements

One possible way of improving the current work is the design of a new volute that produces a reduction of the speed inside it and a decrease of the friction losses. An optimization of this component could cause an ulterior small increment of efficiency around the current working point (where the importance of the volute losses are anyway reduced) but mainly an increase at high flow rate where the BEP is placed, there the volute losses are by far the most important. The consequence of this improvement is therefore a higher maximum efficiency that could eventually get closer to the practically attainable theoretical value of 67% [14].

Another possible improvement is the change of the whole casing. This has the consequence of allowing the use of a more axial impeller and of increasing the radius of the bend of the meridian section. The benefit of this should be seen in a flow that is less likely to separate. More uniformity of the flow means higher efficiency of the impeller.

In the end it must be considered that the present work is only focused on the increase of efficiency of the model with the bigger diameter: Plastic D155. The smaller models (Plastic D142; D136; D128; D110) are then produced by trimming of this impeller to smaller radius. An analysis should be conducted to determine the real effects of the proposed changes on the smaller impellers.

APPENDIX 1: Measurements errors

Quantity	Permissible value	
	grade 1 %	grade 2 %
Flow rate	± 1,5	± 2,5
Speed of rotation	± 0,35	± 1,4
Torque	± 0,9	± 2,0
Pump total head	± 1,0	± 2,5
Driver power input	± 1,0	± 2,0

Permissible values of systematic uncertainties. Table 7 from ISO 9906 [6].

Quantity	Symbol	Grade 1 %	Grade 2 %
Flow rate	e_Q	± 2,0	± 3,5
Speed of rotation	e_n	± 0,5	± 2,0
Torque	e_T	± 1,4	± 3,0
Pump total head	e_H	± 1,5	± 5,5
Driver power input	e_{Pgr}		
Pump power input (computed from torque and speed of rotation)	e_P		
Pump power input (computed from driver power and motor efficiency)	e_P	± 2,0	± 4,0

Permissible values of overall measurement uncertainties. Table 8 from ISO 9906 [6].

Quantity	Symbol	Grade 1 %	Grade 2 %
Overall efficiency (computed from Q , H and P_{gr})	$e_{\eta gr}$	± 2,9	± 6,1
Pump efficiency (computed from Q , H , T and n)	e_{η}	± 2,9	± 6,1
Pump efficiency (computed from Q , H , P_{gr} and η_{mot})	e_{η}	± 3,2	± 6,4
NOTE For taking into account additional uncertainties referred to, losses refer to 10.4.			

Resulting values of the overall uncertainties of efficiency. Table 9 from ISO 9906 [6].

Because of manufacturing uncertainties during completion, geometrical deviations from the drawings are given at every pump.

When comparing the test results with guaranteed values (operation points), tolerances shall be allowed, including the possible deviations in operating dates between the tested pump and a pump without any manufacturing uncertainties.

It should be pointed out that these tolerances in operating behaviour of the pump are relative to the real pump and not to the test conditions and the measuring uncertainties.

To simplify the verification of guaranteed values, the introduction of tolerances factors is recommended.

These tolerance factors, $\pm t_Q$, $\pm t_H$ and t_η on the flow rate, pump total head and pump efficiency, respectively, shall be applied to the guarantee point Q_G, H_G .

In the absence of a specific agreement on the values to be used, the values given in Table 10 shall be used.

Table 10 — Values of tolerance factors

Quantity	Symbol	Grade 1 %	Grade 2 %
Flow rate	t_Q	$\pm 4,5$	± 8
Pump total head	t_H	+ 3	+ 5
Pump efficiency	t_η	- 3	- 5

Other tolerance ranges (e.g. only given by positive tolerance factors) may be agreed in the contract.

The performance of pumps produced in series and with selection made from typical performance curves published in catalogues and pumps with a power input less than 10 kW may vary. Tolerance factors for those pumps are indicated in annex A.

Value of tolerance factors. Chapter 6.3 ISO 9906 [6].

NOTE This annex applies only to the allowable working range of the pump.

A.1 Pumps produced in series with selection made from typical performance curves

The performance curves in catalogues represent the mean (not the minimal) performances of a series of pumps of the same type. This applies also to efficiency and power input. Therefore increased tolerances and even tolerances on power are necessary.

When the manufacturer/supplier makes reference in his catalogue to this annex, the following maximum factors shall be used:

- for flow rate $t_Q = \pm 9 \%$
- for pump total head $t_H = \pm 7 \%$
- for pump power input $t_P = + 9 \%$
- for driver power input $t_{P_{gr}} = + 9 \%$
- for efficiency $t_\eta = - 7 \%$

A.2 Pumps with a driver power input less than 10 kW

For pumps with driver power input less than 10 kW but greater than 1 kW, where friction losses in various mechanical components become relatively important and not easily predictable, the tolerance factors given in Table 10 may not be applicable. In this case the tolerance factors shall be follows:

- flow rate $t_Q = \pm 10 \%$
- pump total head $t_H = \pm 8 \%$

The tolerance factor on efficiency, t_η , if not otherwise agreed, may be calculated as follows:

$$t_\eta = - \left[10 \left(1 - \frac{P_{gr}}{10} \right) + 7 \right] \%$$

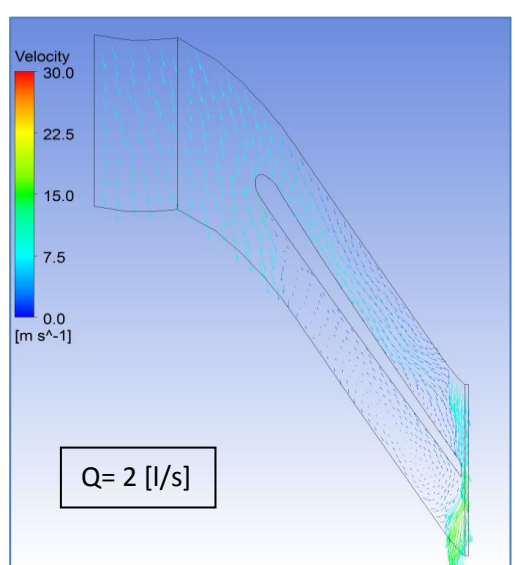
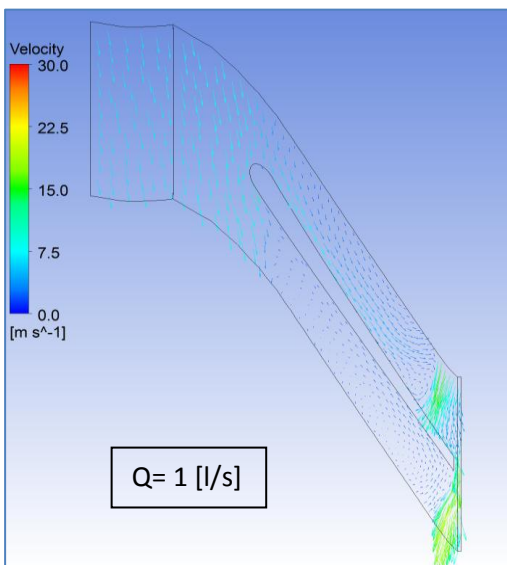
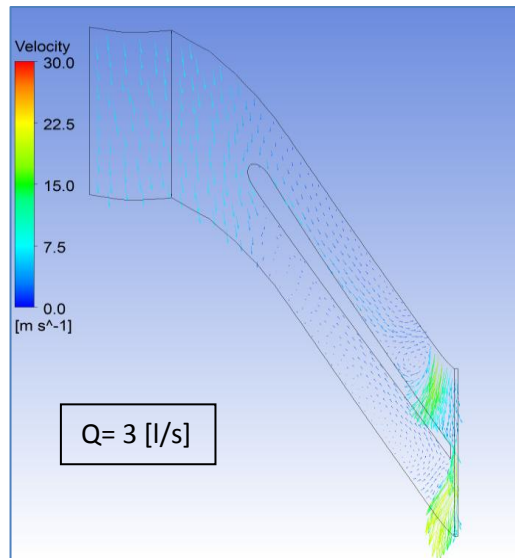
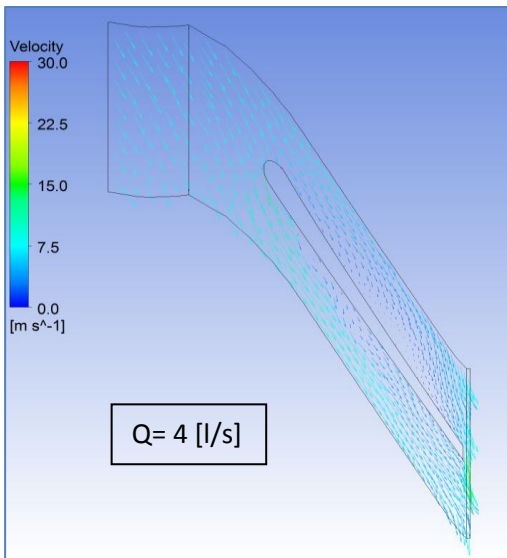
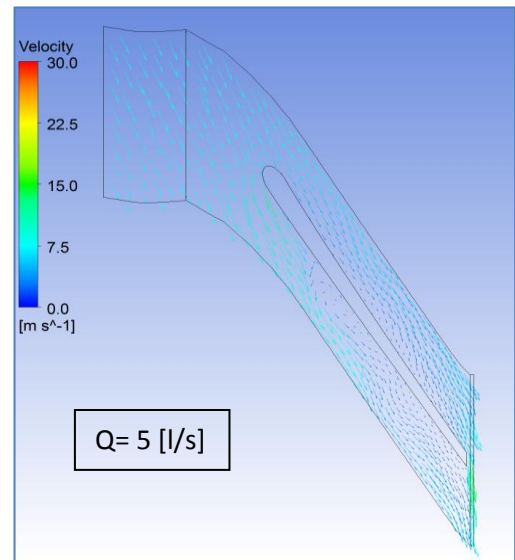
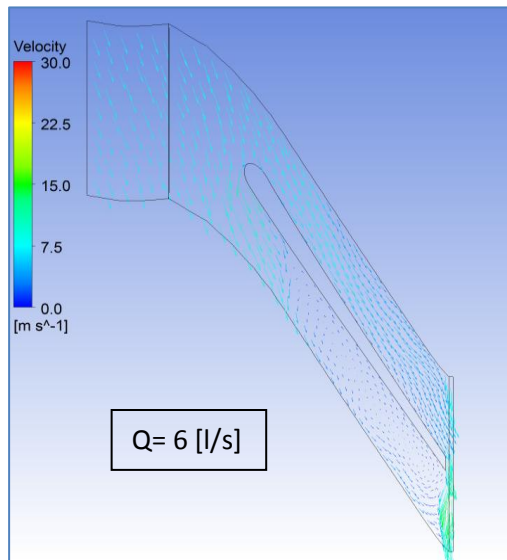
where P_{gr} is the maximum driver power input in kilowatts over the range of operation. A tolerance factor $t_{P_{gr}}$ is allowed using the following formula:

$$t_{P_{gr}} = \sqrt{(7 \%)^2 + t_\eta^2} \%$$

NOTE For pumps with very small power input (less than 1 kW), another special agreement may be decided between the parties.

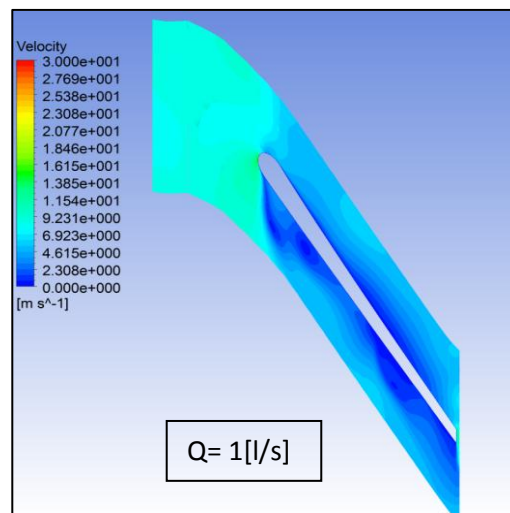
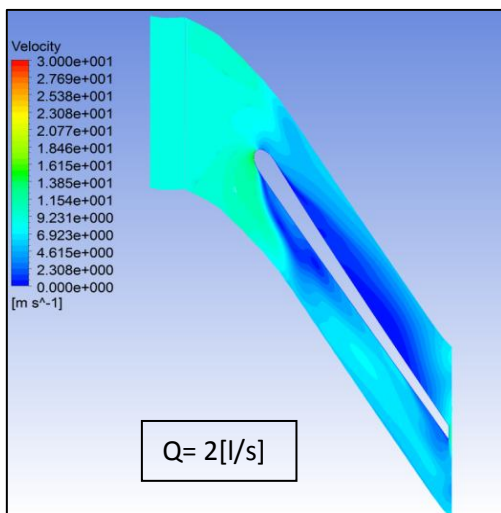
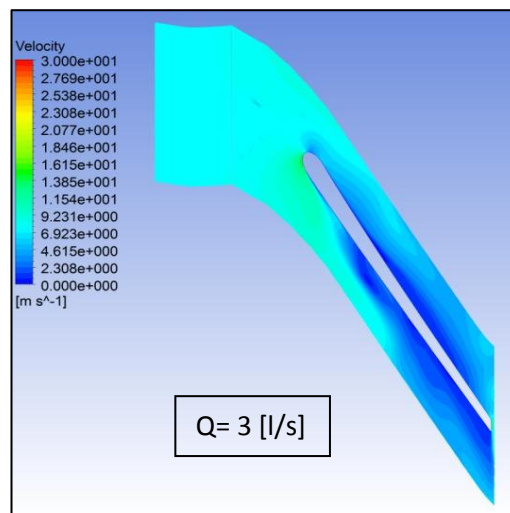
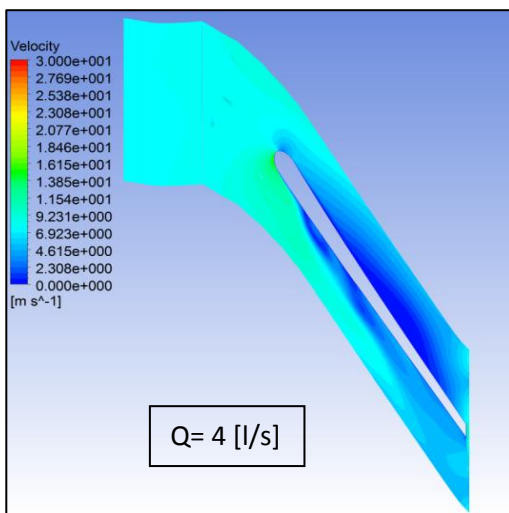
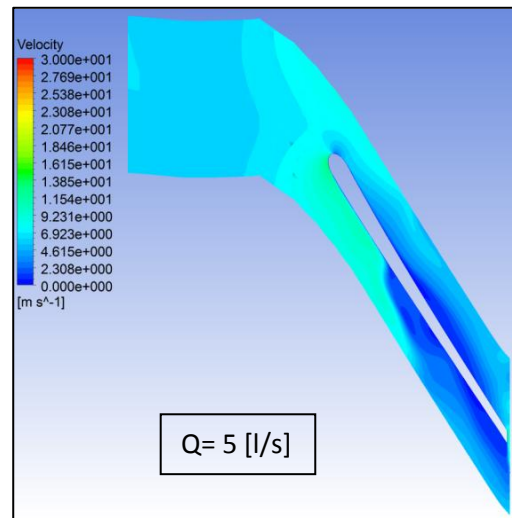
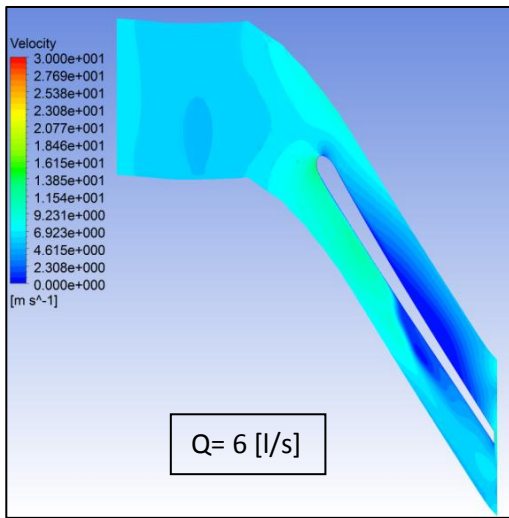
Tolerance factors for pumps produced in series with selection made from typical performance curves and for pumps with a power input less than 10 KW (for grade of accuracy 2). ISO 9906 [6].

APPENDIX 2: Results of the CFD calculation



CFD calculation of the original Plastic D155: velocity vectors in the blade to blade view at decreasing flow rate conditions. 50% of blade height.

APPENDIX 3: Results of the CFD calculation



APPENDIX 4: Cavitation considerations

The problem of cavitation is of a great importance in the pump practice and must never be underestimated. The present situation is supposed to be safe for what concerns this issue because the machine is placed under the level of the water and this does not let the pressure dropping too much at the inlet section. Moreover, in the long service career, no damages nor noise nor vibrations have been recorded. But such is the danger that it is better to look for another prove of the lack of cavitation.

To ensure that the value of NPSHavailable is greater than the NPSHrequired, we have to calculate both of them.

NPSHavailable is the value of the load of the fluid at the entrance of the pump; it is the value available from the system. It can be calculated in a simple way using the following formulation:

$$NPSH_A = \frac{P_{atm}}{\rho * g} - \Delta z - y_{in} - \frac{P_{vapour}}{\rho * g} = 10[m]$$

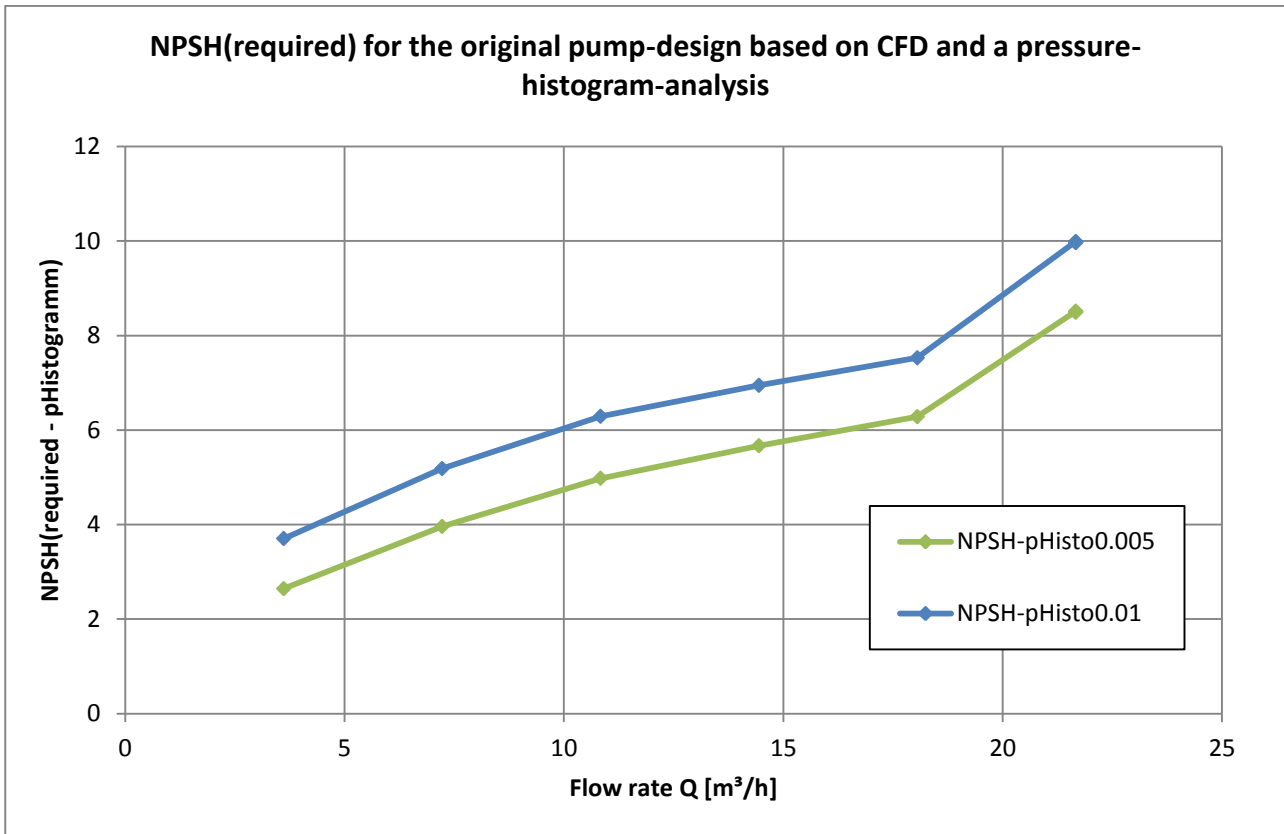
This value is calculated using $P_{atm}=101320$ [Pa] and $P_{vapour}=2400$ [Pa] and the values calculated in other parts of the present work. The value of loss (y_{in}) in the inlet is conservatively calculated with $Q=6$ [l/s] and should be slightly lower when the flow rate decrease. Since this term is negligible, the $NPSH_A$ can be considered constant.

NPSHrequired is the value of positive head required by the pump for a free cavitation behavior. The calculation of this term cannot be done in a simple way but it generally requires experimentation. In this situation the calculation was based on the CFD model using the so called Histogram approach [Benigni]. This method consists in the determination of an equivalent pressure ($P_{Histogram}$) found at a certain distance (x) from the leading edge so that in the x distance all the relative pressure is lower than $P_{Histogram}$. It is then possible to calculate $NPSH_r$ in the following way:

$$NPSH_{r\ Histogram} = \frac{P_{TOT\ in} - P_{Histogram}}{\rho * g}$$

The physical explanation is that the minimum value of relative pressure calculated behind the blade is not necessary a real one, especially when a single phase simulation is done. Moreover the presence of a very small cavity is considered acceptable and therefore imposing the $P > P_{min}$ condition in the entire domain is unnecessarily restrictive. This method has been checked several times (see [3] and [7]) and always proved a good congruence with the experimental data. In the experience of the Hydro Fluid Machinery Department, the value of NPSH3 (corresponding to a loss of head characteristic of 3%. This is the value that is generally used to identify the acceptable NPSHrequired [9]) is placed somewhere between the NPSHhistogram calculated at $x=0,5\%$ and 1% (percentage referred to the total length of the blade).

With this explanation the following graph can be interpreted: $NPSH_{required} (NPSH_{P_{Histo\ 0,01}} < NPSH_{required\ 3\%} < NPSH_{P_{Histo\ 0,005}})$ is always lower than the NPSHavailable in all the functioning range.



NPSH3(required) is placed between the two curves. It is always lower than the NPSH(available)

The same procedure is followed for the improved versions that were developed. For those versions the cavitation is far less concerning and the distance between the NPSHa and NPSHd is greater than in the original version. This comes from the better inflow conditions of these models.

List of symbols

Unless otherwise noted all equations are written in the international system units.

Symbol	Description
A	Area, cross section
a	Shorter distance between two successive blades
BEP	Best Efficiency Point
b	Width of the channel in the meridional section
C	Absolute velocity
C _f	Friction coefficient on a flat plane
CFD	Computational Fluid Dynamic
D, d	Diameter; infinitesimal difference between two values
D _s	Specific diameter
d _n	Hub diameter
e	Error
f	Generic coefficient
g	Gravity acceleration ($g = 9.81 \text{ m/s}^2$, rounded)
H	Head
H _j	Friction losses in the pipes
J _{sp}	Integral over diffuser or volute throat area
K	Coefficient; turbulent kinetic energy
k _{RR}	Disk friction coefficient
L	Length
L _t	Mixing length
LE	Leading edge
I	Work
M	Torque
N _{blades}	Number of blades
NPSH	Net positive suction head
n	Rotational speed (revolutions per minut)
n _q	Specific speed
P	Power
P _u	Usefull power transmitted
P _{rr}	Disk friction power
p	static pressure
Q	Flow rate
Q _{la}	Flow rate through impeller
Q _{le}	Flow rate through diffuser
Q _{sp}	Leakage flow rate
R, r	Radius; curvature radius
Re	Reynolds number
RMS	Root Mean Square residual value
S	Surface or cross section
sax	Axial distance between chasing and shroud
SST	Shear stress transport turbulence model

TE	Trailing edge
t	Time; distance
U,u	Circumferential velocity; velocity parallel to the wall
V	Absolute velocity
W	Relative velocity; weight
y	Distance from the wall
y+	Dimensionless distance from the wall
Z	Geodetic height
α	Angle between absolute velocity and negative component of circumferential velocity
β	Angle between relative velocity and negative component of circumferential velocity
γ	Slip factor
δ	Thickness
Δ	Difference between two values of the same variable
ϵ	Roughness; generic coefficient
ζ	Loss coefficient; load factor
η	Efficiency
η_{vol}	Volumetric efficiency
η_H	Hydraulic efficiency
θ	Angle
λ	Power coefficient; factor
μ	Dynamic viscosity $\mu = \rho \times \nu$
ν	Kinematic viscosity
ρ	Density
τ	Scar stress; blade blocking factor
ϕ	Flow coefficient
ψ	Head coefficient
ω	Rotational speed (radiants per second); turbulent frequency
ω_s	Universal specific speed

List of figures and tables

Figure 1	Two possible ways of regulating the flow rate.	10
Figure 2	Pump characteristics.	11
Figure 3	Balje diagram for single stadium of a pump. Elaborated from [13]	13
Figure 4	Balje diagram for single stadium. Some typical shapes of impellers are also shown. [12]	13
Figure 5	Relation between the impeller shape and the specific speed with constant flow rate.	14
Figure 6	Maximum practically attainable efficiency with respect to specific speed and design flow rate. [14]	15
Figure 7	Field of applications for different nq number pumps. [8]	16
Figure 8	Meridian and planar view of a radial impeller. [9]	16
Figure 9	Sketch of the pump .	18
Table 10	Names of the FP30 series components.	19
Figure 11	Characteristics curves of head and power consumption furnished by the company.	19
Figure 12	Sketch of the test-rig .	25
Figure 13	Detail of the shaft split to insert the torque meter.	28
Figure 14	Torque meter.	27
Figure 15	Sketch of a pressure tapping .	28
Figure 16	Picture of the pressure measurement device.	29
Figure 17	Sketch of the measuring sections. [6]	30
Figure 18	Head characteristics of impellers Plastic D155 number 1.	31
Figure 19	Friction losses on the bearing .	33
Figure 20	Friction losses on the bearing .	34
Figure 21	Effects of the rotational speed on head.	36
Figure 22	Head characteristic of the plastic impellers.	37
Figure 23	Efficiency characteristic of the plastic impellers.	39
Figure 24	Power consumption of impeller 1.	40
Figure 25	Head characteristic of the plastic and cast iron impellers.	41
Figure 26	Efficiency characteristic of the plastic and cast iron impellers.	42
Figure 27	Head characteristic of the plastic impellers with reduced diameter.	43
Figure 28	Efficiency characteristic of the plastic impellers with reduced diameter.	44
Table 29	Reduction of efficiency in plastic impellers with reduced diameter.	44
Figure 30	Head curves of two different impellers and volute.	45
Table 31	Uncertainties.	46
Figure 32	Power balance.	51
Figure 33	Sketch of the meridian section.	53
Figure 34	Test-rig for the measurement of leakage losses.	55
Figure 35	Leakage losses.	56
Figure 36	Localized loss coefficients. [4]	57
Figure 37	Localized loss coefficients . [4]	58

Figure 38	Sections of the volute.	61
Table 39	Table of the calculated losses inside the impeller.	63
Figure 40	Hydraulic efficiencies of single-stage single-entry radial pumps. [9]	67
Figure 41	Head coefficient range for different nq numbers. [9]	68
Figure 42	Head coefficient range for different nq numbers.[9]	70
Figure 43	Possible shapes of the leading edge.	71
Figure 44	Meridian section and main dimensions.	73
Figure 45	Internal (right) and external (left) blade angles distribution in a version of the pump.	74
Table 46	Comparison between original value and ideal ones.	75
Figure 47	Velocity profile of the flow near the surface. Elaborated from [10]	80
Figure 48	Meridian view of the original impeller.	83
Figure 49	Frontal view of the original impeller reconstructed with Blade Gen.	84
Figure 50	Comparison of original impeller and reconstructed one.	84
Figure 51	Drawings of the volute.	85
Figure 52	Three dimensional view of the complete model.	86
Figure 53	Three dimensional view of the detail of the blade.	86
Table 54	Characteristics of the investigated mesh.	87
Figure 55	Characteristics of head of some of the simulated models.	89
Figure 56	Characteristics of efficiency of some of the simulated models.	90
Figure 57	Pressure distribution in meridian view.	93
Figure 58	Pressure distribution in meridian view.	93
Figure 59	Load of the blade.	93
Figure 60	Speed distribution inside the meridian channel and inside the blade to blade plane.	94
Figure 61	Velocity vectors inside the blade to blade channel, around the leading edge.	95
Figure 62	Detail of secondary flow inside the volute.	95
Figure 63	Load of the blades at decreasing flow rate.	96
Figure 64	Stream lines inside the blade to blade channel at decreasing flow rate.	97
Figure 65	Speed distribution in blade to blade channel around the leading edge.	98
Figure 66	Confrontation between expected Jet and wake behavior and blade to blade distribution of velocity. [13]	99
Figure 67	Confrontation between commercial and measured head curves.	102
Figure 68	Confrontation between commercial and measured power consumption curves.	103
Figure 69	Confrontation between commercial and measured efficiency curves.	104
Figure 70	Efficiency split curves of a numerically simulated model.	106
Table 71	Suggested meridian geometry for various nq numbers. Based on Gülich suggestions.	107
Table 72	Intermediate versions.	110
Table 73	Geometrical description of Version 1.	110
Figure 74	Frontal view of version 1.	111
Figure 75	View of version 1.	111
Table 76	Geometrical description of version 3.	112
Figure 77	Frontal view of version 3.	113

Table 78	Geometrical description of version 4.	114
Figure 79	Frontal view of version 4.	114
Table 80	Geometrical description of version 6.	115
Table 81	Geometrical description of version 8.	116
Figure 82	Calculated head curve of version 8.	117
Figure 83	Calculated efficiency curve of version 8.	117
Figure 84	Splitting of efficiency components for original version and version 8.	118
Figure 85	Version 8: Velocity distribution vectors (left) at 80% of blade height; stream lines (right) inside the blade channel at 50% of blade height.	118
Table 86	Geometrical characteristics of version 9.	119
Figure 87	Representation of recirculating flow in the meridian channel. [9]	120
Table 88	Geometrical characteristics of version 2.	120
Figure 89	Frontal view of version 2.	121
Figure 90	Meridian section of version 2.	121
Table 91	Geometrical characteristics of version 5.	122
Table 92	Geometrical characteristics of version 7.	122
Table 93	Geometrical characteristics of version 10.	123
Figure 94	Version 10: Velocity distribution vectors (left) at 80% of blade height; stream lines (right) inside the blade channel at 50% of blade height.	124
Figure 95	Calculated head curve of version10.	124
Figure 96	Calculated efficiency curve of version10.	125
Figure 97	Splitting of components for original version c and version 10.	125
Figure 98	Geometry of impellers Version10 (left) and Version8 (right) confronted with the original impeller.	126
Appendix 1	Measurements errors	131
Appendix 2	CFD calculation of the original Plastic D155: velocity vectors in the blade to blade view at decreasing flow rate conditions. 50% of blade height.	133
Appendix 3	CFD calculation of the original Plastic D155: Velocity of the flow in the blade to view at decreasing flow rate conditions. 50% of blade height.	134
Appendix 4	Cavitation considerations	135

Thanks

Mein Erasmus war ein wunderschönes Erlebnis, eine wichtige Zeit in meinem Leben als Student und als Mann. In Graz habe ich viel Neues gelernt über die Welt und mein Fachgebiet. Für die Möglichkeit um dort zu sein, bin ich Prof. Dossena, Prof. Jaberg und auch der ganzen Büroleitung des Politecnico di Milano und der TU-Graz dankbar.

Ein besonderes Dankeschön geht an Jürgen, dem zuständigen Ingenieur und neuen Freund, der mir sehr viel geholfen hat. Ohne ihn wäre alles viel schwieriger gewesen.

Auch war das ganze Team der HFM äusserst kompetent und sehr freundlich.

Alle diese Leute werde ich nie vergessen; aber die wichtigste Unterstützung kam wie immer von meiner Familie und von Alice.

Bibliography

- [1] Anderson H.H., *Centrifugal pumps and allied machinery*, Elsevier science publisher TD 1994.
- [2] ANSYS CFX-Solver Theory Guide , ed. 2011.
- [3] Benigni H., Jaberg H. and Yeung H., Numerical Simulation of Low Specific Speed American Petroleum Institute Pumps in Part-Load Operation and Comparison With Test Rig Results, *Journal of Fluids Engineering*. 2012.
- [4] Bianchi A., S.U., *Pompe e impianti di sollevamento*, Hoepli editore, 2001.
- [5] B.M. , O.D. , R.S. ; J.P., *Climate change mitigations 2001*, Contribution of working group III to the third assessment report of the Intergovernmental Panel of Climate Change; Cambridge university press.
- [6] BS EN ISO 9906, *Rotodynamic pumps-Hydraulic performance-Acceptance tests-Grades 1 and 2*. 2007.
- [7] Gehrler, A., Benigni, H., and Penninger, G., 2004, Dimensioning and Simulation of Process Pumps, Karlsruhe Pump Users Technical Forum, Karlsruhe, Germany, Sept. 29–30.
- [8] Grabow G., *Optimalbereiche von Fluidenergiemaschinen-Pumpen und Verdichter*, TU Bergakademie Freiberg. 2001.
- [9] Gülich, J. F. *Centrifugal Pump*, Springer edition 2010.
- [10] Kundu, P.K., Cohen, I. M., *Fluid Mechanics*, Academic Press 2004.
- [11] Montenegro, G. e Persico, G.B. , Slides del corso di Tecniche di modellazione di macchine a fluido, anno accademico 2011-2012, Politecnico di Milano.
- [12] Onorati, A. *Dispensa del corso di macchine*, Politecnico di Milano. 2011.
- [13] Osnaghi C., *Teoria delle turbomacchine*, società editrice Esculapio, ed.2006.
- [14] Stoffell B., Vortrag an der TU Graz, 22.06.2006, TU Darmstadt.
- [15] Wilcox D. C., *Turbulence Modeling for CFD*, DWC Industries Inc. La Canada, California 1993.